Development of a 3D bioprinting and standalone bioreactor unit for the production and maintenance of bioscaffolds *in vitro*.

A thesis submitted in fulfillment of the requirements for the degree of

MASTER OF SCIENCE

at the

Biotechnology Innovation Centre

RHODES UNIVERSITY

By

JETHRO HUNDLING

March 2021

Declaration

I declare that this thesis is my own, unaided work. It is being submitted for the degree of Master of Science of Rhodes University. It has not been submitted for any degree or examination at any other university.

_____

Mr. Jethro Hundling

Abstract

The most common method for *in vitro* cell culture currently is to grow a specific cell type in isolation, in monolayer format, adhered to a 2D culture surface. This brings about many limitations in comparison to *in vivo* models due to altered cell phenotypes, as caused by the culturing technique itself, and the lack of naturally occurring cell-to-cell interactions. Three dimensional mammalian cell culture technologies have the potential to overcome these limitations, and provide models more representative of natural systems. Unfortunately, the cost and difficulty associated with achieving sustainable and useful 3D mammalian cell culture is still very high, preventing its widespread adoption across scientific platforms. In this research, we investigate the feasibility of developing and producing a visible light-based 3D stereolithographic bioprinter to produce 3D scaffolds for cell culture. Furthermore, we investigate the possibility of developing and implementing a forced perfusion bioreactor system, which would support the produced scaffold and improve longer-term culture conditions. The developed 3D bioprinter, and bioreactor designs were developed and tested alongside Poly (ethylene glycol) diacrylate (PEGDA), a versatile synthetic scaffold material. PEGDA itself was also evaluated for its printability, robustness in culture conditions over time, and its ability to maintain 3D mammalian cell culture. This research showed that both the developed 3D bioprinter, and bioreactor unit were capable of producing and maintaining an easily modifiable PEGDA scaffold, in culture conditions. In addition, the PEGDA formulation developed was shown to allow for the effective and reproducible 3D cell culture conditions over the medium term, with automated media feeding. The research presented here aimed to illustrate a proof of concept that the low-cost development and production of 3D culture scaffold production and maintenance systems was feasible to the scientific research environment. This technology can then be built upon, into a system that would then allow for the broader adoption and investigation of 3D cell culture as a tool within the scientific community.

Acknowledgments

I would like to acknowledge the ongoing support I have received from my supervisor, Dr. Earl Prinsloo for the duration of my time as a postgraduate student at Rhodes University. Additionally, I would like to thank my lab mates and colleagues: Rose Kadye, John Honiball, Lebohang Makhene, Lucas Lotter, Sidne Fanucci and Mihlali Stoffels, for all of their assistance and advice over the years. Finally, I would like to give special thanks my mom, Gillian Andreas, for her constant love and support, without which I would not have come this far.

Outputs

- John R Honiball, Jethro Hundling, Sidne Fanucci and Earl Prinsloo (2017) A low cost bioprinter for alginate-based hydrogel microextrusion. 2nd International Conference on Tissue Engineering and Regenerative Medicine. Vaal University of Technology, Vanderbiljpark, South Africa. **Oral Presentation**
- Earl Prinsloo, Sidne Fanucci, Rose Kadye, Mihlali Stoffels, Jethro Hundling and John Honiball (May 2019) Towards a bioprinting platform for preclinical and clinical application. SAMRC Advanced Cell Culture Collaborative Meeting, Cape Town. **Workshop Presentation**

Contribution:

Aspects of the proof of concept described in this thesis were included in the presentations listed above.

Table of Contents

List of Figures

List of Tables

List of Equations

List of Abbreviations

2D	2-dimensional
3D	3-dimensional
ABS	Acrylonitrile butadiene styrene
AIM	Adipogenic Induction Media
AM	Additive Manufacturing
CAD	Computer Aided Design
DLP	Digital Light Processing
DMEM	Dubecco's Modified Eagle Medium
EBM	Electron Beam Melting
FBS	Fetal Bovine Serum
FCS	Fetal Calf Serum
FDM	Fused Deposition Modelling
FFF	Fused Filament Fabrication
IBMX	3-isobutyl-1-methylxanthine
IR	Infrared
LED	Light Emitting Diode
MSC	Mesenchymal Stem Cell
NVP	1-vinyl-2 pyrrolidinone
PBS	Phosphate Buffered Solution
PEG	Poly (ethylene glycol)
PEGMA	Poly (ethylene glycol) methacrylate
PEGDA	Poly (ethylene glycol) diacrylate
PI	Propidium iodide
PLA	Poly-lactic acid
PLL	Poly-(L)-Lysine
RTCA	Real Time Cell Analyzer
SEM	Scanning Electron Micrograph
SLA	Stereolithographic
SLM	Selective Laser Melting
SP	Single Plate
TEA	Triethanolamine
USB	Universal Serial Bus
UV	Ultraviolet

List of Symbols

l	Liter
ml	Milliliter
µl	Microliter
m	Meter
cm	Centimeter
mm	Millimeter
µm	Micrometer
kg	Kilogram
g	Gram
mg	Milligram
µg	Microgram
M	Molar
mM	Millimolar
µM	Micromolar
nM	Nanomolar
^{o}C	Degrees Celsius
%	Percent
x	Times
min	Minute
s	Seconds
ms	Milliseconds

1 Chapter 1: Literature Review

1.1 Introduction

All technologies used for the manufacture of structures or objects can be described as falling into two categories, additive or subtractive. Subtractive manufacturing refers to any process in which material is removed from a solid piece, allowing for only the desired product structure to remain. The process of milling is an example of subtractive manufacturing. Additive manufacturing, by comparison, refers to any manufacturing process that deposits material rather than removing it, step by step until the desired product is produced. Additive manufacturing techniques, including three-dimensional (3D) printing, have unique advantages over conventional manufacturing technologies. In addition to being highly flexible in terms of its capacity for rapid prototyping, 3D printing has the potential to allow for the production of complex structures in a relatively short amount of time.

The unique combination of flexibility and precision provided by 3D printing has made it an attractive technology for those in the field of cell biology. In nature, the cells that make up complex organisms exist in complex 3-dimensional matrices. The replication of this microenvironment, termed the cellular niche, is a goal in cell biology, as it allows for an accurate experimental comparison between *in vitro* models and native tissue. However, the complexity required to fully replicate a native tissue and the cellular microenvironment within has remained a challenge in the field. One solution to this problem is to take advantage of advances in 3D printing technology, to mediate the controlled deposition of cells and extracellular matrix components in a spatially defined manner.

1.2 3D printing technologies

The term '3D printing' is relatively broad, and has been used to describe any process whereby a controlled deposition of material is used to produce a spatially defined model in 3-dimensions (3D). This process can be achieved through different techniques, but all rely on the layer-by-layer addition of material to produce a complete physical object (Pandian & Belavek 2016). The use of 3D printing technologies have seen significant adoption by both consumers and manufacturers in the last decade, but its initial conception can be traced back to patents files in the 1970's (Gross, *et. al.,* 2014). The technology began to be more widely adopted in the mid 2000's with the advent of the RepRap project. The RepRap project was the first open-source 3D printing system with the capacity for limited self-replication to be developed and distributed over the internet by volunteers around the globe (Bowyer, 2014). Since then, 3D printing technologies have become widely accessible, with application in a wide range of fields (Pearce et al. 2010). In particular, this trend has allowed for the democratization of the production of scientific equipment, allowing laboratories and individuals to fabricate otherwise exceptionally expensive scientific equipment as needed, at a fraction of its conventional cost (Baden et al. 2015).

1.2.1 Fused Deposition Modelling

The most common form of 3D printing is the Fused Deposition Modelling (FDM) process. This is also referred to as Fused Filament Fabrication (FFF) or Material EXtrusion (MEX), production. The FDM process utilizes a continuous feed of thermoplastic material, which is melted immediately prior to deposition in a heated extruder head. Once deposited, the plastic cools and becomes solid, adding to the 3D model being built. The special deposition of material using this

method is achieved through the computer-controlled motorization of the three axes relative to the extruder end (Dudek 2013).

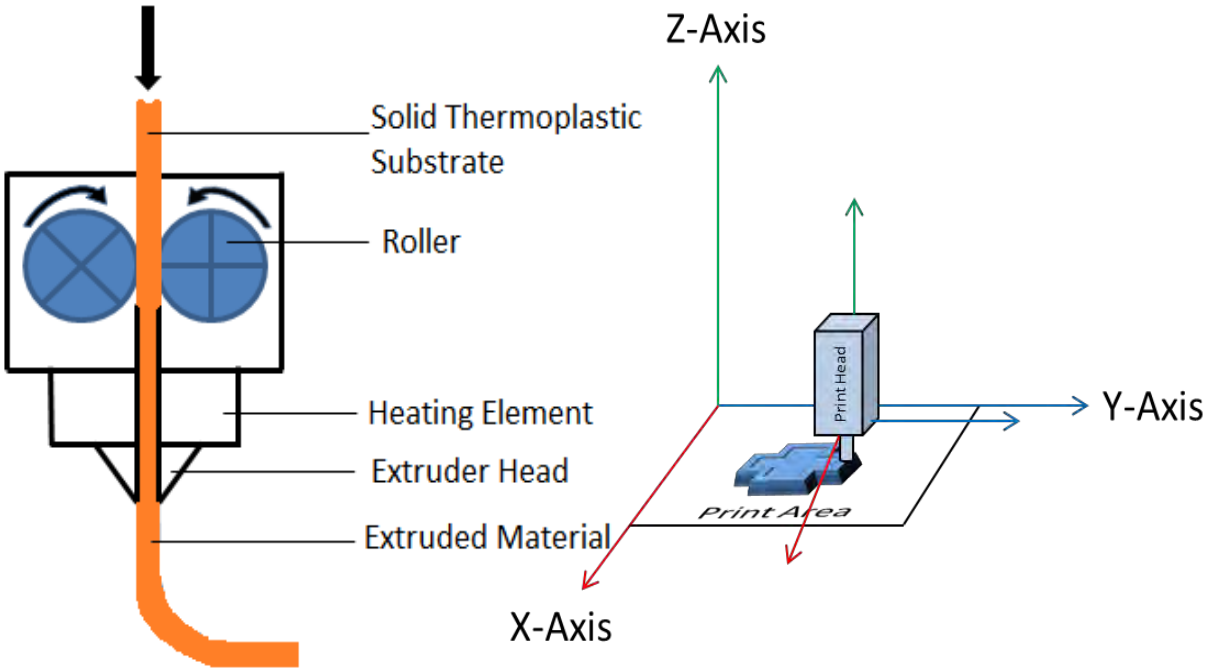

Figure 1.1: A) Cross sectional diagram of the extrusion unit of a conventional FDM 3D printer. B) Diagrammatic representation of the Cartesian planes along which a conventional 3D printer moves to produce an object.

Figure 1.1a shows a cross-section of the print head of an FDM 3D printer, illustrating the extrusion process, while Figure 1.1b illustrates the Cartesian planes along which the extruder is moved to produce a 3D object. FDM printing has become by far the most widely utilized form of the technology for its relative simplicity and low price, as well as range of materials that can be used in this way. Its popularity has also been enhanced through the community driven RepRap project as discussed. Materials such as Polylactic Acid (PLA) and Acrylonitrile Butadiene Styrene (ABS) are most common among enthusiasts (Hwang, et al., 2015), but any material capable of being melted and re-solidifying could be theoretically applied by such a system (Sun, *et al.*, 2015). This gives great variety to the material characteristics of objects potentially able to be produced, making this method of 3D printing suitable for a wide range of applications. FDM printing does have some drawbacks however, as the resolution of any print is limited by the size of the extrusion nozzle diameter,

which defines the smallest theoretical unit that a printer is capable of printing. In addition to this issue, FDM printing can be time consuming relative to other methods of 3D printing and general manufacturing (Brajlih, *et al.*, 2011).

1.2.2 Stereolithographic 3D Printing

Another approach to the process of 3D printing is through stereolithographic (SLA) technologies, also referred to as vat photopolymerization (VPP). SLA 3D printing utilizes photopolymerization to achieve the solidification of consecutive layers from a liquid substrate tank (Taormina, *et al.*, 2018). Photopolymerization, as the name suggests, is the process of polymerization of a monomer based material in reaction to exposure to light (Vitale & Cabral 2016). The light sensitizers used to achieve this reaction are specifically chosen such that the material only reacts to light of a very particular wavelength in order to limit unintended polymerization.

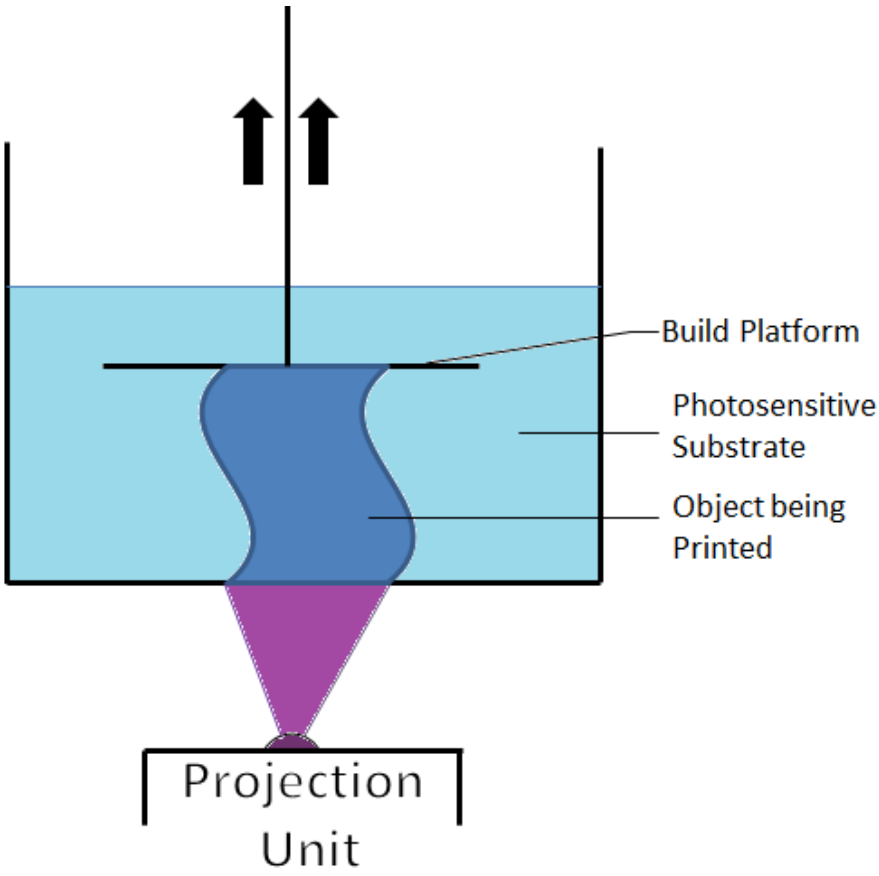

Figure 1.2: Cross section diagrammatic illustration for a conventional SLA/DLP bottom-up 3D printer

The most common wavelength used in SLA based printers are in the UV range (385 nm – 405 nm), being high in energy and preventing conflict with ambient lights. The light sources used in SLA printers can differ, but are most often Digital Light Processing (DLP) projector devices, and less frequently actuated direct lasers. The DLP projection of light onto the resins surface allows for SLA printers with this design to not need motorization of the X and Y axis, as the printer can polymerize the complete layer shape in a single exposure. The Z-axis motor is still required though, in order for layers to be changed during the build process. This factor makes SLA/DLP printers potentially faster than conventional FDM printers that need to move point-to-point on the X and Y axis to complete a solid layer. The major advantage to SLA/DLP printing is the improved print X/Y resolution, which is only limited by the pixel density of the light hitting the resin surface (Finnes 2015). This form of printer is however not without drawbacks. Commercial DLP/SLA 3D printers and the photoactive resins they require are more expensive than the filaments used by their standard FDM counterparts. In a South African context for instance, 1kg of standard PLA filament used for FDM will start at a price of around R 750, while 1L of resin used for SLA/DLP printing will start at around R 1500. Further, SLA printing can require additional post processing that would otherwise not be necessary in an FDM system. The cost of lower end SLA 3D printers is comparable to FDM 3D printers, but higher end models will cost as much as 10 times more. SLA/DLP printers can be configured in a top-down or bottom-up configuration, which refers to the movement of the build plate in the system and the directionality of the light projection (https://theorthocosmos.com/bottom-vs-top-vs-clip-3d-printing/, Accessed 14 Jan 2021).

1.2.3 Selective Laser Melting and Electron Beam Melting

A third type of widely used 3D printing technology is known as Selective Laser Melting (SLM) and Electron Beam Melting (EBM) mechanisms. These two techniques use high energy beams similar to the laser based SLA approach,

except on a powdered solid substrate (Attar 2011; Yap, *et al.*, 2015). These are sometimes referred to as powder bed fusion (PBF) techniques, using directed energy deposition (DED). SLM and EBM printer substrates are powdered metals, which are selectively fused together layer-by-layer through either exposure to a high intensity laser for SLM printers, or a high power electron beam for EBM printers (Murr, *et al.,* 2012). Due to the substrate being solid, these printers are always made in a top-down configuration. Figure 1.3 schematically illustrates the functioning of a SLM or EBM printer. These systems allow for extremely intricate parts to be produced using highly durable and strong metals such as titanium and steel alloys. Both SLM and EBM printers are almost exclusively used for industrial application due to the extremely high associated costs of buying and operating these systems (Sing, *et al.*, 2016). An illustration of the SLM process can be seen in Figure 1.3 below.

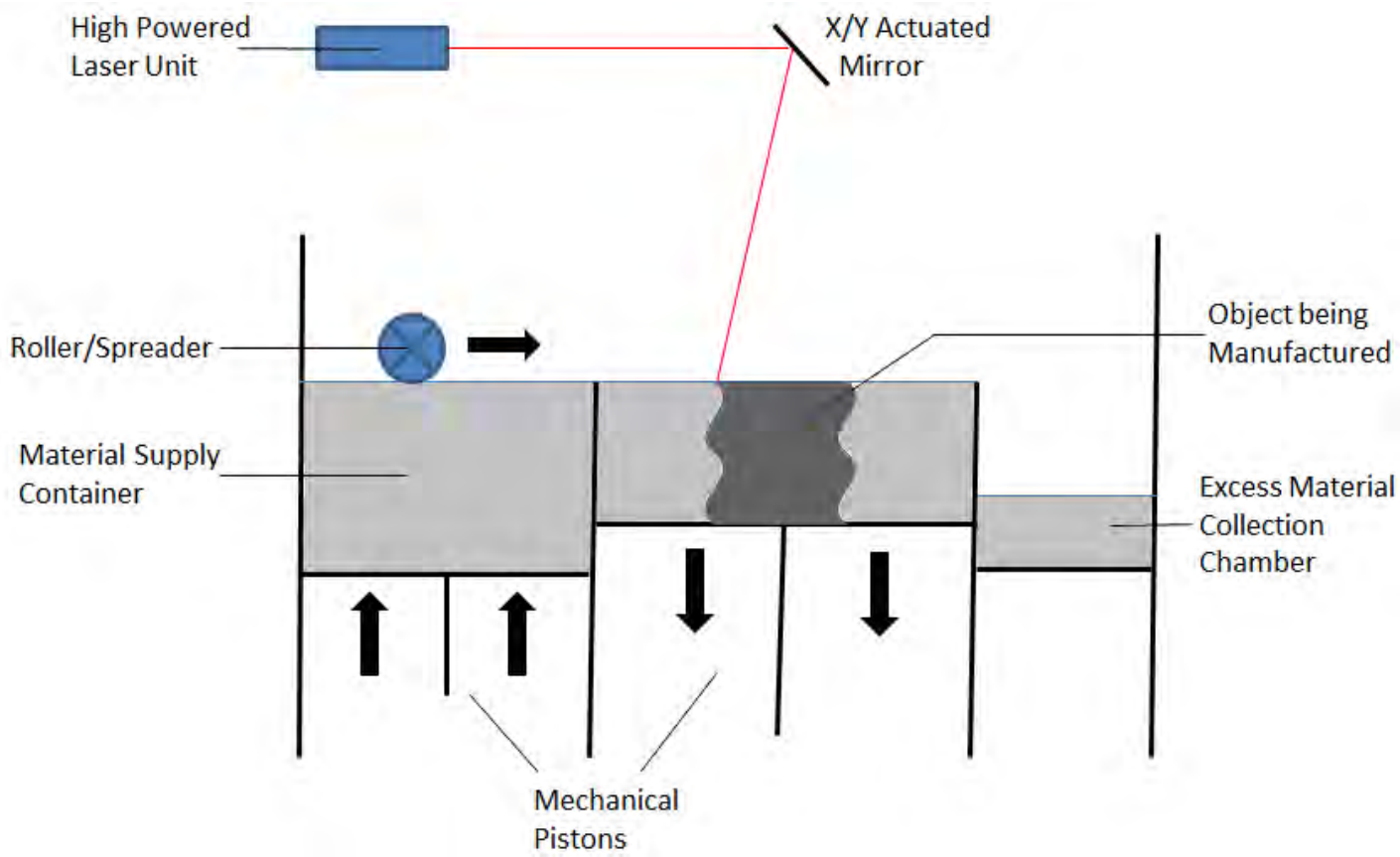

Figure 1.3: Cross-sectioned diagrammatic illustration of a SLM based 3D printing system.

1.3 Additive Manufacturing and Rapid prototyping

A main advantage of additive manufacturing over subtractive manufacturing and casting methods, is the ability to produce much more complex structures that would otherwise be impossible to machine or produce in an injection mold (Kerbrat, *et al.*, 2010; Newman, *et al.,* 2015). Conventional manufacturing techniques could overcome this by producing the object in segmented parts and then combine them in post-processing, but this often leads to parts that are either heavier or are of lower structural integrity. In the case of subtractive manufacturing, there is also often an amount of material that is unrecoverable and wasted after removal, but this can vary based on the exact part being produced and the particular type of additive manufacturing being used (Paris, *et al.*, 2016). One final advantage to additive manufacturing is the capacity for its use in the process of rapid prototyping. Rapid prototyping is the process of testing, updating, and retesting product prototypes in order to arrive at a finalized design as rapidly as possible (Sass & Oxman, 2006). Conventional manufacturing techniques are often unsuitable for this, having much higher turnaround time and cost for producing an even slightly altered product for testing. Additive manufacturing by comparison can produce altered prototypes with virtually no added turnaround time, making it far better suited to this application. This reduced turnover is advantageous to fields in which models need to be constantly updated and revised between prints. The field of tissue engineering is one such example, as 3D structures need to be constantly refined as data is produced on previous generations. The current limitations of this technology, however, is that it is relatively slow in comparison to current mass production techniques when producing multiple copies of an unchanged structure, and is thus often only applicable to the rapid prototyping phase of non-complex product designs (Jain & Kuthe 2013).

While 3D printing technologies are becoming more widely used for conventional part and product production, more recently its application in a wider range of

uses has been explored. One such application is in the realm of biological sciences, through the use of biomaterials in the place of conventional plastics or metals for printing materials.

1.4 Biomaterials

A biomaterial is a substance that is engineered to interact with biological systems, or is biologically compatible in some way (O'Brien, 2011). Biomaterials often take the form of supporting hydrogel scaffolds that allow for the growth of cells in 3D. This is achieved by utilizing specific biomaterials that form cross-linked polymer matrices or scaffolds with qualities sufficient to support sustained cell culture growth (Nair & Laurencin, 2007). It is important that these qualities, including pore size, density and elastic modulus of the scaffold, suit the specific application and cell type. Cell types found in the soft tissue, for instance the brain or adipose tissues, would require a scaffold with greater elasticity in relation to a cell of a hard tissue such as the bone(Leipzig & Shoichet, 2009; Pennesi, *et al.,* 2011). A vast array of matrix options exists to suit systems of various characteristics, but all can be categorized as either naturally derived, or synthetically produced, and each with its own unique properties (Tibbitt & Anseth, 2009). Table 1.1 lists a number of both natural and synthetic biomaterials, with some of their associated properties as an example of this diversity.

Table 1.1: Examples of both natural and synthetic biomaterials and general properties associated with each category. (Tarun, G. 2011)[1] (Seliktar, D., 2012)[2] (Almany & Seliktar, 2005)[3] (Gyles, et al., 2017) (Leberfinger, A. et al., 2017)[4] (Caliari and Burdick, 2016)[5]

Natural Biomaterials	Properties	Synthetic Biomateirals	Properties
Collagen[1,2,3,5,]	Biocompatible; Bioadheasive; Biodegradable in physiological conditions; Poor mechanical properties.	Polyethylene Glycol (PEG)[3,56]	Easily modifiable; Poor cellular adhesion; Biodegradable.
Fibrin[1,3,5,6]	Rapid solidification; Bioadheasive; Poor mechanical properties.	Calcium Phosphate[1]	Biocompatible; Resists biodegradation; Easily modifiable; Good mechanical strength.
Agarose[5]	Low cell adhesion; Cheap/Easily accessible; Rapid solidification.	Polyacrylamide[2,4,6]	High cellular adhesion; High capacity for swelling; Maintains integrity at low crosslinking concentrations.
Hyaluronic Acid[1,4,5,6]	Poor mechanical properties; Biodegradable.	Poly(lactic-co-glycolic acid)[1,4,]	Low mechanical strength; Modifiable biodegradation profile; Biocompatible.
Chitosan[1,4,5]	Biocompatible; Biodegradable; Poor mechanical properties.	Hydroxyapatite[1]	High mechanical strength; Brittle.
Alginate[1,4,5,6]	Good stability; Poor cellular attachment; Cheap/Easily accessible.	Gelatin methacryloyl[5]	Easily degradable; High mechanical strength; Slow polymerisation.

1.4.1 Natural Hydrogels

Naturally derived biomaterials, as the name suggests, are those that already occur and exist within the natural environment of the cell *in vivo.* Thus, these materials are extracted directly from a biological source (Drury & Mooney, 2003). Commonly used biomaterials that are used as scaffolds or scaffold components for cell culture include collagen, fibrin and hyaluronic acid (Yahia, 2015). Collagen, for example, makes up around 20% of all protein in the human body, and is thus present in the extracellular matrix of numerous cell systems. When in use as a hydrogel scaffold, collagen can self-assemble under physiological conditions to produce a cross-linked polymer scaffold at appropriate densities for cell attachment and encapsulation (Antoine, *et al.*, 2014).

A

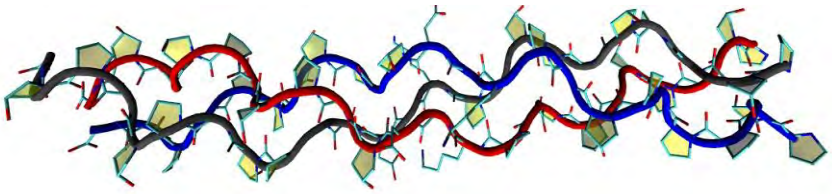

B

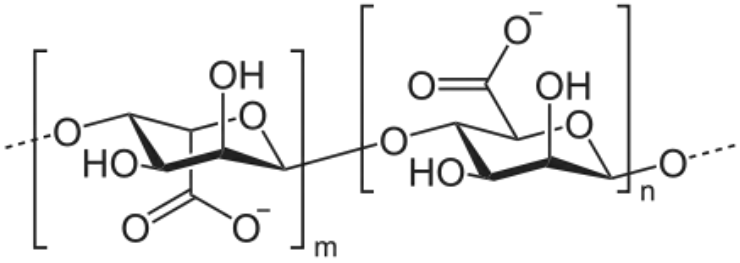

Figure 1.4: [1]A: Structure of a triple helix tropocollagen strand, each comprised of individual crosslinked amnio acid subunits. [2]B: Chemical structure of crosslinked alginate polymer.

[1]https://commons.wikimedia.org/wiki/File:Collagen_%28triple_helix_protein_with_schematic_ribbons%29.jpg
[2]https://commons.wikimedia.org/wiki/File:Alginat.svg

Fibrin is another such material found in the body that is naturally involved in the process of wound clotting. This same reaction can be induced experimentally to produce hydrogels of specific densities and crosslinking characteristics (Ahmed, *et al.*, 2008). Unlike collagen and fibrin, which are produced naturally in mammalian systems, biological hydrogels can be derived from other sources. Alginate, a polysaccharide derived from brown algae, is one such example. Alginate hydrogels rely on crosslinking through ionic bonding, and have the ability to be dissolved, recovering encapsulated cells for analysis. Alginate does not naturally allow for cellular attachment and is usually modified to promote binding through the addition of bioactive compound, or to adapt its innate characteristics to suit a given application (Augst, *et al.,* 2006).

The use of biologically derived materials is intended to provide a better culturing environment through the use of a material that already exists as part of the niche matrix in which the cell type naturally occurs. Having adapted to naturally attach and survive within such matrices usually allows for improved cell attachment, growth characteristics and physiological homogeneity (Edalat, *et al.*, 2012). In addition, and for the same reason, hydrogel scaffolds produced from natural materials often require little to no functionalization prior to cell seeding.

However, the use of biological materials does come with drawbacks that must be considered. The greatest challenge when working with matrices native to the normal *in vivo* environment of the cell, is the susceptibility of such materials to degradation (Tan & Marra, 2010). The degradability of these materials often makes long-term cell culture almost impossible. In addition, biologically derived gels can vary in quality between batches and sources, or contain cytokines and growth factors, both of which would impact cell growth and metabolism (Caliari & Burdick, 2016).

1.4.2 Synthetic Hydrogels

An alternative to organically derived materials for hydrogel production, synthetic materials can also be used to similar effect. Unlike 'natural' hydrogels, synthetic scaffolds make use of materials that are not found in biological systems (Ahmed, 2015). These are usually consisting of long chain cross-linked polymers that are biologically inert, and easily controllable in terms of their structures and pore sizes (Cheung, *et al.*, 2007). Polyacrylamide and polyethylene glycol (PEG) are both examples of such biomaterials, and are among the best studied in this category (Almany & Seliktar, 2005; Kandow, *et al.*, 2007). Both materials are readily available and can be structurally controlled down to the microscale. This manipulation is achieved by control of characteristics at the time of polymerization such as temperature and density, influencing the physical characteristics of the resulting hydrogel.

These materials can also be chemically modified, as in the case of Poly (ethylene glycol) diacrylate (PEGDA). Derived from standard PEG, PEGDA is modified through the addition of acrylate ester groups at either end of the polymer chain. PEGDA remains hydrophilic and non-cytotoxic, while gaining altered crosslinking characteristics. Notably, PEGDA exhibits an increased propensity for light-based crosslinking and polymerization, making it a popular choice for photoencapsulation and light based 3D bioprinting.

A

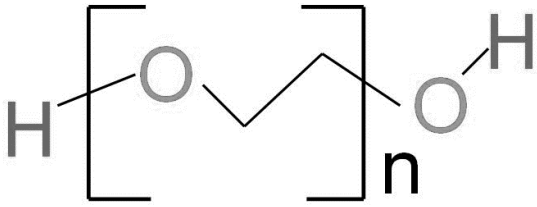

B

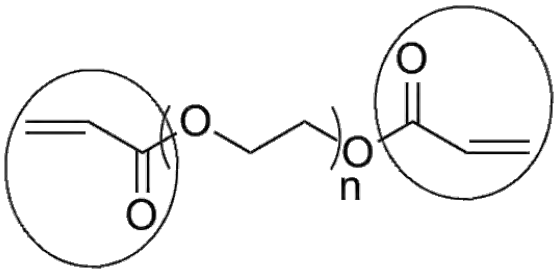

Figure 1.5: [1]A: Chemical structure of the Polyethylene Glycol (PEG) polymer structure. [2]B: PEG modified with two acrylate end groups to produce PEGDA (Polyethylene Glycol Diacrylate).

[1]https://commons.wikimedia.org/wiki/File:Chemical_structure_of_polyethylene_glycol_(PEG).jpg
[2]https://commons.wikimedia.org/wiki/File:End_group_example.png

Materials such as these perfect for systems where fine structural control is necessary, a benefit that is not often shared by standard biologically based scaffolds (Chiu *et al.*, 2011). In addition, most synthetic materials will resist biological degradation (Thankam & Muthu, 2014) and can often prevent undesired cellular responses due to low biocompatibility. This brings about additional challenges for synthetic materials, as being biologically inert often inhibits the proper attachment and growth of cells in culture. Furthermore, such materials can even have a toxic effect on the cells if the materials are not fully polymerized or begin to leach (El-Sherbiny & Yacoub, 2013).

In order to overcome these challenges, but retain the benefits of synthetic scaffolds, they are often used in conjunction with natural elements or biologically functionalized to produce more effective conditions (Deforest, *et al.*, 2010)(Weber, *et al.*, 2007) . Hydrogels that combine elements or materials of both biological and synthetic origins are termed semi-synthetic, and aim to alleviate some of the shortcomings of each class for a desired application. Synthetic scaffolds such as PEG for example, has poor biocompatibility as

previously mentioned, making it unsuitable for long term cell attachment. To overcome this synthetic hydrogels can be functionalized by the addition of biologically active molecules on their surface, facilitating attachment Seliktar, et al., 2012). Another example is the work done by Engler et al, who used a polyacrylamide hydrogel base layered with a collagen outer layer to investigate the effect of material elasticity on directing differentiation in stem cells (Engler, *et al.,* 2006).

1.5 Bioprinting technologies

That application of biomaterials through 3D printing-based techniques is termed 'bioprinting'. Bioprinting allows for the functionality of biomaterials to be implemented in a spatially defined manner, a factor important for several biological applications including tissue engineering and disease modelling. However, the unique sensitivity of biomaterials and biological systems require special consideration when deciding on the printing system to be used. Three main types of bioprinter have been widely utilized, namely inkjet bioprinting, extrusion based bioprinting, and light-based/laser bioprinting (Zhu et al. 2016).

1.5.1 Inkjet bioprinting

Inkjet bioprinting involves the sequential deposition of biomaterial in droplet form with extremely high precision and resolution. Akin to conventional 2D paper printers, inkjet bioprinter use a variety of methods to produce droplets as low as picoliter volumes, which are jetted out at a defined point. This then is achieved in a layer-by-layer fashion, until the desired structure is complete (Derby 2008).

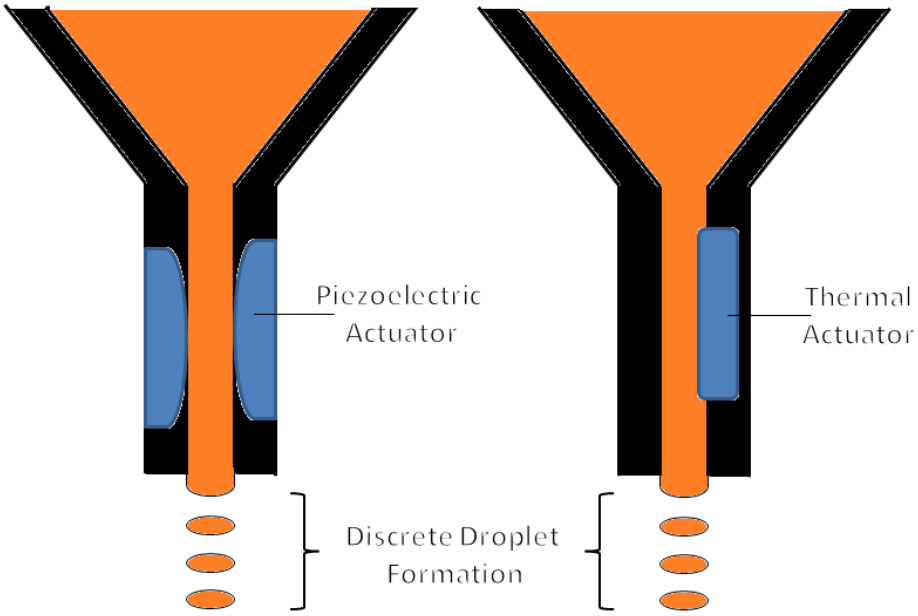

Figure 1.6: Diagrammatic representation of thermal and piezoelectric extrusion in an inkjet bioprinter (Gungor-Ozkerim, et al., 2018).

While this has been achieved in a number of ways, most methods of inkjet bioprinting are through thermal and piezoelectric extrusion. Thermal extrusion as the name suggests works by heating the print head, causing a pressure increase resulting in the expulsion of a small jet of material (Cui, *et al.*, 2012). Piezoelectric printers on the other hand utilize piezoelectric actuators that resonate in response to pulses of applied current. This resonation produces an acoustic waveform within the print head, which can drive out small amounts of material in a controlled manner (Ameri, *et al.*, 2017). Other forms of inkjet printers that differ in method of material do exist but are far less frequently used. The process of inkjet extrusion can be seen in Figure 1.4. While inkjet bioprinters can deposit material with exceptionally high accuracy and precision, they do suffer from a number of drawbacks. One such drawback is the extremely long print times associated with printing in such ultra-small volumes. This can become an issue when applying cells that are sensitive to long removal times from culture conditions. In addition, inkjet bioprinters are limited in the biomaterials that can be used in such a system. Highly viscous materials for example will often not be effectively released by the ultra-small nozzles due to inherently high surface tensions (Hospodiuk, *et al.*, 2017). Finally, the jetting

process itself has been shown to be potentially harmful to cells as a result of the localized temperature increases in the case of thermal inkjet bioprinting, and increases in pressures in the case of both piezoelectric and thermal methods (Godar, 2018). However, with proper optimization, the harmful effects on the cells can be minimized to maintain high cell viability (Gudapati, *et al.*, 2016).

1.5.2 Extrusion Bioprinting

An extrusion bioprinter functions by depositing a biomaterial through pneumatic or mechanical force. This differs from regular FDM 3D printers however, as the substrate being printed is already in a form that does not require melting prior to extrusion. Just as in a conventional FDM 3D printer however, the spatial control of deposition is carried out by tri-axial/cartesian axis motor driven design (Pati, *et al.*, 2015). The biomaterial being printed in extrusion-based bioprinters is held in a reservoir and can then be extruded in a semi-continuous manner as needed. Systems using pneumatic pressure to achieve this can suffer from compression-lag, making mechanical extrusion the most popular method of extrusion in this category (Ozbolat & Hospodiuk, 2016). In comparison to inkjet bioprinters, extrusion based bioprinters can make use of a much wider range of materials and can potentially produce larger structures in a shortened amount of time. The disadvantage, however, is the loss of print resolution due to the larger extruder diameter and greater minimum deposition volume. Like inkjet printers though, extrusion printers also suffer from the effects of pressure on living cells when being forced through the extrusion nozzle during printing (Tambi, *et al.,* 2014). The most common method to overcome this is by simply seeding the scaffold material with cells post print, but this is not always possible depending on the specific application, or type of materials being used. An example of when this solution may not be applicable would be a multi-material scaffold in which the target zone for growth may not be isolated from a conjoined material component intended to stay cell-free, or indeed the target zone may not outwardly accessible to cellular infiltration at all. Nevertheless,

extrusion bioprinting remains a valuable technique for 3D bioprinting in a number of applications. An illustration of the extrusion-based mechanism is illustrated in Figure 1.6.

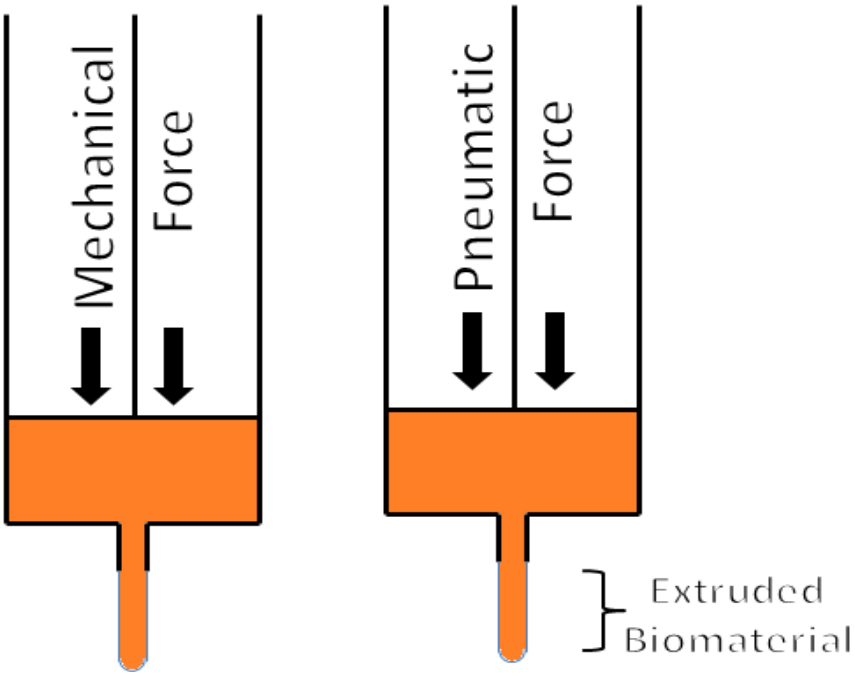

Figure 1.7: Diagrammatic representation of the mechanism of material deposition in an extrusion based bioprinter (Gungor-Ozkerim, et al., 2018)

1.5.3 Stereolithographic bioprinting

The final approach to 3D bioprinting, stereolithography, takes inspiration from conventional stereolithographic (SLA) printers that use light to selectively catalyze the polymerization of a liquid substrate to produce a single object in a layer-by-layer format (Raman & Bashir 2015). As in conventional printers, the light source can differ between printers and will be selected based on the photoactive material to be polymerized. 3D SLA bioprinters can also be designed in both a top-down and bottom-up approach, assuming the material being printed can effectively remain attached to a build plate. Most commonly, light in the UV wavelength is used as the curing agent due to its high energy, but light in the visible spectrum has also been used (Lim, *et al.* 2016). The majority of SLA bioprinters utilized digital light processing (DLP) displays or projectors to

catalyze polymerization of biomaterial, but direct laser-based approaches have also been demonstrated for application in bioprinting. Figure 1.7 illustrates the functioning of a top-down SLA DLP bioprinter in operation.

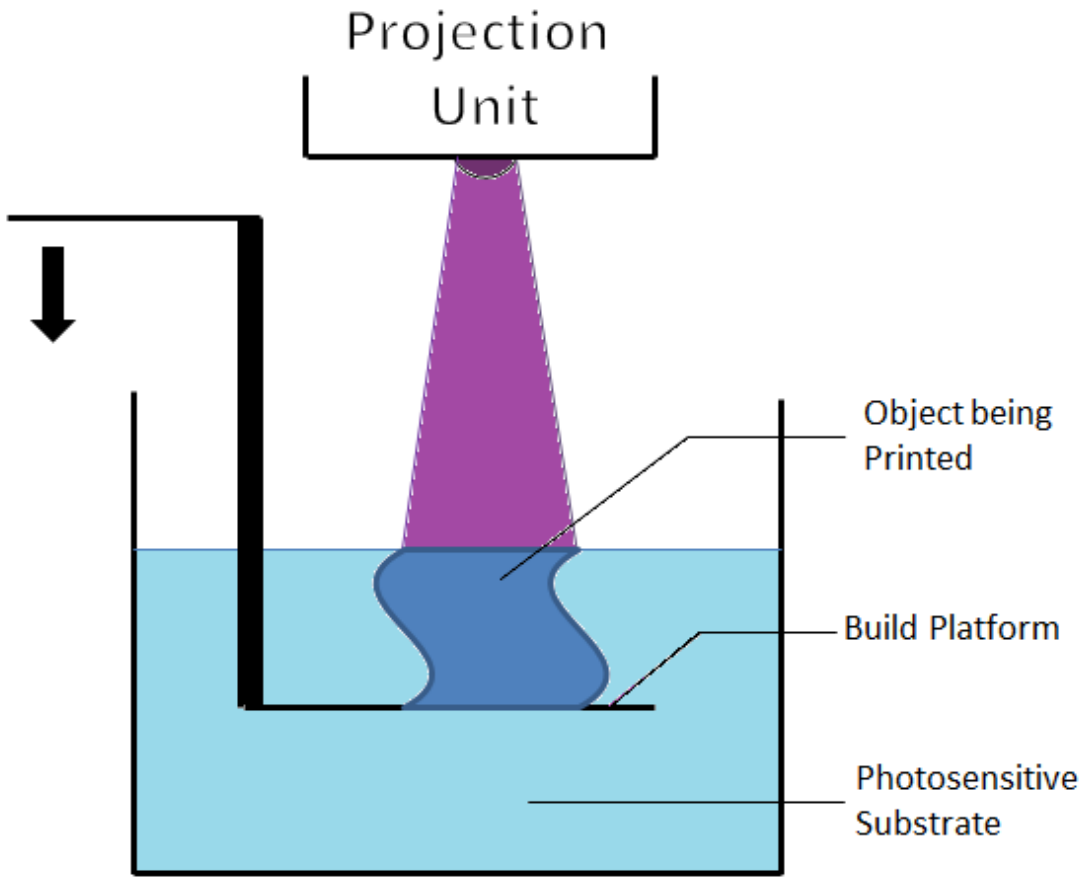

Figure 1.8: Mechanism of action in a top-down configured SLA/DLP 3D bioprinter

The wavelength and intensity of light should be carefully considered in any application in which cells are live-printed, to minimize any harmful effect. This is especially true for UV-based approaches, as light in the UV spectrum can have significant mutagenic effects (Wang, *et al.*, 2015). This effect is caused through the direct action of UV light on DNA strands, inducing various forms of damage including the formation of thymine dimers, DNA strand breaks, and cytosine to thymine substitutions (Brash, *et al.,* 1991). Further, the action of UV can indirectly cause genotoxicity through the production of reactive oxygen species (ROS) through small molecule activation. The ROS in the cellular environment

then induce DNA damage through oxidative base damage and further DNA strand breaks (Ikehata & Ono, 2011).

The chemistry of the substrate used in stereolithographic bioprinting should also be carefully evaluated for its potential cellular toxicity (Arcaute, *et al.* 2014). With the increased popularity of stereolithographic approaches, a wide range of photoinitiators have become available for this application. Photoinitiators are responsible for the absorption of light at specific wavelength to produce a reactive species, catalyzing the polymerization reaction of a substrate (Nguyen & West 2002). However, photoinitiators and other light sensitizing compounds can have a toxic effect on cells, meaning a balance needs to be struck between toxicity and light sensitivity (Bail, *et al.*, 2013). It is critical when using a stereolithographic bioprinting method that all of these factors be considered to ensure the culture is not negatively. (Williams, *et al.,* 2005).

1.6 Approaches to 3D bioprinting design

All 3D printing systems, regardless of type, share the same pre-printing workflow. This consists of initial design of an object in a Computer Aided Design (CAD) software, followed by the 'slicing' of the design to produce discrete instructions that are then read by the printer. This is no different for bioprinting techniques. Depending on the application however, bioprinting can add additional challenges due to the inherent complexity in biological systems. To overcome these challenges, specialized design approaches such as generative design and biomimicry can be employed to produce bioprints that are more effective in their given application. Critically, it is important to identify the appropriate biomaterials to be used, to enhance the success of a print (Lee & Yeong 2016).

1.6.1 Biomimicry

Biomimicry is an approach to innovation that seeks to replicate naturally occurring systems as templates for design (Passino, 2005). Such methods of technological development stem from the thought that naturally occurring systems already present tried and tested models for success. Specifically for *in vitro* cellular culture and tissue engineering, biomimicry represents a method that replicates the patterning and functioning of the system, as it would be found *in vivo* (Yamada & Cukierman, 2007). Absolute replication is of course, never fully achievable, as the complexity of natural systems is far too great. However, the production of systems that mimic that found naturally is often an effective method to allow for improved functionality and more accurate biological comparisons (Huh, *et al.*, 2012). This is an especially applicable approach when considering 3D cell culture, which often expressly seeks to produce cultures and conditions that mimic natural systems. When intending to produce a cellular system to mimic and replicate one occurring naturally, it is important to consider any and all factors that would be present normally. This includes all aspects of the cellular niche environment, such as physical, chemical and cellular cues (Pampaloni, *et al.*, 2007; Zhang, 2012). Physical characteristics of the culturing environments are arguably the most overlooked in terms of conventional cell culture techniques but can be more accurately replicated within 3D scaffolding systems. These physical factors should be carefully chosen within a scaffold environment to produce a topography and elastic modulus relevant to the culture type involved (Khoruzhenko, 2011). This approach has been especially taken up in the fields of tissue replacement and regenerative medicine. Biodegradable scaffolds seeded with regenerative cells are becoming commonplace to replace lost tissues, but integration of these scaffolds relies heavily on the compatibility of the material scaffold with the natural system (Antoine, *et al.,* 2014).

An example of applied biomimicry is demonstrated by Anjem and colleagues, in the development of semi-synthetic injectable hydrogel scaffolds to be used in conjunction with adipose-derived mesenchymal stem cells for a more effective

method of application for cell therapies in cartilage repair. In this instance, the researchers noted the need for hydrogels employed in this application to be extremely mechanically resistant and have mechanical properties closely matching that of the native tissue. This approach mimics the naturally occurring cartilage constructs they aim to repair and prevents destruction of the scaffold *in situ*. In addition to the mechano-physical queues being provided to the cells by this biomimetic scaffold, additional materials were included in the hydrogel cocktail to enhance chondrogenic differentiation (Anjum, *et al*., 2017).

1.6.1.1 Generative Design

While biomimicry has the potential to produce bioprints with better relevance to *in vivo* conditions, it is not always the most appropriate design choice in cases where this is not the overall goal. An example of this would be in designing a scaffold intended to enhance surface area available for cell culture. In this case the emulation of the natural conditions found *in vivo* for the intended cell type might not be relevant, and thus a new approach is required. The approach of generative design can be applied in cases such as these. Generative design is a computer-based method of design that begins with defining the goals and parameters of the form that needs to be produced (Krish 2011). Through algorithmic design, a generative design program then rapidly produces and tests a huge number of design choices (generations), selecting for those that best fit the inputted specifications and requirements. While generative design technology could be used in bioprinting to produce more effective bioscaffolds, it is also widely used in conventional 3D printing and material sciences to produce materials with more advanced properties (Fantini & Curto 2018)(du Plessis, *et al.,* 2019).

1.7 3D cell culture

The culture of mammalian cells *in vitro* has been a powerful tool across a variety of fields. The use of culturing techniques has allowed for numerous advancements in medicine and in aiding our understanding of human biology on the whole (Phelan 2007). Current techniques that allow for the culture and experimentation using mammalian cells usually involve the culturing of a specific cell type in a 2-dimensional (2D) monolayer format (Freshney 2011). Despite the essential contributions made in the past using these techniques, the growth of cells in this manner does have documented drawbacks, because of which, cells cease to be truly representative of their *in vivo* counterparts (Imamura et al. 2015). This in turn limits the results of any such experimental set up intended to provide information of an *in vivo* system. In addition, current techniques often produce limited cell proliferation and maximum cell capacity, a major limitation in experimental set ups requiring larger quantities of cells for analysis. It has been suggested that the development of 3-dimensional (3D) culture systems may provide a more physiologically applicable and comparable alternative to current 2D systems (Edmondson *et al.*, 2014; Duval *et al.,* 2017).

1.7.1 Mammalian Cells *in vivo*

In the *in vivo* environment, each mammalian cell exists within a complex system of extracellular matrices, stimulating factors and other cells of various types all collected in a specific 3D environment (Zhang et al., 2003). We refer to this combination of factors that make up the environment in which a cell is maintained, the cellular 'niche'. This niche environment differs between cell types, depending on the specific requirements needed for proper cell functioning and survival (Kfoury & Scadden, 2015). In addition, the cellular niche acts as one cohesive environment to ensure cells are properly regulated and able to perform their specific function (Scadden, 2006). Aside from somatic cells, mammalian

stem cells have their differentiation potential regulated by these factors, and thus exist in more specialized niche environments within the body (Wang & Wagers, 2011). Figure 1.8 below gives a representation of some of the factors that make up the cellular niche microenvironment.

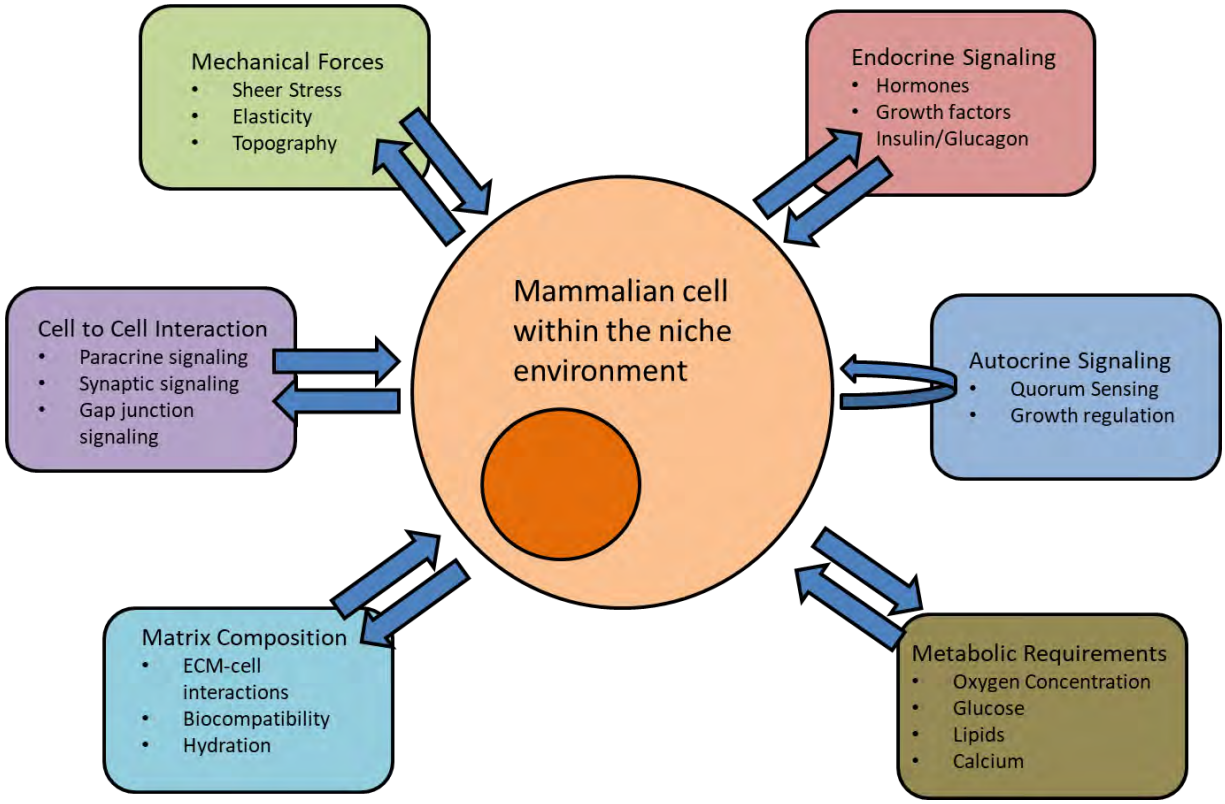

Figure 1.9: Factors contributing to the mammalian cell niche microenvironment in vivo. (Scadden, 2006) (Ventre & Netti, 2016) (Pennesi, et al., 2011).

The understanding of cellular niche environments is critical for reproducing the factors that are required to properly maintain cells in a natural state, allowing for the improvement of cell culture techniques (Ahmad *et al.,* 2007). When taken out of the niche environment and cultured *in vitro*, cells will be altered in response to, and depending on, the change in their external stimuli. This includes changes to their morphology (Matsuda *et al.*, 2010) to adapt to environmental/mechanical changes and changes to their gene expression profile, and thus proteome, in response to an altered external signaling profile (Zaitseva *et al.*, 2006). It is because of this fact, that techniques used to culture cells *ex vivo*

are currently unable to fully replicate the natural state that would be present within the normal *in vivo* environment. This becomes especially important in cultures intended to replicate a specific cell or stem cell niche, as any deviation from the naturally occurring system will negatively impact the results produced (He, *et al.*, 2014).

1.7.2 Cell culture in 3D vs 2D

Current culture systems generally rely on the adherence of a specific cell type onto a 2D surface of a specialized culture dish or flask. This format of culture induces cells to grow in a flattened, 2 dimensional, and monolayer format. Cell culture carried out in 2D does undeniably have many benefits in terms of convenience of culture and experimentation. Cells in a monolayer, for instance, are visually accessible and thus any changes in the culture can be observed microscopically (Lamhamedi-Cherradi *et al.*, 2014). In addition, single cells are easily distinguishable and any changes due to experimental conditions can be easily discerned through microscopy (Hess *et al.*, 2010).

This technique becomes problematic when trying to produce systems that mimic features observed *in vivo*, for both experimental and practical purposes. Cells cultured in 2D are forced into an unnatural morphology, very different to that of their *in vivo* counterparts. It has been shown that cells, across many cell lines, will become significantly flattened with an increased diameter (Gospodarowicz, *et al.*, 1978). This is in part as a result of being adhered to only a single surface, inducing the cells to adapt and flatten, in order to provide an increased surface area for sufficient attachment (Edmondson *et al.,* 2014). In addition, this flattened conformation allows greater nutrient and molecular transfer through the upward face of the cell, without which, cells produced in such an environment would likely not survive. Finally, cells cultured in a 2D format only

have access to cell-to-cell contact via their horizontal plane, an unnatural state relative to that found in most situations *in vivo* (Page, *et al.*, 2013).

This change in microenvironment experienced by the cells does not only impact their morphology, but also has a profound impact on their genetic, transcriptive and translative profile (Kenny *et al.*, 2007; Schmidt *et al.*, 2013). This was as a direct result of the altered signals being given to the cells in the foreign microenvironment. These signals are mainly in the form of mehanotransductive feedback pathways, altered cell-to-cell signaling pathways, and in response to the lack of naturally occurring soluble factors in the nutrient media (Birgersdotter, *et al.*, 2005). It must also be mentioned that the choice of cells that result in sustained *in vitro* cultures have also been put through a selective protocol to retain those that have the ability to be cultured in this unnatural format. This selection in itself has an impact on the genetic and phenotypic characteristics of any cell lines used, thus adding to the disparity between the culture and the cell type *in vivo* (Browne & Al-Rubeai, 2007). Finally, the continual culture of mammalian cells has been shown to produce gradual mutations in a passage dependent manner (Kim *et al.,* 2017). Nikitina and colleagues demonstrated that a significant fraction of hMSCs when placed in standard culture conditions would develop significant genetic abnormalities, diverging from the normal karyotype within 12 passages (Nikitina *et al.,* 2018). In conjunction, these issues result in the production of cells that are indeed similar, but often not fully comparable to their *in vivo* counterparts.

To rectify the issues caused by 2D cell culture techniques, it has become increasingly clear that 3 dimensional cultures can better mimic the microenvironment of cells as found *in vivo* (Tibbitt & Anseth, 2009). It has been shown in multiple cell types, that cells cultured in 3D scaffold and gel systems have improved morphology, expression profiles and response to various toxins in relation to that, which is found in their *in vivo* counterparts (Sun, *et al.*, 2006; Lee, *et al.,* 2009). A 3D cell culture works by allowing attachment to the cell

culture in all directions, as opposed to a flat 2-dimensional plane. This is achieved using 3D biomaterials that allow for this attachment, thus more effectively solving the negative impacts caused by monolayer cell culture. Cells cultured in a 3-dimensional scaffold can form connections in all directions, to both each other and the scaffold material used, producing a morphology more characteristic of that found *in vivo,* thus improving upon systems relying on 2D adherence (Cukierman, *et al.*, 2001). The choice of material used in any 3D system can additionally be chosen and modified to more effectively replicate the specific microenvironment of any specific cell type *in vivo,* including factors such as matrix functionalization, firmness, cell spacing and pore size(Saha, *et al.*, 2007; Lutolf, *et al.*, 2009) . A summary of the differences between cells cultured in 2D vs 3D conditions can be seen in Table 1.2.

Table 1.2: Comparative summary of the differences between 2D and 3D culture in vitro. (Pollack, et al., 2019) (Matsuda, Y. et al., 2010) (Imamura, Y. et al., 2015) (Antoni, D. et al., 2015) (Schmidt, et al., 2013)

Cells in 2D	Cells in 3D
Flattened morphology, with cellular attachment on a single side	3D morphology, with cellular attachment in all directions
Cells connect in a monolayer on a 2D surface	Cells can form in complex 3D structures
Cell to cell interaction limited	Cell to cell interaction can take place in all directions
Gene expression altered from that found in the native environment	Gene expression more representative to that found *in vivo*
No mimicry of natural tissue architecture	Mimicry of natural tissue architectures possible
No limitation of nutrient or signalling molecule availability	Variable nutrient and signalling molecule availability
High reproducibility and high culture proliferation rates	Low reproducibility and low culture proliferation rate
Culture conditions and protocols are highly standardised	Culture conditions and protocols are not standardised
Simplified results interpretation due to low variability in conditions	Increased complexity in result interpretation due to high variability in culture conditions

1.8 Applications of 3D cell culture

1.8.1 Drug development

The culture of mammalian cell in 3D format already has a number of established uses; with further development the technology has the potential to be used for a number of additional applications. Currently, in the pharmaceutical industry, the static monoculture of primary liver hepatocytes is commonplace for use in novel drug assays (Takayama *et al.,* 2013). However, persistent issues of hepatocyte longevity and sustained viability are major limitations to such tests (Meli, *et al.*, 2012). This is especially true in the cases of drugs that are slow clearing, or the metabolites of which are slowly produced for example theophylline or tolbutamide (Di & Obach, 2015). It has been shown, for example, that the 3D culture of hepatocytes in flow through based bioreactor systems provide significant improvement to all of these issues (Hongisto *et al.,* 2013). Drug development and testing companies are beginning to implement these technologies to better screen for drug efficacy, but further development is needed and is still being carried out to provide systems that can more accurately replicate the effect of drugs of cells *in vivo* (Gupta *et al.,* 2016).

1.8.2 Disease Modeling

In addition to the improvement of drug screening, 3D co-culture technologies have the potential to provide a few other research opportunities. One such example is the potential for systems to be developed that mimic the diseased states of human cells in an *in vitro* environment. These cultures could be used to provide a model to study specific diseases in an intricate manner, without the need for an actual human patient or animal model (Brennand *et al.,* 2011). Such a system could then be extended to not only research specific characteristics of a

disease, but also as mentioned before, conduct improved drug screening trials. This would also provide a more accurate look into a particular disease, over current 'disease in a dish' based monoculture systems (Vargo-Gogola & Rosen, 2007). A recent paper by Park et al. demonstrated this by developing a triculture 3D culture system that more accurately reproduced the hallmarks of neuroinflammation and neurodegeneration of Parkinson's disease. Such a system can allow for the reproducible testing of potential drugs to produce results more indicative of the *in vivo* cellular response (Park *et al.*, 2018).

1.8.3 Cell therapies

Cell culture in 3D as a technology also lends itself not only to novel research, but also to use in direct therapies for a variety of illnesses. Indeed, the development and application of 3D cell constructs for cell replacement therapies are becoming available for some illnesses such as Parkinson's (Carlson, *et al.*, 2016). This has in the past been limited to therapies carried out through the direct transplant of tissue or cells from a donor. However, the development of systems that can more effectively proliferate and maintain specific cell and stem cell populations *in vitro* before transplantation would allow for the number and the effectiveness of such therapies to improve. Chen *et al.* in 2015 demonstrated this potential through the use of a 3D Ca-alginate bioscaffold for the proliferation of autologous human osteoblasts prior to transplantation. The system they developed produced cells of higher viability and with greater expression of bone-related genes when compared with conventional culture methods, illustrating the potential for 3D cell culture to facilitate improved cell therapies (Chen, *et al.,* 2015).

1.8.4 Tissue and organ replacement

Improving upon the development of cell therapies is the possibility to replicate entire organs or tissues *in vitro* using multicellular composite systems. Such

technologies are far from fully developed but are constantly being improved with the ultimate goal of being able to effectively grow new, ready for transplant organs from their undifferentiated cellular components (Sekine *et al.,* 2013). Many researchers have already proved the viability of such systems by producing simple skin and cartilage tissue transplants that effectively integrated into the patient once transplanted (Horch, *et al.*, 2005). It was shown viable to produce larger structures too, such as fully vascularized ears, illustrating the potential to create even more complex organs and tissues in the future (Mannoor *et al.,* 2013). A more recent example is the work done by Gregorian *et al*, in developing a lung model, encased in a functional intravascular network, created using photopolymerised hydrogels (Gregorian *et al.,* 2019). While this was a far cry from a functional lung, this work demonstrates the capacity of 3D bioprinting techniques to produce highly complex and modifiable architectures for replication in *in vivo* structures. Despite modern advances however, effective replication of the complexity of natural systems remains a challenge in the production of transplantable tissues and organs (Kurniawan, 2019). In addition, sufficiently rapid vascularization and maintenance of cells in larger scale 3D cultures remains an issue (Min, *et al.,* 2019).

1.9 Bioreactors

A bioreactor can be defined as an apparatus in which a biological process or system is carried out in a controlled manner (Nagel *et al.,* 1992). With regard to mammalian cell culture, a bioreactor refers to a configuration of several culturing elements with the intention of providing improved culturing environments for increased cellular yield and survival. Bioreactors are needed as a natural extension of 3D cell culture techniques, as cells seeded on a 3D scaffold require maintenance under specific conditions to ensure engraftment, survival and proliferation (Selden and Fuller, 2018). There are many types of bioreactor that attempt to do this, each method coming with specific drawbacks and advantages.

1.9.1 Types of bioreactor setup

Bioreactor systems can vary in size, from small scale systems and lab on chip-based approaches best suited for analytical application (Powers *et al.,* 2002), to large-scale cell culture reactors that use thousands of liters of media supporting billions of cells more suited to biological product production or effluent treatment (Briggs *et al.,* 2007). With the number of different materials, set up designs, scales and cell types that are available, bioreactors can be used to produce a potentially limitless variety of culturing conditions for cell growth and research. Due to the range of potential set ups, it is difficult to classify bioreactors into discreet categories. Broadly, bioreactors are categorized by feeding method, either being batch, fed-batch or continuous. However, bioreactors can otherwise be categorized by their other characteristics, such as method of cellular attachment, function or scale (Spier, *et al.,* 2011).

In terms of the method of attachment used, or lack thereof, mammalian bioreactors utilize either an attached surface on which cells are able to grow, or a suspension system in which cells grow in a free floating liquid environment (Lutolf & Hubbell, 2005). Set ups can then be further separated by their methods of cell feeding, using batch, fed-batch or continuous methods (Mulukutla, *et al.*, 2012). A diagrammatic representation of these can be seen in Figure 1.9.

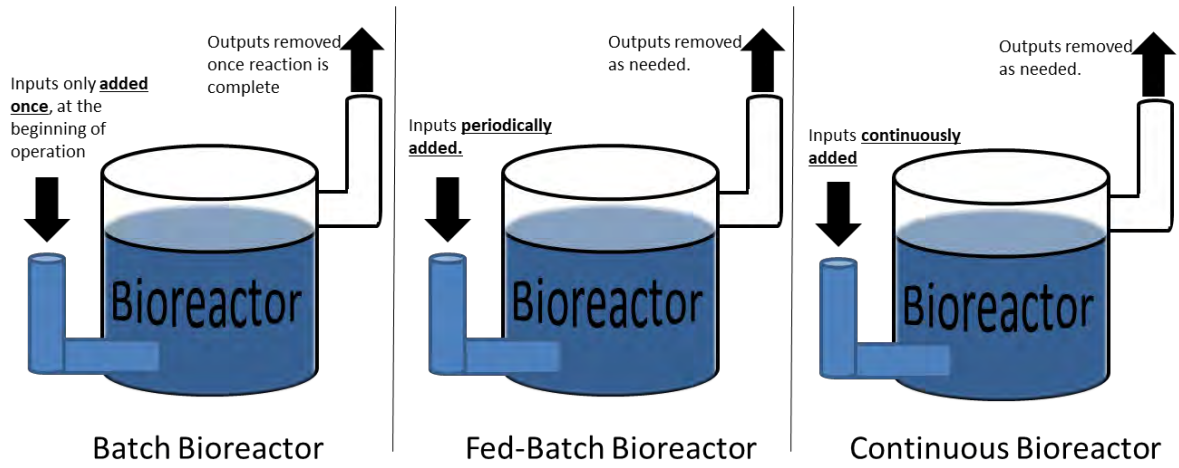

Figure 1.10: Diagrammatic representation of bioreactor technologies separated by feeding methods.

In batch methods, only a single feeding of media is provided to the cells at the beginning of culture. This method is often not used for mammalian cell culture, as it drastically limits the life span of the cells due to their nutritional needs. Fed-batch techniques are likely the most commonly used for laboratory scale operations, providing consistent and regimented feedings of fresh media to the culture as required. Fed-batch techniques are often preferred, as they require very little specialized equipment and materials. Standard 2D cell culture flasks are an example of a simple fed-batch system, as the culture media is periodically replaced as needed. Finally, continuous methods allow for fresh media to constantly be flowing into the system. Continuous methods require a specialized media pump and reservoir systems, and is not suited to all bioreactor setups, but does provide the advantage of constant and consistent nutrient supply to the culture (Mulukutla *et al.,* 2012). Some popular bioreactor set-ups for laboratory scaled experiments include 'spinner flask' bioreactors, in which a cell-seeded scaffold is suspended in media that is continuously circulated by a stir bar (Sucosky, *et al*, 2004). Another example is perfusion-based bioreactors that use pump based systems to force media through the cell scaffold within the vessel (Hidalgo-Bastida, *et al.*, 2012). Examples of these bioreactor technologies can be seen in Figure 1.10. Both of these bioreactor technologies attempt to eliminate oxygen and nutrient gradients within the bioscaffolds through constant movement of media through the system.

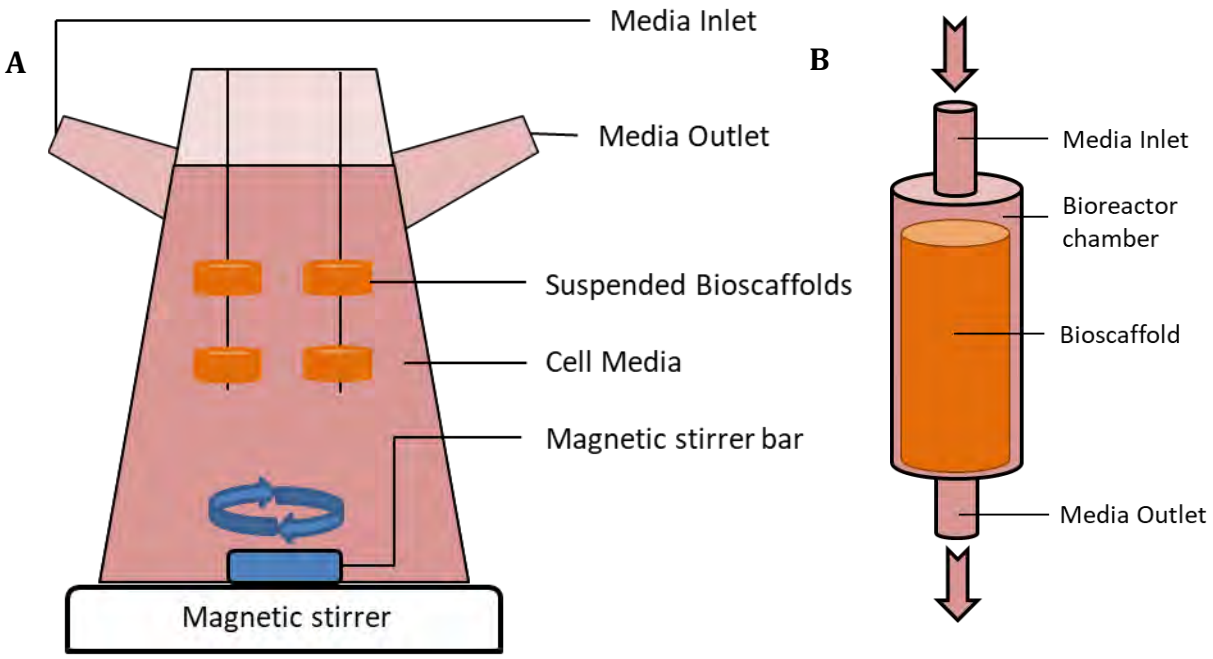

Figure 1.11: Diagrammatic representations of A: A spinner flask bioreactor; and B: A forced perfusion based bioreactor.

Depending on the experimental design, a specific mammalian cell bioreactor set up will be chosen to meet the desired goals. Regardless of the set up itself, several factors need to be considered when implementing any type of bioreactor, due to the inherent needs of the mammalian cells to be cultured. In line with these needs, a bioreactor must control the levels of oxygen, carbon dioxide and nutrients that are available, as well as regulate temperature and pH. This is usually done through the continuous monitoring (through the use of inlayed sensors) and maintenance (through variable control of the bioreactor inputs) as demonstrated by Obom et al 2014. These factors of course also come with the added challenge of maintaining strict sterility.

Depending on the reactor and objectives, additional control must be maintained over factors such as cellular organization and differential growth stimuli (Obradovic, *et al.*, 1999; Abu-Absi *et al.,* 2011). Standard monolayer and suspension-based culturing methods achieve all these basic requirements by a simple method of fed-batch replenishment of fresh media in an open-air environment. This, however, becomes more difficult when attempting to produce cultures within a more complex physical environment, such as those within enclosed 3-dimensional culturing conditions. This is due to the natural formation of gradients across any 3D scaffold or system, or the uneven distribution of

media within. Leung *et al* illustrated this by demonstrating the uneven oxygen distribution within cell-laden collagen hydrogels. To overcome these challenges, 3D systems often employ methods of stirring or forced perfusion of media, to properly distribute nutrients, dissolved gasses and waste products in and out of the system (Sen, *et al.*, 2001).

In summary, the following initial requirements should be considered when deciding on a mammalian bioreactor setup, with any additional factors being drawn from the specific experimental or economic goals of the system.

Table 1.3: Summery of universal considerations for mammalian cell bioreactors.

Physical requirements	Chemical requirements
• **Supply and removal of media to facilitate sufficient chemical exchange.** • **Temperature maintenance.** • **Sterility maintenance.**	• pH maintenance. • Nutrient availability. • Sufficient removal of biological waste products. • Control of dissolved gasses (CO_2/O_2)

1.10 Problem Statement

It is becoming increasingly apparent that the monolayer culture of mammalian cells provides an insufficient comparison between the native and *ex vivo* tissue characteristics. This difference can be attributed at least in part to the mechano-physical and spatial differences placed on cells within the 2D culture environment, subsequently diminishing its application in fields in which biomimicry of native tissue is desirable. In the fields of pharmaceutics, tissue engineering and disease modelling, this issue is being overcome through the

increasingly widespread adoption of 3D tissue culture techniques. One such approach is to leverage the process of additive manufacturing for the layer-by-layer production of culture tissues in a spatially controlled manner. This is then used in conjunction with an array of biocompatible materials to create artificial culture environments or artificial niches that better reflect the desired characteristics needed for a given application, in a process termed "bioprinting". Bioprinting, while not being a new concept, is still in its infancy as an applied technology and thus has large associated costs and limited accessibility. This lack of accessibility has resulted in relatively few research groups adopting the technology despite its benefits, thus novel approaches to 3D bioprinting are desirable to alleviate this problem. The development of an affordable system, able to effectively produce a wide range of 3D biocompatible structures that could then be maintained over time, could allow for more widely utilized 3D culture technologies to be adopted by the scientific industries.

1.11 Research Questions

- Can a visible light bioprinter be built that is capable of spatially defined 3D hydrogel scaffold production?
- Can Poly (ethylene glycol) diacrylate be 3D printed and used as an effective hydrogel scaffold to support the proliferation of mammalian cell cultures *in vitro?*
- Can a small-scale bioreactor system be built to support the growth of mammalian cultures on a 3D printed PEGDA hydrogel scaffold?

1.11 Aims and Objectives

The aims and objectives of the study are described below:

1. ***The development and construction of a DLP based 3D bioprinter.***

The objectives linked to this aim were set to:

1.1 Design and complete construction of the printer structural framework.

1) CAD Design of the structural framework.
2) Cutting of the 20x20mm T-slot aluminum profiles to the correct lengths.
3) Production of connective corner brackets through conventional 3D printing.
4) Construction of the printer structural framework.

1.2 Production and implementation of X- and Z-axis components.

1) Production of axis components through conventional CAD based design and 3D printing.
2) Assembly of the x- and z-axis within the structural framework.
3) Mounting of the z-axis build plate onto the z-axis.
4) Mounting of the x-axis base plate onto the x-axis.

1.3 Mount projector unit

1) Production of mounting brackets through conventional 3D printing techniques.
2) Mounting of the DLP projector unit to the printer structural framework.

1.4 Implement motor and projector electronic control components.

1) Connect Arduino Uno R3 and CNC Shield motor control unit to the z- and x-axis control motors, and to a controlling PC.
2) Flash Arduino Uno R3 with firmware for motor control

1.5 Troubleshoot issues and optimize bioprinter.

2. ***Construct the structural and mechanical components of the bioreactor unit***

The objectives linked to this aim were set to:

2.1 Design and fabricate the bioreactor chamber.

1) Bioreactor chambers were designed using CAD-based software.

2) Bioreactors were synthesized using SLA/DLP resin-based 3D printing techniques.

2.2 Develop and produce the media reservoir and feeding systems.

1) A syringe-based media feeding system was designed using CAD-based software, and parts printed using conventional 3D printing techniques.
2) A central motor system was implemented to control the flow of media through the system.
3) The motor was connected to a controlling PC via Arduino UNO R3 with CNC-shield.
4) The bioreactor chamber was implemented such that media could be fed through as controlled by the connected PC.

3. ***Produce a 3D scaffold capable of supporting mammalian cells in vitro.***

The objectives linked to this aim were set to:

3.1 Define and optimize the PEGDA scaffold formula to be tested as a cell scaffold material

3.2 Illustrate the efficacy of the PEGDA cocktail to be used as a material for visible light based bioprinting.

1) Prints of varying complexity were attempted using the defined PEGDA scaffold material.
2) Define the printing characteristics of PEGDA for the given application.

3.3 Investigate the swelling characteristics of PEGDA in standard cell culture media over time.

1) Produce polymerized PEGDA disks of uniform consistency and size.
2) Immerse the PEGDA disks in standard culture media and measure disk diameter increase over time at standard culture conditions over time.

3.4 3T3-L1 preadipocyte cell line efficacy was confirmed though endpoint differentiation testing with Oil red-O staining

3.5 Investigate the toxicity of PEGDA cocktail components on mammalian cell culture.

3.6 Achieve cell culture on the produced PEGDA scaffold outside of the bioreactor system.

2 Chapter 2: Development and Construction of a Multimaterial DLP visible light 3D bioprinter

2.1 Introduction

Digital Light Processing (DLP) 3D printing is an increasingly popular approach to 3D printing as it allows for a number of advantages over conventional extrusion-based technologies (Jasveer and Jianbin, 2018). A subset of stereolithographic (SLA) 3D printing, DLP 3D printing utilizes computer controlled projected light to solidify a photo-curable substrate in a layer-by-layer fashion (Taormina, *et al.*, 2018). While conventional extrusion based printers are limited in resolution by the minimum width of the extrusion nozzle, DLP based printers are limited rather by the definition in the object projected, thus providing a much finer range for detail (Finnes, 2015). Additionally, DLP printers can often handle greater levels of overhang within prints as each layer is solidified as a single piece, as opposed to using the conventional outline and fill-in method. These factors make DLP based printing techniques ideal for applications in which print resolution and complexity are highly valued. One such field in which this is becoming increasingly recognized, is in the area of bioprinting, in which biological scaffolds need to be produced to replicate the complexity of native biological tissues (Zhu *et al.,* 2016).

The following section outlines the criteria and rational used in the development of a novel 3D DLP/SLA bioprinter.

2.2 Initial development criteria and design rational

Development of the bioprinting unit began by outlining specific criteria and functionality that should be adhered for the creation of the final product. Bioprinting as a term encompasses a very wide range of processes and

techniques, and it was thus imperative that a clear set of functionalities were kept in mind when deciding on the desired criteria.

There are a number of methods by which 3D printers and bioprinters achieve controlled substrate deposition and solidification, each with their own advantages and disadvantages. A stereolithographic (SLA) technique that utilizes digital light projection (DLP) to create solidified objects was ultimately chosen for the development of this printer due to the wide range of substrates to which the technique could be applied, and the precision at which objects can be produced. Conventional extrusion-based printers are limited in that the resolution of the print cannot exceed the diameter of the extrusion nozzle, as this dictates the size of the thinnest 'line' that the printer is able to produce. DLP based printers can achieve higher print resolutions as they are limited rather by the smallest pixel of light they can project onto the photoactive resin surface. In this way, DLP printers can theoretically produce more precise structures, but suffer from other issues that can reduce printing definition, including scattering of light and substrate swelling. Scattering refers to the undesired reflection of light by the printing substrate, causing areas intended to remain hollow or empty to polymerize (Persano et al. 2018). Swelling is the effect whereby upon polymerization, the substrate swells slightly in all directions, increasing the size of the smallest theoretical unit that could be printed (Arcaute et al. 2014). Some substrates suffer from this more than others and are an important factor to consider in substrate selection. Both issues, however, can be minimized through substrate choice, compositional alterations of the substrate itself, and general system optimization. DLP 3D printers conventionally use either UV or visible light to cause solidification of the substrate, and this was the next design criteria to be decided.

It was decided that the printer developed should utilize visible light based DLP stereolithographic polymerization to produce its solidified layers of substrate material. Using visible light as opposed to the more commonly used UV based

systems provided several advantages. First and foremost, visible light does not cause the damaging effect that is exhibited by UV light exposure on cells. The implementation of visible light polymerization would allow for the possibility of 'live prints', in which the substrate contains live cells before and during the printing process, enhancing penetration within the 3D scaffolds produced. The high intensity of light needed to achieve rapid polymerization was a concern in this regard and was addressed later in this research (See section 4.2.5). The experimental range that this functionality would allow made visible light an ideal choice for the development of the bioprinter unit. The major disadvantage with regard to the use of visible light photoinitiation was the need for the apparatus and polymer would need to be housed in a darkened casing, to prevent unintentional and spontaneous polymerization by external light sources.

To further increase the versatility of the developed bioprinter, it was decided to include the functionality to have more than one tank within the printer unit. Conventionally, DLP 3D printers simply use only a Z-axis motor-controlled build platform that is lowered and raised within a single substrate tank. Adding space for additional tanks to contain separate substrates would provide increased experimental and functional flexibility, adding the ability to produce structures of multiple substrates from a single print. The disadvantage to this is that it means the final printer design would be substantially larger than single tank designs.

The final preliminary decision to be made was between using a bottom-up or top-down based DLP layout. DLP printers come in two distinct conformational layouts, with reference to the direction from which the projecting unit shines onto the substrate tank. Bottom up designs feature a projector below the resin tank, shining up through a clear tank bottom. The build platforms in these designs are thus lowered to the bottom of the tank, with the platform rising as the print progresses. The major advantage to this design structure is that it can allow for a very small relative tank volume, as the height of the tank does not

limit the maximum height of the final prints produced. This design however can have issues with print attachment, as the first layers of each print compete for adherence to both the build platform and the bottom of the substrate tank. Top-down systems feature a projector suspended above a substrate tank shining down. The build platform in this set up thus begins just below the surface of the substrate liquid. Printers set up in this way have less of an issue with adherence, as the build platform is the only contact surface present during the initial print layers. However, a much larger substrate tank with greater substrate volumes is often required. This is because the maximum depth that the build plate can travel in the tank is the limiting factor with respect to print height. Ultimately, it was decided to utilise a top-down set up for the development of the bioprinter unit for the reasons mentioned. It was intended for the printer to theoretically be able to utilize a variety of substrates with varying adherence profiles, and the top-down method would allow for a more reliable set-up overall in this regard.

In summary criteria for the bioprinter unit were decided to be as follows:

- Utilize digital light projection (DLP) for substrate polymerization.
- Use light of a visible wavelength.
- Have functionality to use multiple substrate simultaneously.
- Be oriented in a top-down printing configuration.

With these criteria in mind, a 3D bioprinter system was designed and constructed as follows in Section 2.3.

2.3 Methods and Materials

2.3.1 Computer Aided Design (CAD) Software and 3D printing

To produce the 3D models that would then be printed to produce the components of the bioprinter, the software package SketchUp was used. It can be downloaded from https://www.sketchup.com/download. The version used was

17.0.18899 (Win 64-bit). Additionally, within the SketchUp program, the extension "SketchUp STL" was added to allow models to be exported in the .stl format used by the 3D printing software Cura. This extension can be found here https://extensions.sketchup.com/en/content/sketchup-stl, but can also be easily navigated to, through the in program "Extension Warehouse" functionality.

The slicing program Cura was used to convert the designed 3D models from an .stl format to a .gcode file that could then be executed by a conventional 3D printer to produce the part. The 3D printer used for this purpose was a Wanhao Duplicator i3 (3D Printing Store, South Africa). The print material used to print all designed parts for the 3D bioprinter was 1.75 mm PLA filament (Verbatim). The version of Cura used was v15.04.4 for windows 64-bit. It can be downloaded at the following address: https://ultimaker.com/en/products/ultimaker-cura-software.

Printing parameters were as follows:

Table 2.1: Printing parameters for designed structural parts during construction of the 3D bioprinting unit.

Print Parameter:	Value Set:
Extruder Temperature	200˚C
Bed Temperature	50˚C
Layer Height	100 µm
Printing Speed	50 mm/sec
Infill Percentage	100%

2.3.2 Bill of materials

A summary list of components and materials used in the construction of the 3D bioprinting unit can be seen in Table 2.2 below. The costing and sources for each item was included. Where possible, components were sourced locally in

Grahamstown, South Africa. Materials and component parts were ordered from various online outlets when not available locally.

Table 2.2: Bill of materials of components and materials used in the construction of the 3D bioprinting unit.

Item	Dimentions/Size	Source	Price per Unit	Quantity Required	Price Total
Threaded rod	450 mm x 8 mm	Albany Enginering	R54.95	1	R54.95
Stainless steel rods	450 mm x 8 mm	Albany Engineering	R60.00	4	R240.00
Aquarium tank for printer resin bath	N/A	The hoof and hound	R71.80	1	R71.80
Mounting Tape	N/A	Builders Warehouse	R32.42	1	R32.42
Nuts and bolts (20 pack)	4mm x 12mm	Builders Warehouse	R47.57	16	R761.12
Stainless steel build platform	130mm x 180 mm	R and S Plumbing	R76.00	1	R76.00
1.6 mm steel plate	540mm x 290mm	Albany Engineering	R45.50	1	R45.50
T-slot aluminium profile	20 mm x 20 mm x 1 m	Hobbytronics	R62.07	11	R682.77
Polylactic acid fliament (single spool)	20 m	www.3dprintingstore.co.za	R300.00	2	R600.00
NEMA 17 Stepper motor	N/A	www.3dprintingstore.co.za	R239.00	2	R478.00
GT2 Timing belt	1 m	www.3dprintingstore.co.za	R49.95	1	R49.95
LMUU8 linear bearings (pair)	N/A	www.3dprintingstore.co.za	R39.00	5	R195.00
Timing belt tensioner	N/A	www.3dprintingstore.co.za	R22.00	1	R22.00
GT2 belt pulley	N/A	www.diyelectronics.co.za	R29.95	2	R59.90
Optoma HD141X projector	N/A	www.amazon.com	R7 000.00	1	R7 000.00
ARDUINO CNC SHIELD V3 KIT	N/A	www.diyelectronics.co.za	R499.95	1	R499.95
608ZZ radial bearings	N/A	www.3dprintingstore.co.za	R9.95	1	R9.95
T8 brass nut	N/A	www.3dprintingstore.co.za	R39.95	1	R39.95
Flexible Coupling	N/A	www.3dprintingstore.co.za	R79.95	1	R79.95
Total					R10 999.21

2.3.3 Printer frame development and construction

The first component of the printer to be designed and constructed, the outer frame of the printer would provide a support structure to the entire unit. It was crucial that this structure be sufficiently robust and rigid, to allow for the mounting and attachment of all subsequent components. The frame structure described can be seen in Figure 2.1 below. The frame was constructed of 20mm x 20mm T-slot aluminium profiles of various lengths (Figure 1.2B). This material was chosen for being lightweight, strong and allows easy attachment via 4 mm x 12 mm bolts and associated nuts. Individual fame components were conjoined using a standard 3D printed corner bracket (Figure 2.11A). The frames overarching rectangular shape was designed to allow enough internal capacity to hold at least two 5 litre substrate tanks on the X-axis, and enough vertical height to produce a 3D construct of 100 mm tall at a minimum. Additional support beams were added to the back wall of the frame to support the Z-axis, and two more to the top of the frame on which to mount the projector (Figure 2.1C).

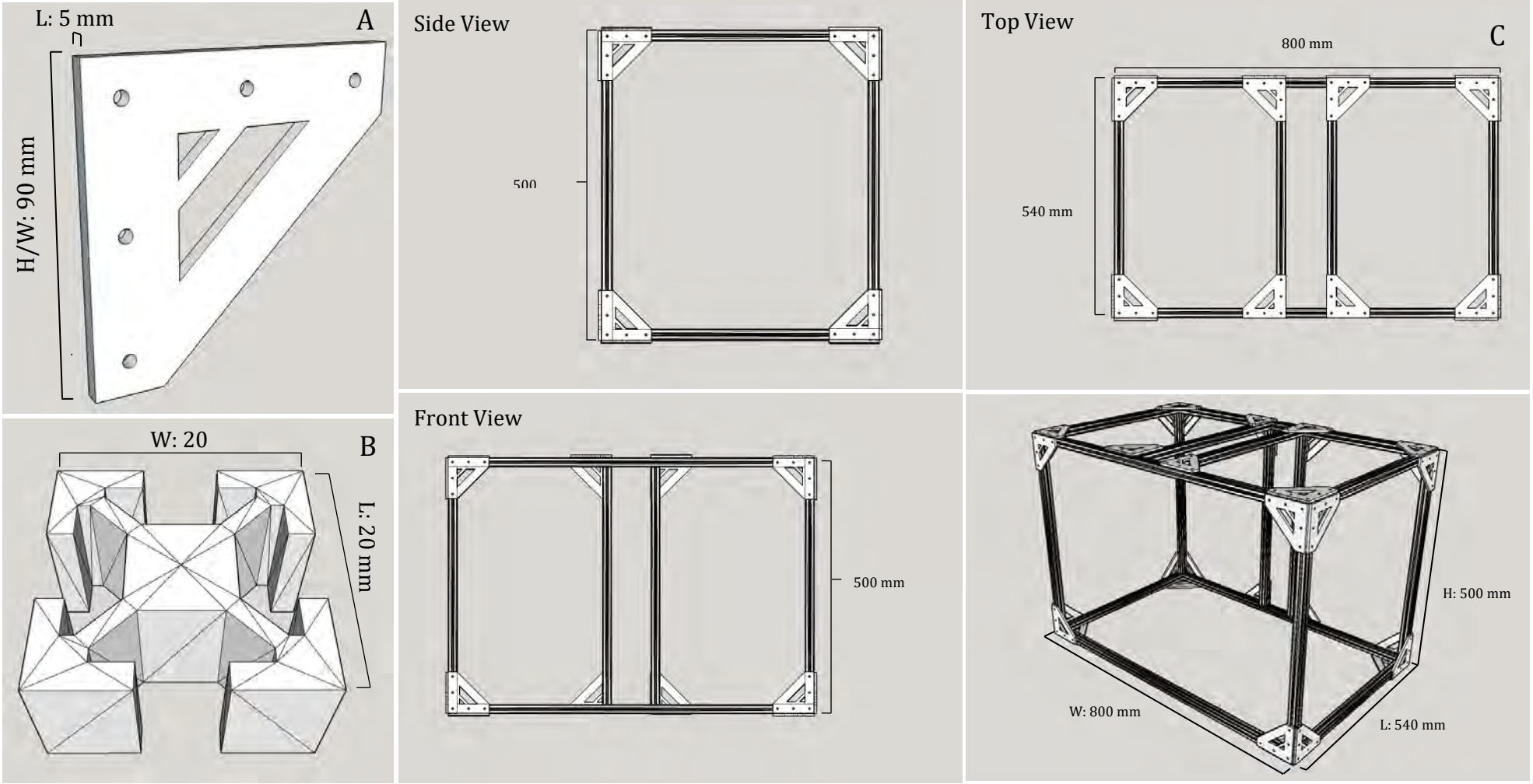

Figure 2.1: Schematic representation of prototype frame. A: The 3D printed corner connecting brackets. B: Cross-sectioned unit of the T-Slot aluminum profiles. C: The assembled frame of the 3D bioprinter composed of aluminum profiles joined by the corner connector

The aluminium frame was joined together via 5 mm thick 3D printed PLA corner connectors, designed to connect two aluminium extrusions together at a right angle (Figure 2.1A). These were fixed in place by attachment via 4 mm x 12 mm bolts and associated nuts, fitting into the T-slot shape of the profiles. These connectors (Figure 2.1B) were designed to only connect two extrusions per piece, to allow for modular assembly and disassembly of individual parts of the frame during development, to allow for more rapid prototyping and alterations. The overall frame size produced was 800 mm wide, 540 mm long and 500 mm in height, giving an approximate total calculated internal volume of 0.216 m^3.

2.3.4 Z-carriage development and construction

The Z-axis carriage provides vertical movement to the printer and holds the build platform that is lowered and raised to produce print layers. In-text part numbers described pertain to the completed Z-axis carriage assembly in Figure 2.2. The Z-axis consists of a vertical lead screw driven linear slide controlled by a central 1.8° 200 steps/rev 1.7A NEMA 17 stepper motor (11) located at the base of the printer, fixed to the two supporting frame components (1) running up the back via a 3D printed bracket (PLA with 50% print infill). Attached to the stepper motor via a coupler (10) is 450 mm long, 8 mm diameter threaded rod (9) that when turned, provides the Z-axis translation to the attached build plate connector (6) at a pitch of 2 mm. This is achieved though connection between the two parts by a T8 brass nut (5), fixed to the build plate connector. Running parallel to the threaded rod are two smooth rods (3) that also attached to the build plate connector via LMUU8 linear bearings (4) to prevent rotation and maintain stability during vertical translation. Both the two smooth rods and central threaded rod are attached at their top to a frame mounted 3D printed brace (2) to insure they remain in place and aligned. Both the base motor and top brace are firmly anchored to the printer frame via 4 mm x 12 mm bolts and nuts. Fixed to the build plate connector are three 4 mm x 200 mm threaded rods (7)

running down to attach the build plate (8) to the Z-axis, held in place by 4 mm nuts above and below each connection point. These were used to secure the build plate in place below the build plate connector with a sufficient overhang to allow the plate to dip into the substrate tank without contacting the side. Figure 2.2 illustrates the completed Z-axis assembly.

2.3.4.1 Build Platform

The build platform is the part of the printer on which printed objects are sequentially built and must be sequentially lowered into the substrate tank as the print progresses. The build plate was made of a 130mm x 180 mm piece of 1mm thick polished stainless steel. This was connected at one end by three 160 mm long, 4 mm diameter threaded rods that provided connection from the build plate up to the Z-Axis adapter. The adapter was mounted to the Z-axis by two linear bearings on either end to connect to the two vertical smooth rods, and by the central threaded rod nut that provided vertical translation during rotation of the threaded rod at a 0.8 mm pitch. This configuration allowed for the build plate to travel from freely between the base plate and the projector during Z-axis translation.

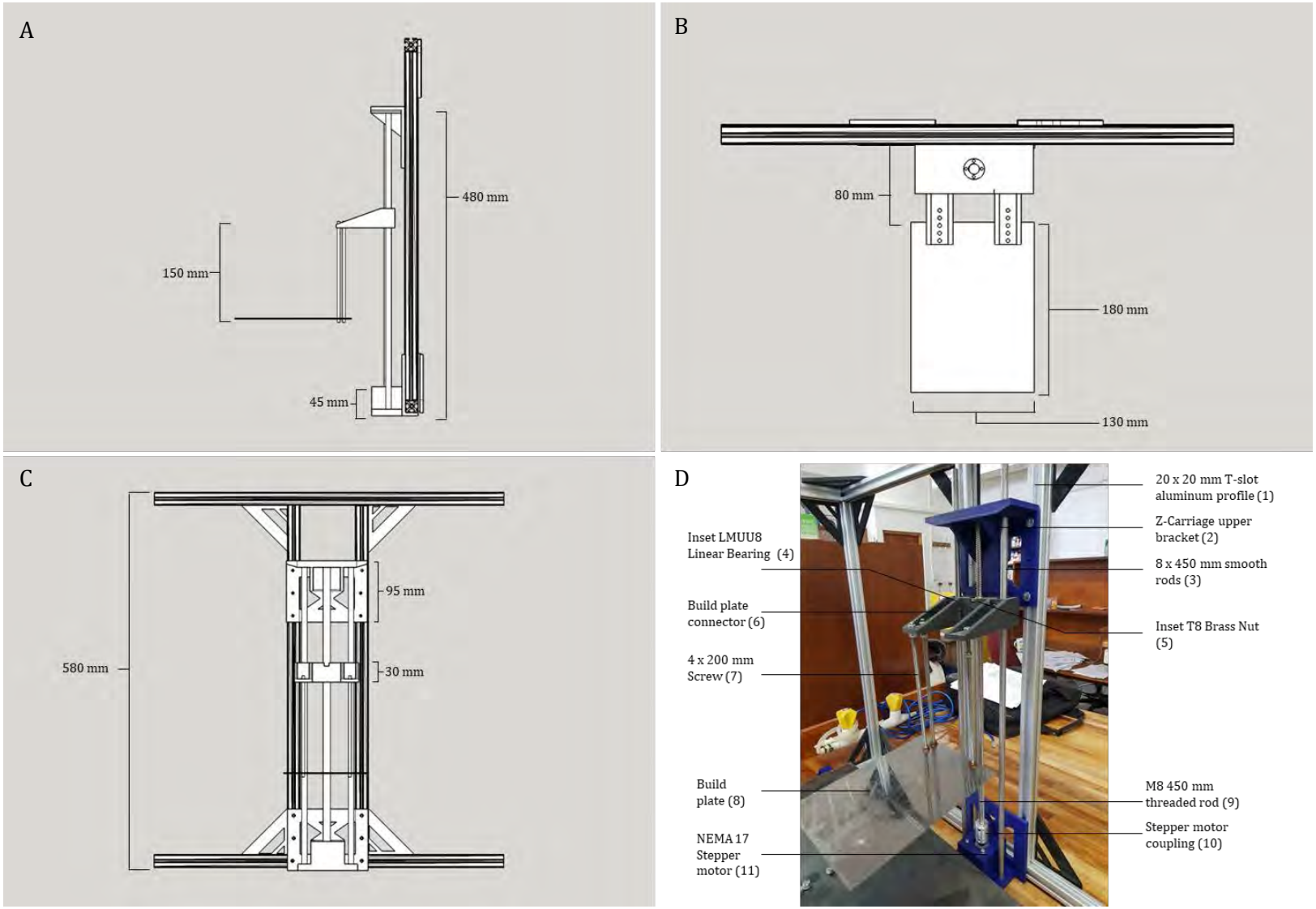

Figure 2.2: Schematic and image showing the constructed Z-axis of the completed 3D bioprinter unit and its individual components (1 -11). A: Side view perspective; B: Top view perspective; C: Front view perspective. D: Constructed Z-axis with individual components labeled.

2.3.5 X-carriage development and construction

The X-axis carriage provides horizontal translation to the printer and holds the substrate tanks. The X-axis was implemented in accordance with the criteria to include multi-substrate functionality to the printer. All in-text part numbers pertain to the parts illustrated in Figure 2.3 (1-11) of the completed X-axis assembly. The X-axis consists of a two parallel smooth rods (2) connected at either end via adapters (1) that attach to the frame suspending them 50 mm above the floor of the printer. The two smooth rods (2) are positioned approximately 240 mm apart. Between the rods runs a parallel GT2 timing belt (4) with tensioner (10), also connected at either end to the frame. To the one side, the belt is attached to the frame via a stepper motor (5) with pulley attachment (6), attached to the frame by a 3D printed mounting bracket. This motor provides movement to the X-axis via the timing belt. Opposite the motor holding the other end of the belt is simply a 3D printed bracket (4) with a GT2 pulley attachment (6) to allow free rotation when acted on by the belt. Finally, a 1.6mm thick steel baseplate (540mm x 290mm) (7) is mounted atop the two parallel steel beams via four 3D printed adapters (8) that connect the plate to the beams via two LMUU8 linear bearings per adapter (9), allowing free horizontal movement. The timing belt is attached to the underside of the plate via an adapter component (11) attached via four 4 mm x 12 mm bolts and associated nuts. This set up allows for the free movement of the platform horizontally along the bottom of the printer, allowing enough freedom of movement for any part of the plate to reach the central region of the printer (under which the projector is mounted). All parts attached to the frame are attached by 4 mm x 12 mm bolts and connecting nuts. Figure 2.3 illustrates the completed X-axis assembly, and Figure 2.4 illustrates the CAD model of the same.

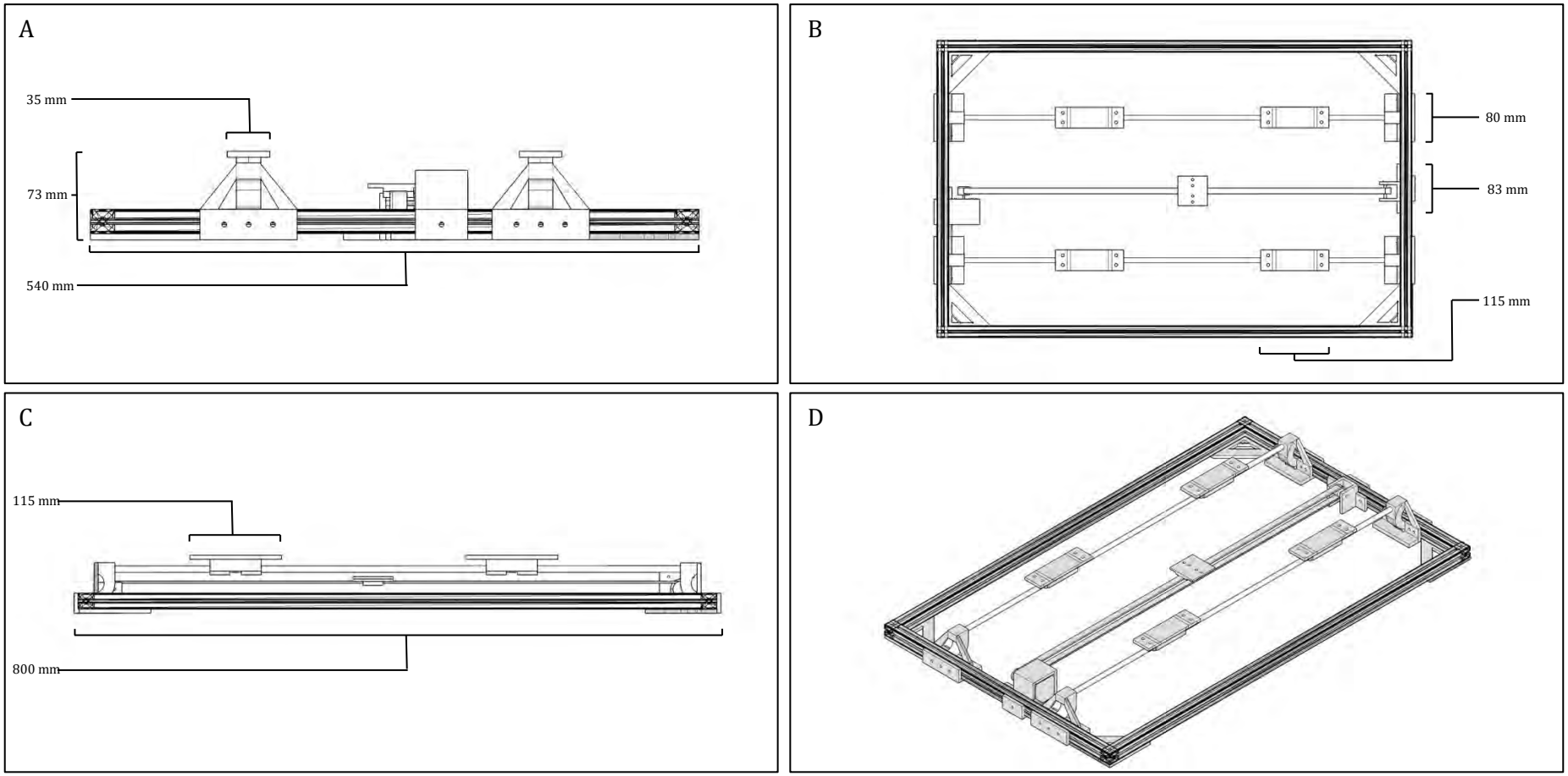

Figure 2.3: CAD model of the complete X-Axis assembly of the completed 3D bioprinting unit. A: Side view; B: Top view; C: Front view; D: Front perspective view.

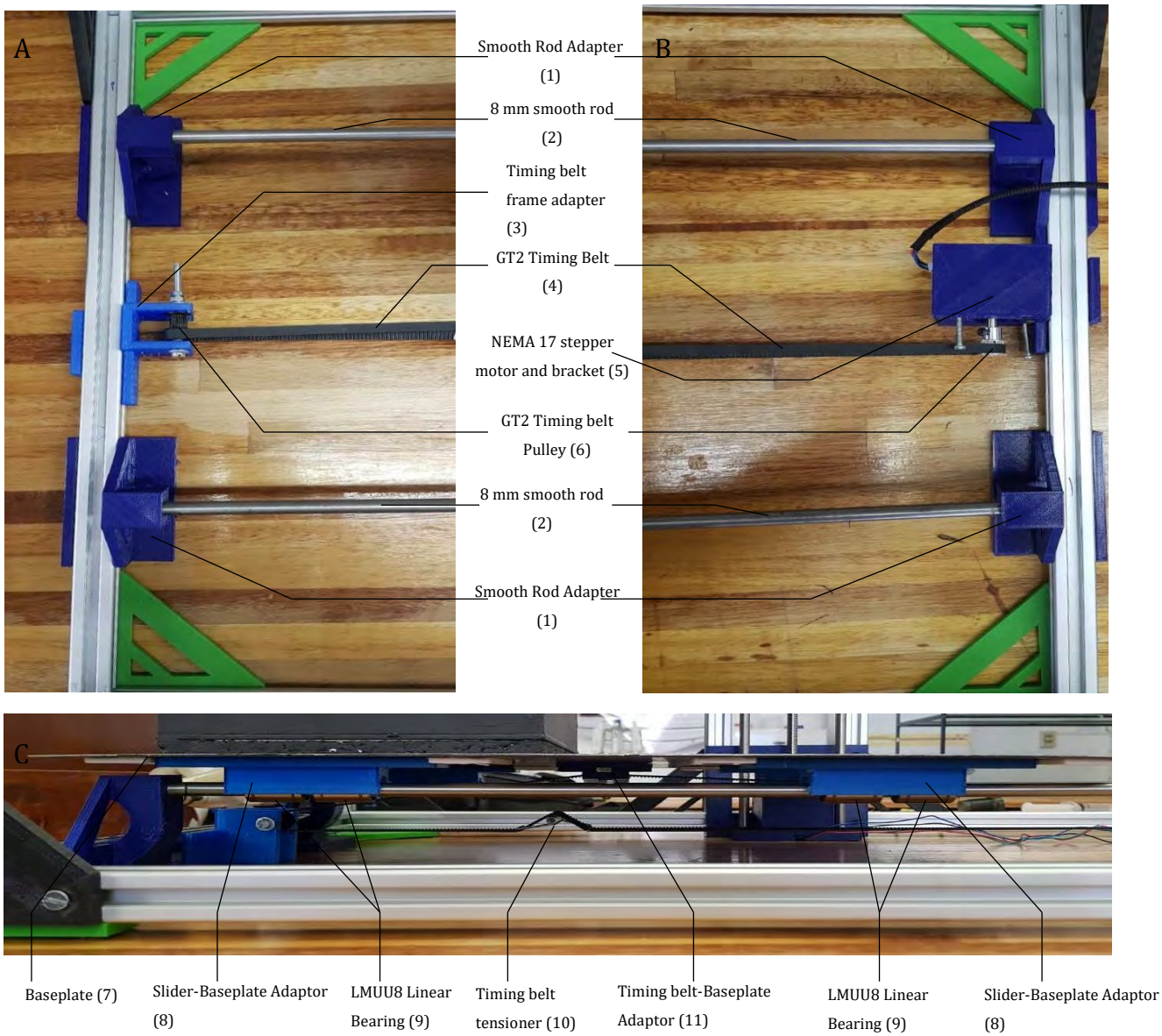

Figure 2.4: Images of the complete X-Axis assembly of the completed 3D bioprinting unit with individual components numbered (1-11). A: Top view of the left side frame-mounted sub-assembly; B: Top view of the right side frame-mounted sub-assembly; C: Side view of the frame mounted sub assembly.

3.3.6 Projector Mounting and support

The projector unit provides the controlled light exposure required to polymerize the liquid substrate within the printer. Two 50 mm long, 20mm x 20mm T-slot aluminium profiles (5) were mounted to the two support beams running along the top of the printer frame. These were mounted perpendicular to the support frame components via an upper connecting bracket (1). To these two vertical extrusions, the Optoma HD projector (Model HD141X) was attached facing downwards, connected by a 3D printed mounting adapter (3) to the two vertical extrusions (5). Each of the mounting brackets used to attach the projector were made to be fully adjustable to easily modify projector location along the Y and Z-axis, to allow fine-tuning of the printer, before being fastened into place. Once mounted in the correct position (based on distance from the resin surface), the power supply (2) and HDMI digital input (4) were connected to the projector. The projector and mounting assembly can be seen in Figure 2.5.

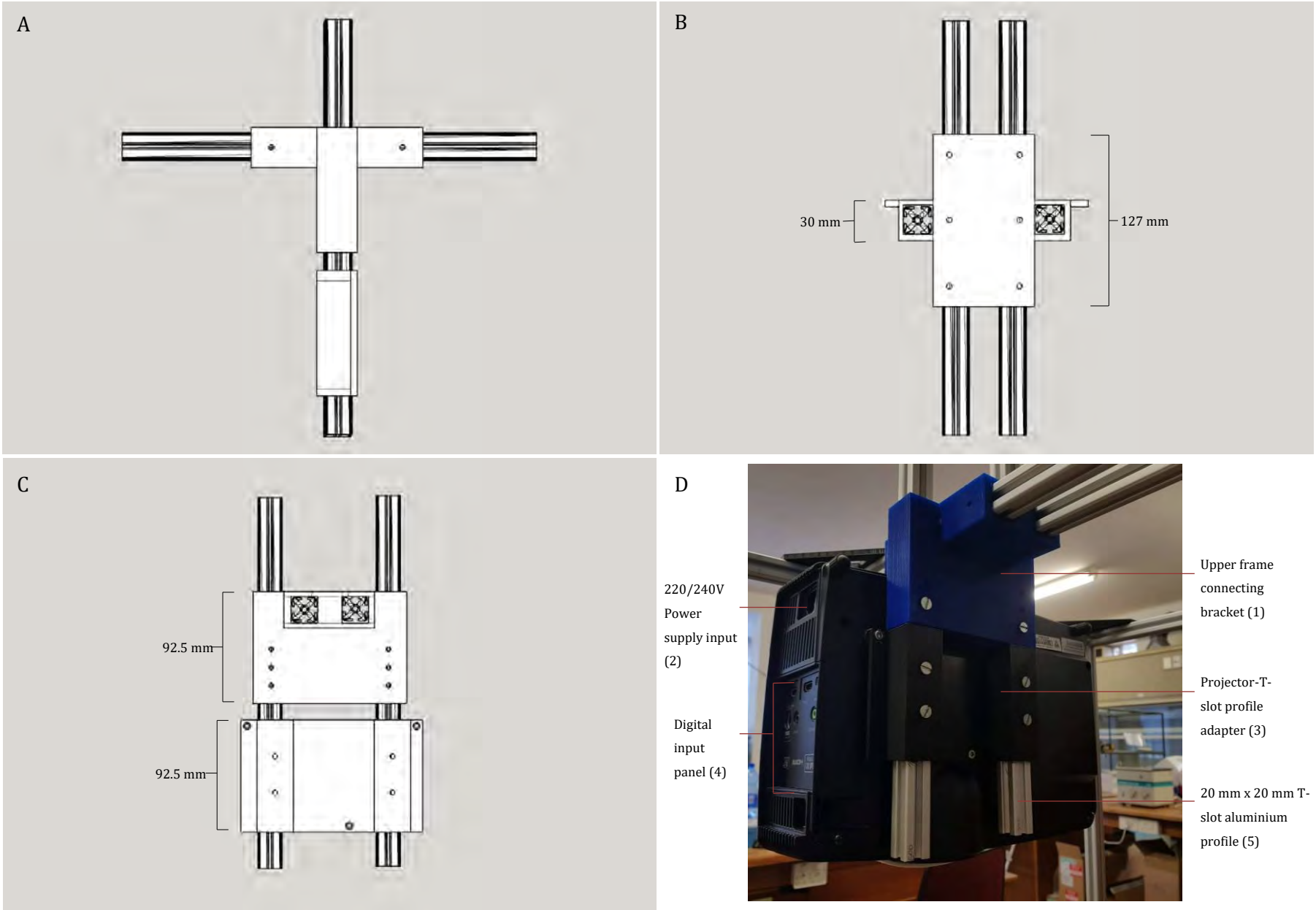

Figure 2.5: Image of the mounted projector unit its final position in the 3D bioprinter unit with individual components annotated (1-5). A: Side view; B: Top View; C: Front View; D: Completed projector mounting system, with individual components annotated

2.3.7 Electronics and Control Hardware

The two motors (Z-and X-axis) and projector unit were configured to be controlled simultaneously by a standard personal computer with Windows 10 operating system. The projector itself was connected to the PC via HDMI-HDMI cable, and powered by a standard 220/240V electrical outlet cable. To allow control of the motors directly via the PC, it was connected to an Arduino UNO R3 control board with CNC-shield, depicted in Figure 2.6 and Figure 2.7. The Arduino CNC shield was pinned with three A4988 motor control drivers and heat sinks, for the X, Y and Z-axis control points. The PC to Arduino connection was achieved via standard USB-A to USB-B cable. The stepper motors were connected to the CNC-shield with the Z-axis motor connected to the Z-axis output pins and the X-axis motor to the Z-axis output pins. The orientation of the pins was as shown in Figure 2.6, such that the negative ends were facing away from the power inlets. A generic 12V power supply unit, connected to the power inlet connections on the board, powered the Arduino UNO R3 control board and CNC shield (V3.0). Board specifications for the Arduino UNO and CNC shield can be found here (https://store.arduino.cc/arduino-uno-rev3) and here (https://blog.protoneer.co.nz/arduino-cnc-shield/) respectively. Figure 2.8 at the end of this section illustrates the electronics setup as a schematic, to illustrate the connections more clearly between the various individual components.

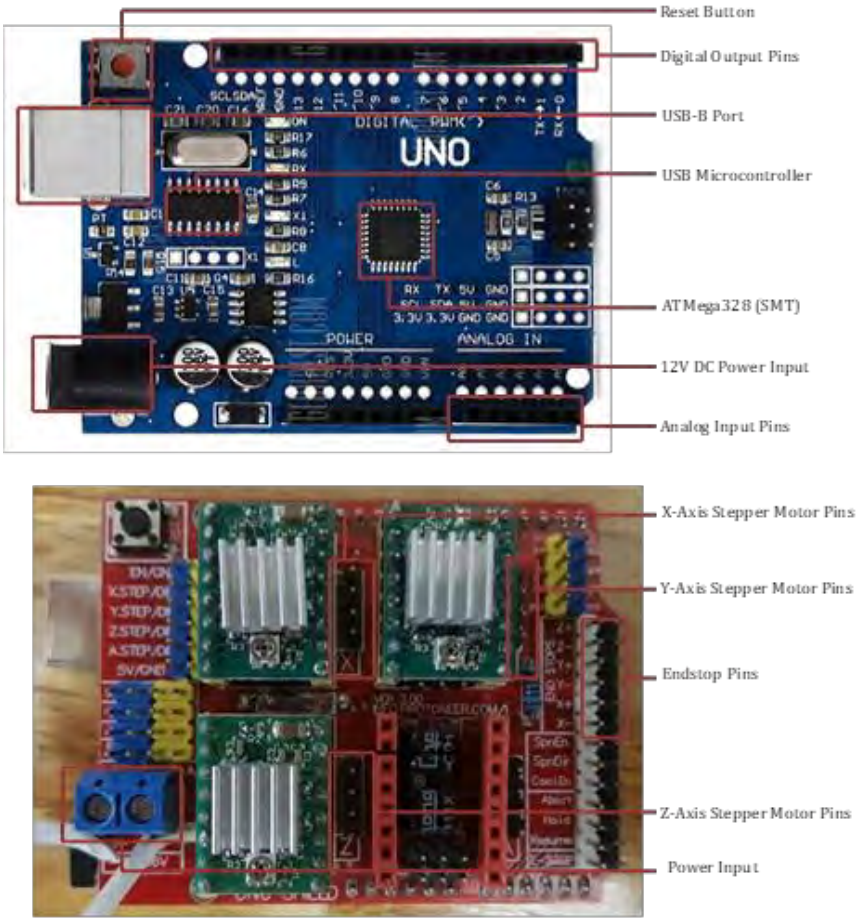

Figure 2.6: Labelled schematic of the Arduino UNO R3 control board and CNC shield with individual components annotated.

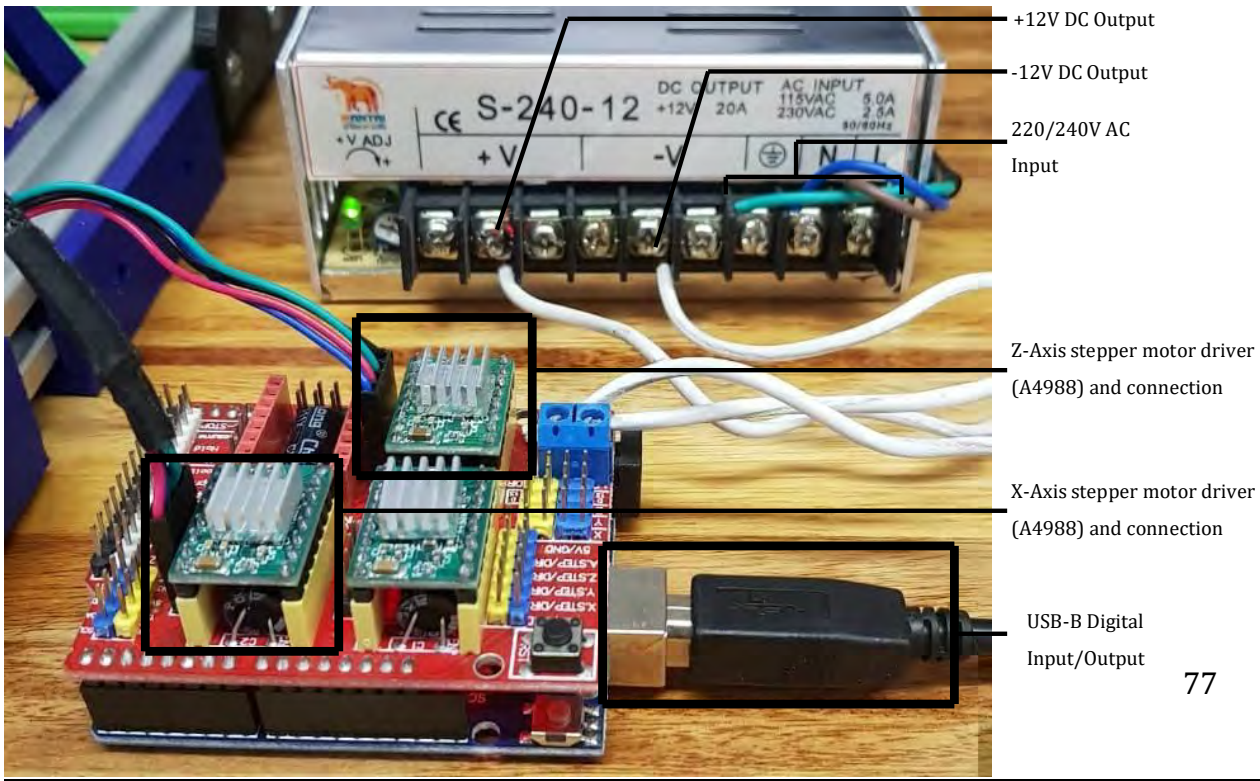

Figure 2.7: Annotated schematic of the Arduino UNO R3 control board with connected CNC-shield in the working configuration in the bioprinting unit. Individual relevant components and connections are annotated.

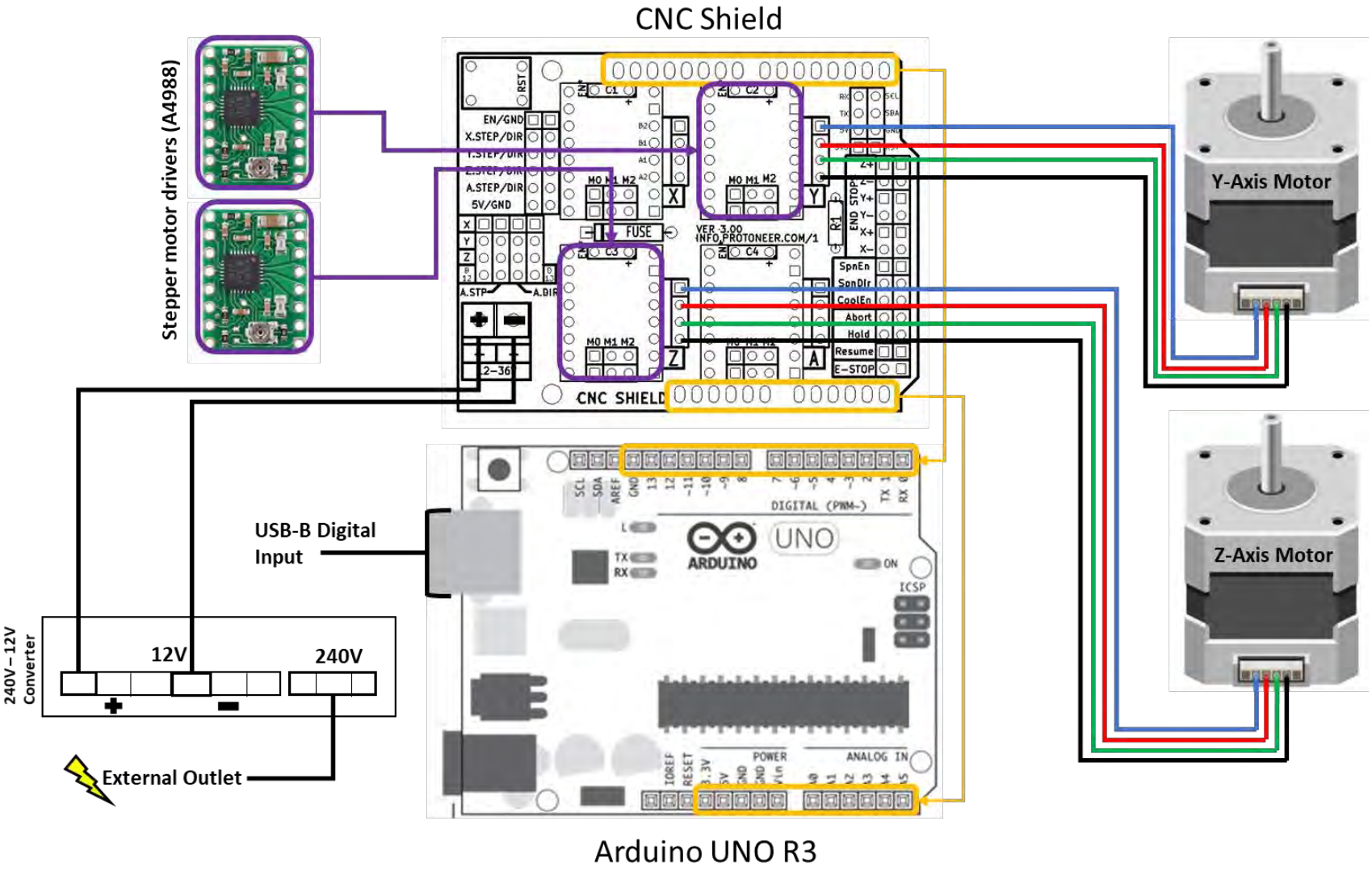

Figure 2.8: Schematic illustration of the Arduino-CNC setup for the completed prototype 3D bioprinting system

2.3.8 Firmware and Software

The Arduino UNO R3 control board was connected to the controlling PC via USB-B to USB-A as described previously. The Arduino Integrated Development Environment (IDE) (v1.8.5) was loaded and the scan for device option selected. Arduino IDE downloadable from "https://www.arduino.cc/en/Main/Software?". The connected Arduino UNO R3 board was detected by the software and selected, ensuring the baud rate was set to 115200. GRBL v0.9 firmware was downloaded from "https://github.com/grbl/grbl", decompressed, and saved locally to the Arduino IDE libraries folder. Within the Arduino IDE, the GRBL firmware was selected, compiled and uploaded to the Arduino UNO R3 board.

The open source software Creation Workshop (CW) was used for the general control of both motors on the printer, slicing of .stl 3D models, and execution of the print protocol. It was downloaded from "http://www.wanhaosupport.com/downloads/download/2-wanhao-duplicator-d7/1-creation-workshop-pre-configured-1-0-0-75". Within the CW software environment, a baud rate of 115200 and the appropriate COM port were selected, before connecting to the Arduino UNO R3. Once connected, the Z-axis was calibrated by entering the line "$102=4000" into the command prompt of the CW software and pressing enter. This command modifies the Z-axis motor output steps_per_mm function to correctly suit the connected hardware. The corrected value was calculated according to the formula:

Equation 2.1: Calculation to determine the correct ratio of motor steps to translation distance, used to modify the GRBL firmware to match the connected hardware.

$$steps\ per\ mm = \frac{motor\ steps\ per\ revolution\ \times\ driver\ microstep}{Thread\ pitch}$$

$$steps\ per\ mm = \frac{200\ \times\ 16}{0.8}$$

$$steps\ per\ mm = 4000$$

This change permanently modifies the GRBL firmware on the local EEPROM (electronically erasable programmable read-only memory) on the Arduino UNO control board, and thus only needs to be altered once. The EEPROM allows contains the system firmware, which is statically maintained on the board between uses, and remains unchanged unless overwritten, as done here. The following settings were then entered into the CW software under a custom printing profile:

Table 2.3: Settings used for Creation Workshop software for printing using the developed 3D bioprinting unit.

Parameter	Value
Z-Axis Lift Distance	0.6 mm
Z-Axis Lift Speed	200 mm/min
Z-Axis Retract Speed	200 mm/min
Slide/Tilt Value	0
Build Direction	Top Down
Lift and Sequence Time	7000 ms
Anti-Aliasing	1.5

This profile was found to consistently produce prints of approximately 100 µm layer height, later discussed in Chapter 4.3.6.

To produce the 3D models that would then be exported to Creation Workshop for printing, the 3D modelling software SketchUp was used. It can be downloaded from https://www.sketchup.com/download (v17.0.18899 (Win 64-bit)). Additionally, within the SketchUp program, the extension "SketchUp STL" was added to allow models to be exported in the .stl format required by Creation workshop. This extension can be found here https://extensions.sketchup.com/en/content/sketchup-stl , but can also be easily navigated to, through the in program "add extension" functionality.

2.4 Troubleshooting and Discussion

Once assembled, the 3D bioprinting unit began working as expected, with only minor technical challenges being presented. This section will outline essential troubleshooting carried out during the construction and testing of the functional prototype presented here. The proof of concept bioprinting unit is shown in Figure 2.9 below.

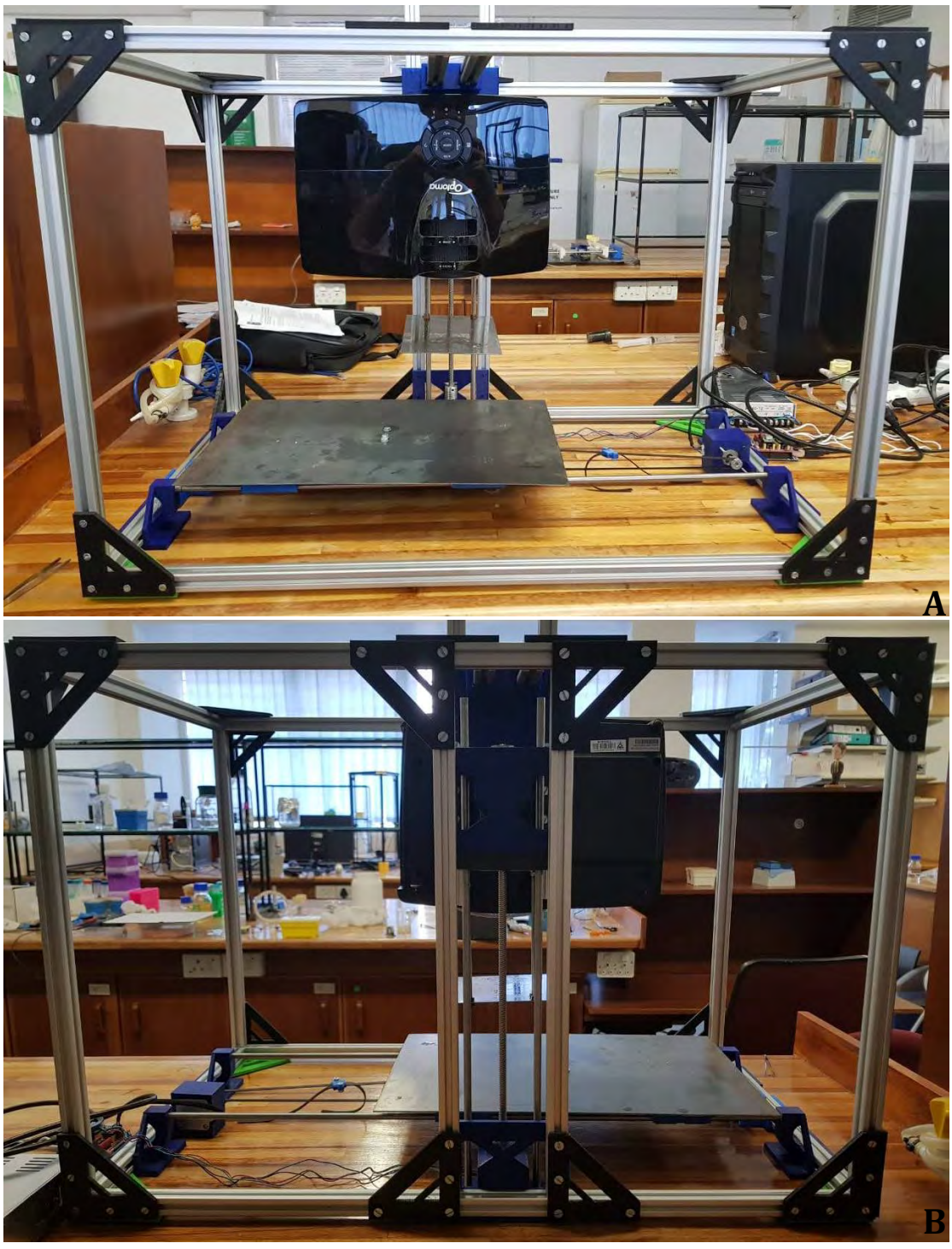

Figure 2.9: Completed visible light-based 3D bioprinting unit. A: Front perspective. B: Rear perspective.

2.4.1 Structural Integrity

The completed frame design performed well, being able to hold all the interior components in place, including the suspended Optoma HD projector. During motor operation, the frame proved to be riged enough for only inconsequential vibrational movement to be observed. The frame was also reasonably light thanks to the use of aluminium in its construction, allowing for moving of the unit to be relatively easy. The corner brackets, as explained in the Materials & Method section (2.3.3) of this report, were designed with modification in mind rather than structural integrity. The design acted as intended, allowing individual parts and indeed entire profiles to be slid in and out of the frame with relative ease without requiring disassembly on a larger scale. This design feature should be improved upon in future iterations through the production of a single corner part that would replace the three individual modular ones, providing better structural integrity. A potential design for this more robust part can be seen below in Figure 2.10 (B), in comparison to the existing part Figure 2.10 (A).

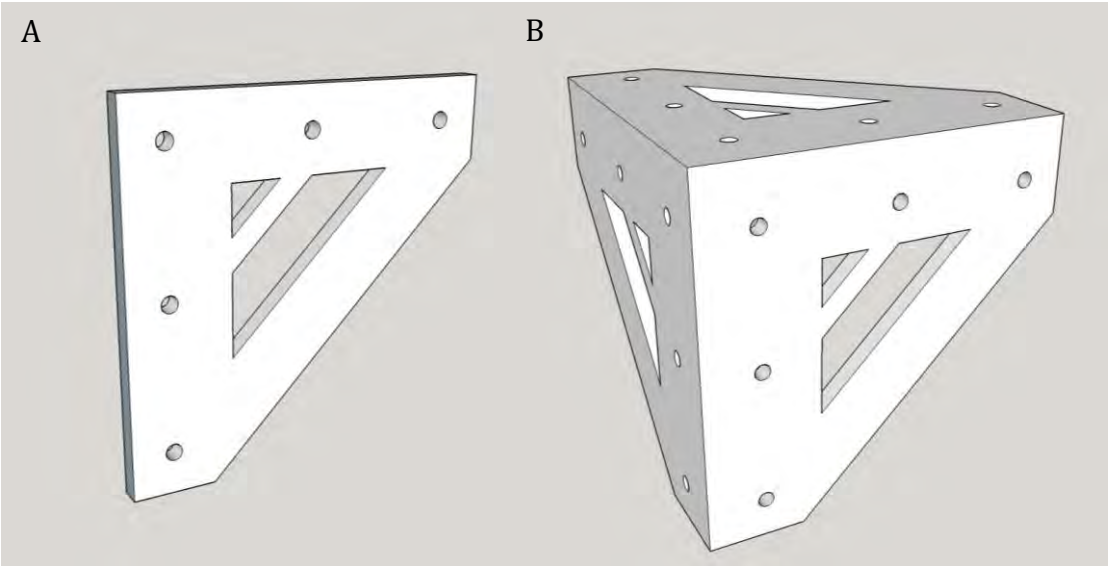

Figure 2.10: Computer modelled design for: A. Implemented corner part (used in triplicate per corner); B. Proposed corner part; for implementation on the frame of the developed bioprinting unit.

The proposed corner part would in essence consist of a fused version of the original part, but should provide improved overall rigidity. The lack of easy modifiability should not be an issue in future iterations, as the exact design used will be much more clearly defined prior to building with lessons learned though this research. However, the improved part would need to be printed on a well-calibrated 3D printer, to ensure perfect right angles between each axis of the part.

2.4.2 X-axis

The X-axis controlled base plate was implemented to allow the printer to accommodate two separate substrate tanks, and allow autonomous switching between them as required. Once assembled and connected, the base plate was able to smoothly move in accordance with commands sent via the Creation Workshop software. The plate itself consisted of a 600 mm by 400 mm, 2 mm thick steel plate riding on a linear rail system connected on the underside at each corner. To test this axis effectiveness, it was put under full load of 10 kg of water (5kg centred on each side along the length of the plate) and operation was tested (Data not shown). Despite the load, the motor was comfortably able to slide the bed along the axis without issue. The same result was found when the bed was unevenly loaded (5 kg on a single side), with the motor effectively moving the weight to the desired position as defined by the input command. Once the bed was loaded with a filled substrate tank (~5 kg), the issue of 'sloshing' became apparent. When under the dynamic load, the shifting weight would move the bed around at the destination location of a move command. To combat this, two strategies seemed to be effective. Greatly reducing the speed of the move commands would successfully prevent this issue, but seemed to strain the motor and would add to print time when this feature was utilized. An alternate solution was to break the translation up into shorter bursts that prevented the build-up of excess momentum in a single direction. This is ultimately an issue faced by

bottom-up based SLA designs. Utilising a top-down style printer, the volume of the substrate required is far lower, and thus would be much easier for the motor to move.

To overcome this issue without compromise, future iterations should consider the implementation of a heavier duty motor (eg. NEMA 23) and larger timing belt, to resist the movements of a dynamic bed load. Alternately, the belt driven system could be replaced with a threaded rod-based system that would be more robust, but likely slower. Replacing the build plate itself with a lighter material, reducing the overall weight of the system itself, can further enhance this. The dual substrate print functionality was unfortunately never utilized in this research, and improvements that can be made in this area will undoubtedly become clear as work continues.

2.4.3 Z-Axis

The Z-axis controlled movement of the build plate itself during printing, as defined by the print protocol sent to the motor by the control software. Once installed, the motor turn smoothly, responding to Z-axis commands sent through the Creation Workshop control software. However, once utilized within a print protocol, the distance mismatch earlier discussed in the software section became apparent and was solved.

An additional issue identified however was the build plate itself. Initial designs used a steel plate made from 1.5 mm thick steel, the same as was used for the base plate of the X-axis. This however proved to be too heavy for the mounting configuration to maintain level and rusting of the platform was a concern, so this was exchanged for a 1 mm thick stainless-steel plate to overcome these issues.

Once these issues had been resolved, the Z-axis became fully functional. The motor was capable of reasonably high-speed translations along the Z-axis in defined steps. When moved through the substrate solution during printing, the build plate showed no signs of deflection or slowing. Despite this, future iterations of this design should consider the implementation of a semi-perforated build plate. This may avoid potential deflection of the build platform in more viscous substrates, and may decrease substrate movement in the tank when changing layers. To further decrease the weight of the overhanging build plate to reduce change in the plate angle over time, a lighter material such as aluminium or robust plastic should be considered for future iterations.

2.4.4 Projection Unit

The projector unit consists of an Optoma (Model HD141X) Full HD projector mounted to top of the printer facing down towards the substrate tank and projects onto the build platform. The bracket holding the projector was designed so the projector would be suspended such that the projected image covered the build platform. This ultimately yielded a range of approximately 15 cm from the substrate surface with the tank filled with 5 litres of material. Positioning in this manner was done to ensure that a maximum amount of the build area could be utilized for printing without adjustment. It is also important to note with a 3D printer in this configuration is that the projector distance must be calibrated to a specific level in relation to the substrate surface, and that level must then be maintained, or the projector recalibrated between prints. This is due to the projected image widening in all directions as the print starting position begins gaining distance away from the projection point. If this is unmaintained, each subsequent print will start further from the projection point as material is expended, and the degree to which the size of each subsequent print increases in relation to its expected size is magnified. This would be made worse by radiant heat from the projector causing evaporation from the substrate, but this was not

as issue in this research due to the open plan of the printer. In addition, the change in volume due to material removal from printing was not a significant issue, as the printed scaffolds only removed a tiny volume of material after each print in relation to the overall tank volume. These effects were nonetheless monitored to allow for consistent print characteristics between prints, but smaller systems will undoubtedly be more sensitive to this issue than the system produced here. This was achieved by ensuring before each print that the projection area remained at the full size of the build plate, and adjusting either the substrate volume, or projector height to ensure that it did. To correct for the issue entirely, a corrective lens could be developed to counteract this effect. In essence a corrective lens would convert the outgoing projected image into one that is linear, and does not expand with distance. Alternately, a short throw lens could be implemented, to better suit the image throw distance in this application, minimising the impact of distance change to image size substantially.

2.4.5 Software Integration

Testing began through integration of the control software with the hardware components, via the CNC-shield and UNO control board. It was initially found that the Creation Workshop printing software was not compatible with recent versions (1.0 and up) of the GRBL firmware flashed on the Arduino UNO R3 control board This was resolved by downgrading to archived v0.9 GRBL firmware (https://github.com/grbl/grbl). This fix was not ideal, as it could prevent testing with alternate software that may require a more updated version of GRBL without re-flashing of the firmware; it was concluded to not be an issue within the context of this research. It was interesting to note that the popular open source control software Universal G-code sender (available at https://github.com/winder/Universal-G-Code-Sender) also had difficulty in connecting with more recent versions of grbl, but had no issue once downgraded

to grbl v0.9. While not ultimately used in this project, Universal G-code Sender remains popular in similar DIY applications.

Once connected, the Creation Workshop was seamlessly able to control the motors and projector, and could successfully slice 3D .stl models into executable g-code prints. However, a difference was immediately seen between the inputted layer height software setting and the actual layer height seen in the Z-axis movement during printing. Despite calibrating the firmware based on the hardware used (as discussed in section 2.3.8) this mismatch between software output and actual axis movement remained an issue. This may be attributed to a firmware translation issue, but the cause was ultimately not determined. A software fix was not found to work around this issue, and rather the straightforward solution of inputting the layer height as a derived value from the desired layer height was used.

Conveniently, this value could be determined by simply dividing the intended layer height by 10. An unfortunate side effect of this fix was that it forced the program to dramatically overestimate the number of slices that were needed for a given print. To compensate, imported .stl models intended for print were scaled down to 10% in ratio in only their Z-axis dimensions prior to slicing using Creation Workshop's scaling functionality. Once this step had been performed, the printer showed to output both the correct layer height, and the appropriate number of layers to produce prints that matched the initial intended design. The accuracy of this method of layer input height correction was later confirmed though microscopic analysis of cross-sections of completed scaffold prints in Chapter 4. This workaround was functional, but not at all ideal. Future iterations of this project should attempt to pinpoint the cause of this issue, and implement a permanent solution.

In summary, a table highlighting all of the major troubleshooting steps taken can be seen below in Table 2.4.

Table 2.4: List of major issues identified during the development of the 3D bioprinting unit and the troubleshooting steps implemented to correct them.

Issue Identified	Troubleshooting steps taken
Mismatch between print software and motor hardware causing altered print layer height.	Altered model scale to account for this mismatch and produce prints of the correct layer height.
Substrate reservoir weight too great for smooth translation between tanks.	Translation broken up into shorter moves, allowing proper destination coordinates to be conserved.
Steel build-plate weight too great to maintain level surface due to sagging.	Thinner and thus lighter build-plate made of stainless steel used.
Changing focal distance due to substrate volume changes.	Monitoring of volume levels and adjustment of projector height to adapt to change over time.

3 Chapter 3: Development and construction of a proof-of-concept continuous flow bioreactor unit with standalone syringe pump system

3.1 Introduction

A bioreactor is a broad term used to describe any chamber, usually enclosed, used to support a biologically active system in a controlled manner (Nagel, *et al.*, 1992). Bioreactor designs thus vary greatly, as the overall design of the reactor will depend entirely on the requirements of the system it is intended to support. This can range from massive industrial scale bioreactors used for biological product production or waste management (Briggs, *et al.,* 2007), down to nano-scale bioreactors for application in protein kinetic investigations (Vriezema, *et al.,* 2005). Aside from scale, bioreactors also vary in feeding mechanisms and attachment profiles (or lack thereof), based on what is most appropriate for the system it is designed for. The biochemical or biological kinetics of any designed system must be also carefully considered and controlled to produce the desired conditions. The physical factors influencing the kinetics of any bioreactor are the volume, shape of the reactor chamber, pressure, and flow rate in the case of continuously fed bioreactors. Other factors that influence this are temperature, media composition and the characteristics of the biological components within the reactor, among others.

The dilution rate of a continuous bioreactor system, such as the one described in this chapter, can be expressed as a relationship between the inputted media flow rate, and the total bioreactor volume. This relationship can be illustrated is the following formula:

Equation 3.1: Formula for dilution rate (D), as measured by the flow rate (F) divided by the vessel volume (V)

$$D = \frac{F}{V}$$

In this case, D represents the rate of dilution; F represents the flow rate of the reactor (volume over time), while V represents the total reactor volume. This calculation can provide information on the total input media being passed over the surface area of the bioreactors internal surface over time. This can then be accurately adjusted to achieve a specific condition, for example, to balance the dilution rate against the growth rate of cells within the reactor. It is critical to understand the kinetics of any bioreactor system, in order for all of the relevant variables to be controlled, to achieve a desired outcome (Bielser, *et al.,* 2018).

The presented work illustrates the design, development and production of a continuous flow, perfusion-based bioreactor and media supply unit capable of supporting hydrogel scaffolds produced by the 3D bioprinting unit described in Chapter 2.

3.2 Criteria for bioreactor design

In this research, the bioreactor designed was intended to support the hydrogel scaffold produced by the 3D bioprinter described earlier. In addition, this scaffold held within the bioreactor would in turn be used to support the growth of mammalian cells in accordance with the overall aims of the research. It was important for the system as a whole to be designed with this in mind, as the size of the completed unit would need to be able to fit comfortably within a standard size mammalian cell incubator.

When designing the bioreactor system, a number of key characteristics were considered. First and foremost was nutrient availability. Previous research in the field of 3D culture scaffolds has described the issue of uneven culture survival within the scaffolds due to uneven nutrient distribution through the system (Rouwkema, *et al.,* 2009)(Malda, *et al.,* 2007). A non-homogenous culture environment can lead to unintentional cell death or differentiation within some regions within the scaffold and prevents long or even medium-term cell culture from being possible. To counter this, it was decided that one of the criteria for the bioreactor design was to develop a system that uses a perfusion-based flow-through approach to nutrient delivery. A perfusion-based system works by actively forcing nutrient media through the system, ensuring that all parts of the contained scaffold were receiving a constant supply of new nutrients to maintain cell health. In addition, a perfusion-based system would allow for effective nutrient distribution when supporting both porous and non-porous scaffold materials. Figure 3.1 illustrates this concept in more detail, showing how media is passed through a biological scaffold to provide a constant supply of nutrients to the system.

Figure 3.1: Diagrammatic representation of a forced perfusion based bioreactor.

Other considerations for design criteria include the need for an autonomous control system for the reactor. In order to support long-term cell culture, the system designed would need to be able to regulate and carry out the consistent flow-through of nutrient media over time, without constant human input.

Without continuous input, the scaffold would develop a nutrient gradient as discussed, leading to loss of viability and uncontrolled changes within the bioreactor. An operator would be unable to provide this consistent long-term input manually, thus an automated system must be employed. In addition, the control system would need to be easily modifiable to easily alter the flow rate of media into the system as required. This would allow for the easy optimization of the system once fully operational, in terms of its ability to produce a sustainable and well-defined cell culture environment.

It is also critical that a continuous bioreactor be able to reach a steady state operation with whatever organism it is intended to grow. In essence this means that the flow of media leaving the reactor be in balance with the time required for the cells in suspension are able to replicate. If replication exceeds flowrate, then the reactor will become overgrown, if flow rate exceeds replication, then the culture will be washed out. This can be calculated by comparing the doubling time of the culture, to the bioreactor's specific residence time (μ). Residence time is simply the time a particle is expected to remain in the bioreactor chamber given a specific bioreactor volume and flow rate and can be calculated as follows:

First, D = dilution rate is calculated as a function of F = Flow rate divided by V = volume of the system:

Equation 3.2: Formula for dilution rate (D), as measured by the flow rate (F) divided by the vessel volume (V)

$$D = \frac{F}{V}$$

Residence time (μ) of a particle within the reactor is then then simply calculated by the equivalent relationship:

Equation 3.3: Particle residence time (μ), as an inverse proportion to the dilution rate (D).

$$\mu = \frac{1}{D}$$

In a steady state continuous bioreactor, the residence time (μ) should be equal to the culture doubling time. This calculation however, is primarily intended to

examine the balance of a bioreactor culture growing in suspension, as an adherent culture would resist the washing-out effect to some extent. Regardless, this calculation can help with diagnosing the health of a bioreactor setup and should be considered.

Finally, it was critical that the bioreactor chamber itself be easily accessed, to allow for the insertion and removal of culture scaffolds during and after experimentation. However, once closed the chamber should remain watertight, in order to prevent the leakage of cell media, and prevent external contamination.

In summary, the criteria for the design and development of the bioreactor unit are as follows:

- Utilise a continuous perfusion-based bioreactor chamber design
- Unit should be compact enough to be held within a standard, CO_2 regulated, mammalian cell culture incubator.
- Able to be autonomously controlled over extended periods.
- Be compatible with the scaffold produced by the 3D printer (as described in Chapter 2)
- Allow for easy disassembly after testing, while remaining watertight once assembled.

3.3 Materials and Methods

3.3.1 Computer Aided Design (CAD) Software and 3D Printing

The 3D printing used to produce the structural components of the syringe based pumping system were designed and printed as described in Chapter 2, section 3.1.

The production of the bioreactor parts were carried out using a Wanhao Duplicator 7 DLP 3D printer (AMS3D Pty (Ltd)), with the Wanhao black UV resin. Parts for the bioreactor were designed and converted to .stl formats using the Sketchup design software as earlier described. The slicing and printing of parts using the Wanhao Duplicator 7 was performed using the software Creation Workshop (v1.0.0.54 windows 64-bit) that can be downloaded here: http://www.wanhao3dprinter.com/Down/ShowArticle.asp?ArticleID=83. All parts were printed using a 50 µm layer height, with an exposure time of 7000 ms and a structure infill of 100%. Post print, all constructs were rinsed in isopropanol and allowed to dry in daylight for at least 30 minutes before use.

3.3.2 Bill of materials

The following table summarizes the components and materials used in the construction of the bioreactor and media pumping system. Prices and sources for each item are included.

Table 3.1: Bill of materials detailing the components and materials used in the construction of bioreactor and media pumping system

Item	Source	Price per Unit	Quantity Required	Price Total
1.6 mm steel plate (400mm x 200 mm)	Albany Enginering	R31,50	1	R31,50
20 ml lure-slip syringes	Luer and Wallace Pharmacy	R3,50	2	R7,00
Dual Shaft NEMA 17 stepper motor	www.3dprintingstore.co.za	R189,00	1	R189,00
Wanhao 3D printing resin (1l)	www.diyelectronics.co.za	R595,00	1	R595,00
Stainless steel rod (8 mm)	Albany Enginering	R60,00	2	R120,00
608ZZ radial bearings	www.3dprintingstore.co.za	R9,95	2	R19,90
T8 brass nut	www.3dprintingstore.co.za	R39,95	2	R79,90
4 mm Tygon silicone tubing (15m roll)	RS Components	R505,03	1	R505,03
5mm to 8mm Flexible Coupling	www.3dprintingstore.co.za	R79,95	2	R159,90
LMUU8 linear bearing	www.3dprintingstore.co.za	R39,00	4	R156,00
Total				R1 863,23

3.3.3 Development and production of the input-output/reciprocal syringe based pumping system.

The pumping system is the component responsible for maintaining the reservoirs of fresh and expended cell culture media, as well as facilitating the transfer between the two through the bioreactor chamber itself. The system was designed such that the two syringe reservoirs would mirror each other in terms of input and output, in order to minimize backpressure though the system. A figure illustrating the reciprocal pumping system can be seen in Figure 3.2 below.

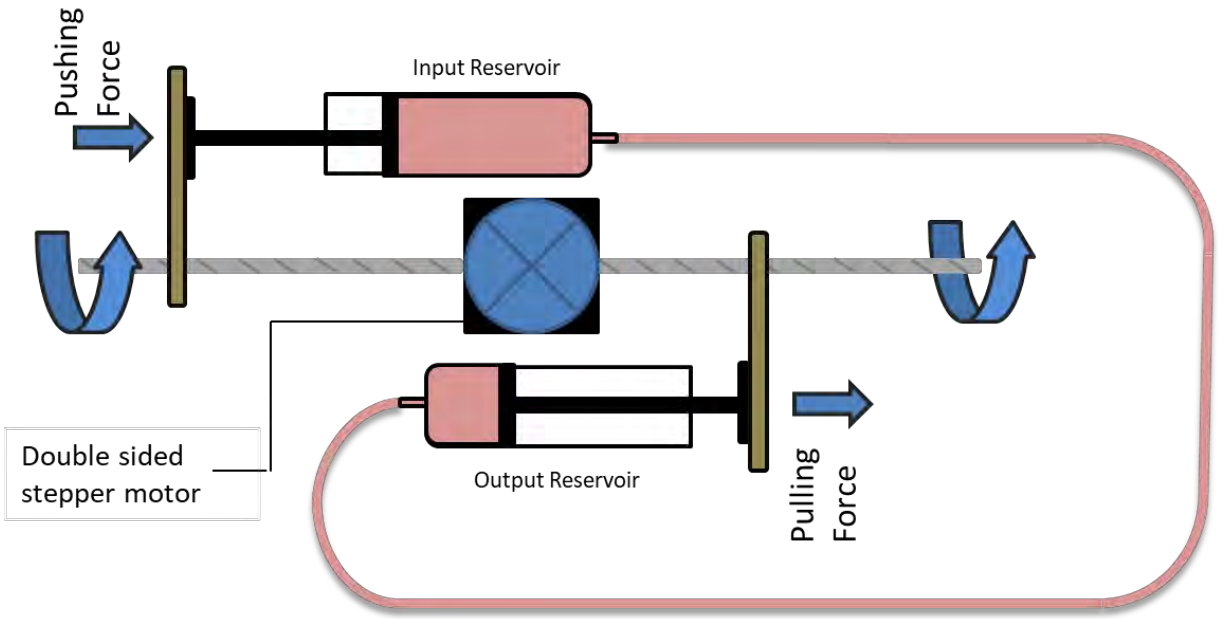

Figure 3.2: Diagrammatic representation of the single motor, dual syringe pump system.

The bioreactor pumping system is shown in Figure 3.3 and Figure 3.4, with each number in this section corresponding to a specific part for clarity. The entire unit was mounted on a 400 mm x 200 mm steel plate, giving the system rigidity. Located centrally on the plate, a dual shaft NEMA17 stepper motor (2) was mounted via a 3D printed bracket (1). The CAD design of this bracket is shown in Figure 3.3A. This motor was extended by two 8 mm diameter leadscrews (4)

running lengthways for 100 mm in either direction. It was decided to use a single dual shaft motor as opposed to two single shaft motors in an effort to reduce the size of the overall unit. On either side of the motor, two 25 ml syringes (3; 8) were mounted facing opposite directions, attached to the same bracket (1) mounting the central motor. These syringes acted as the reservoirs for input and output media and from the system during operation. Running along either side of the unit are two parallel 8 mm smooth rods (9), fixed in place by two outer brackets (10). The design of the outer brackets is shown in Figure 3.3D. These stainless steel beams allowed for the system to resist the torsion created by the motor during horizontal movement. The two end-stop brackets were also attached to the central threaded rod at either side via 8 mm freely rotating 608ZZ radial bearings (5), and were firmly attached to the base plate using M4 mm x 10 mm nuts and attached bolts. These provided firm ends to the set-up, keeping the smooth rods in place while proving stability to the rotating central leadscrew; this formed the basis of a linear rail. Finally, two 3D printed connective bars (3) are placed such that they connect the syringe extruders to the central threaded rod and both side mounted stainless steel beams. The design of the connective bars is shown in Figure 3.3B. The bar was connected to both smooth rods using LMUU8 linear bearings driven by a leadscrew and connected via a central T8 brass nut (6), allowing horizontal translation when the leadscrew rotated. The 3D printed connective bars each also passively attached to their respective syringe extruder such that during horizontal translation, the syringe plunger would either be pushed further into the syringe or pulled out, depending on direction. The two reservoirs were connected to either end of the bioreactor chamber itself via 300 mm pieces of 4 mm inner diameter Tygon silicone tubing (7). Figure 3.3 and 3.4 below illustrates the components used in the completed syringe pump system as described and their place within the completed setup; Figure 3.4 shows these components in attached to the finalised pumping system. Finally, Figure 3.5, Figure 3.6 and Figure 3.7 show the CAD models of the three 3D printed components used in the completed syringe based pumping system.

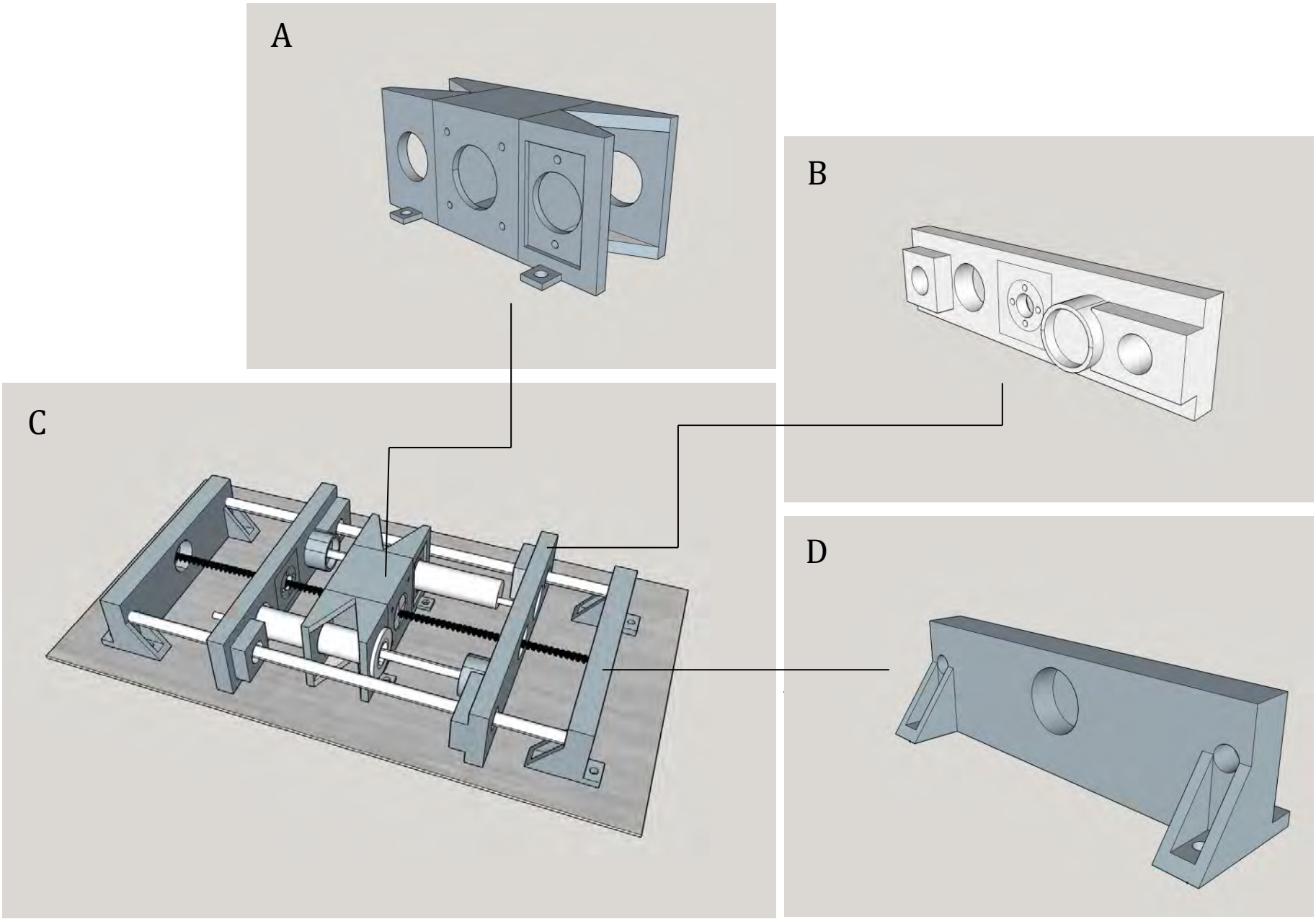

Figure 3.3: CAD model of the 3D printed components of the media pump system, and their place within the completed setup. A: Central motor and syringe mount; B: Connective bar; C: Completed media pump setup; D: Outer bracket.

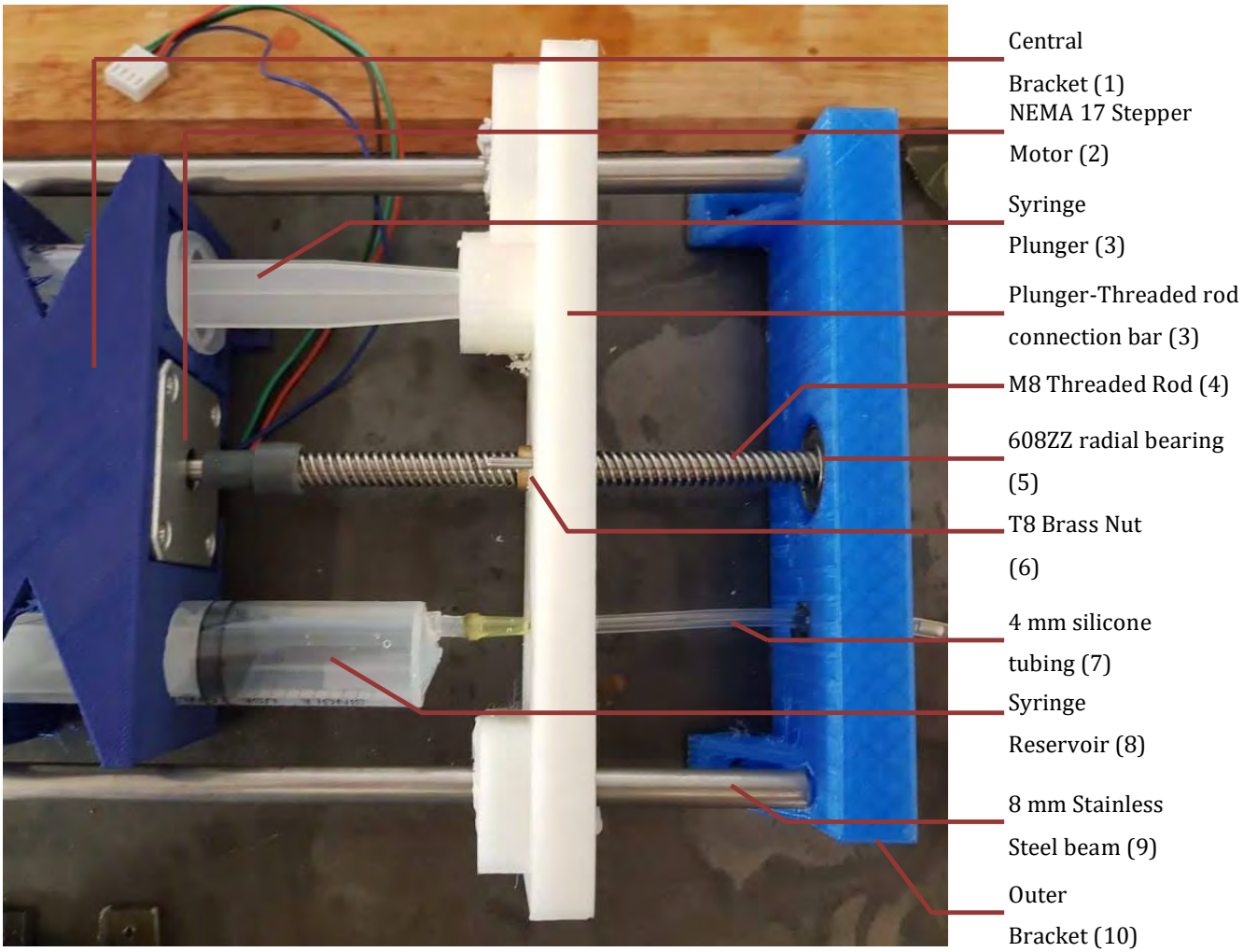

Figure 3.4: Top-down view of the right side of the symmetrical syringe-pump assembly. Individual components are annotated (1-10)

Individual printing components are further detailed in Figure 3.5, Figure 3.6 and Figure 3.7 below:

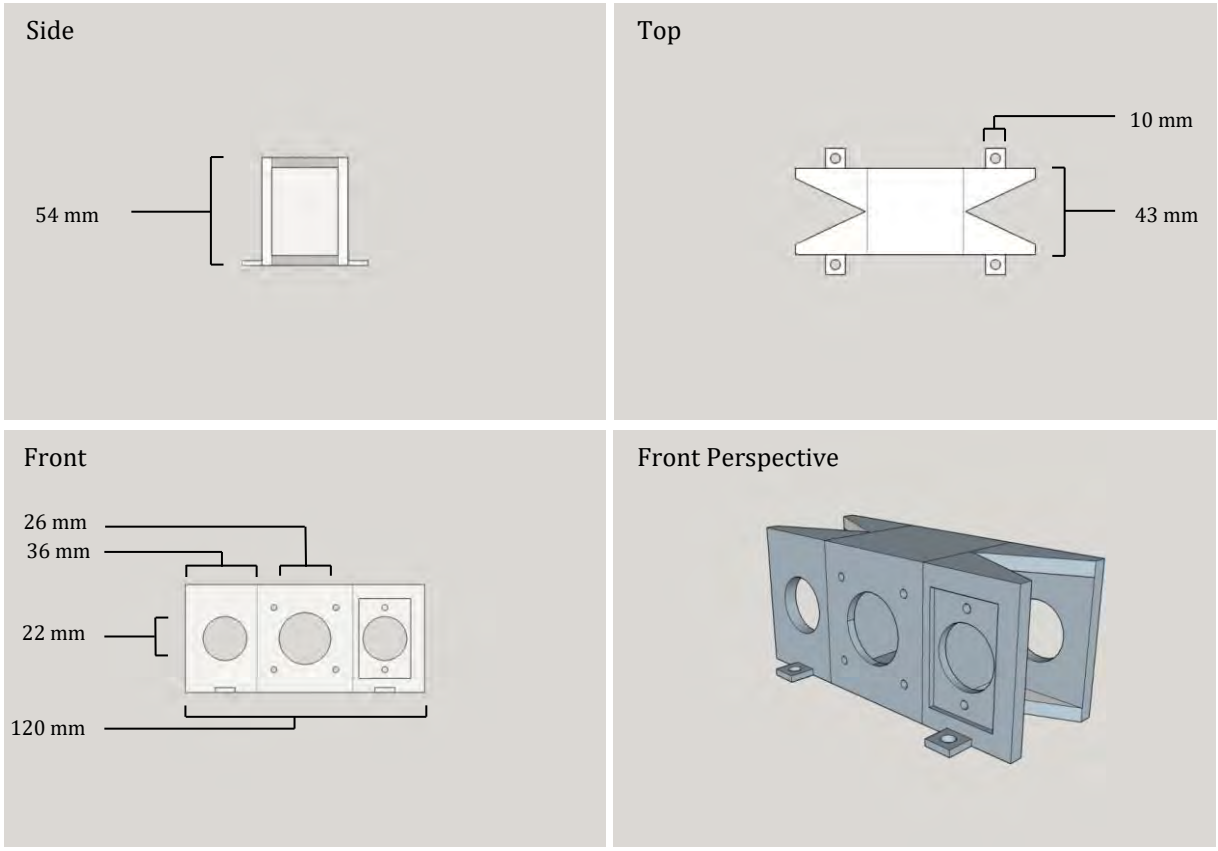

Figure 3.5: CAD model of the 3D printed central motor and syringe mount of the completed motorized media pumping system.

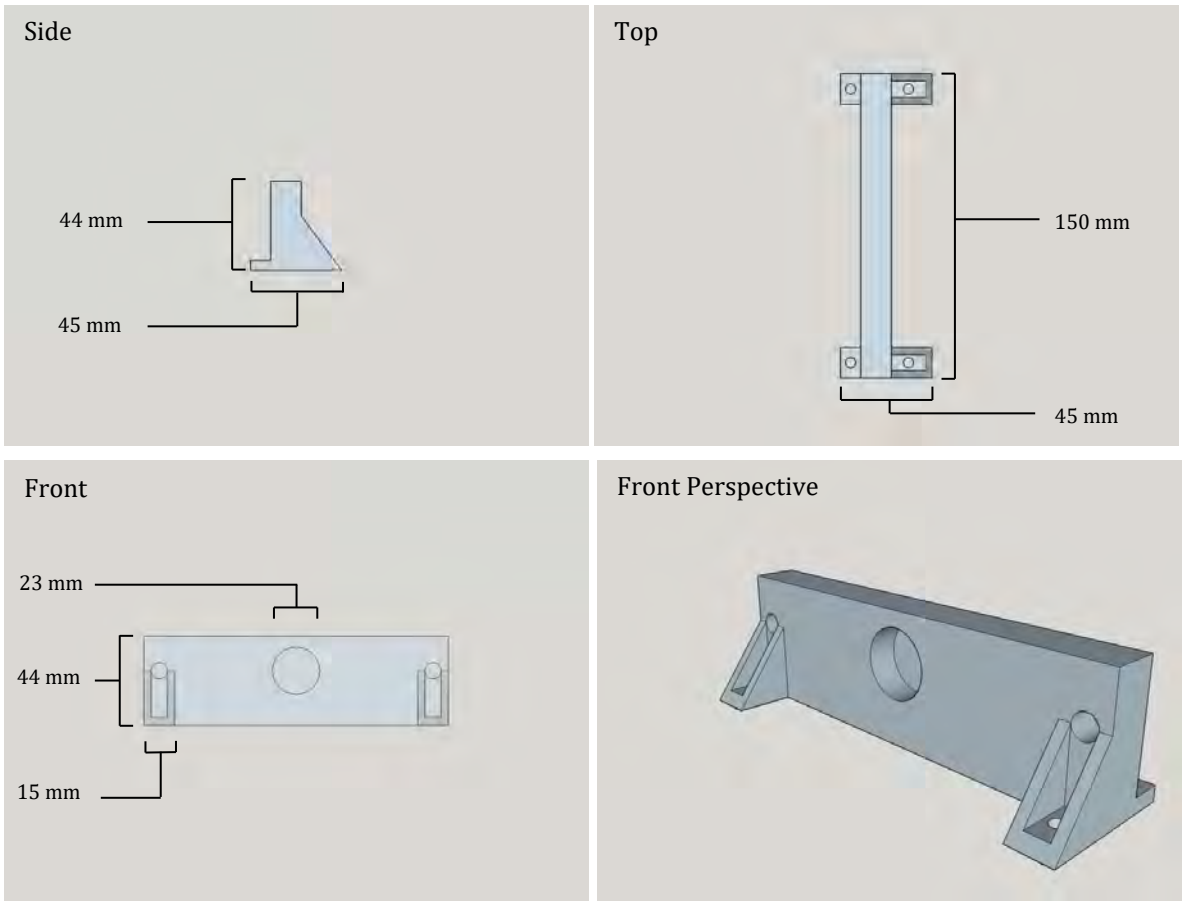

Figure 3.7: CAD model of the 3D printed outer bracket component of the completed motorized media pumping system.

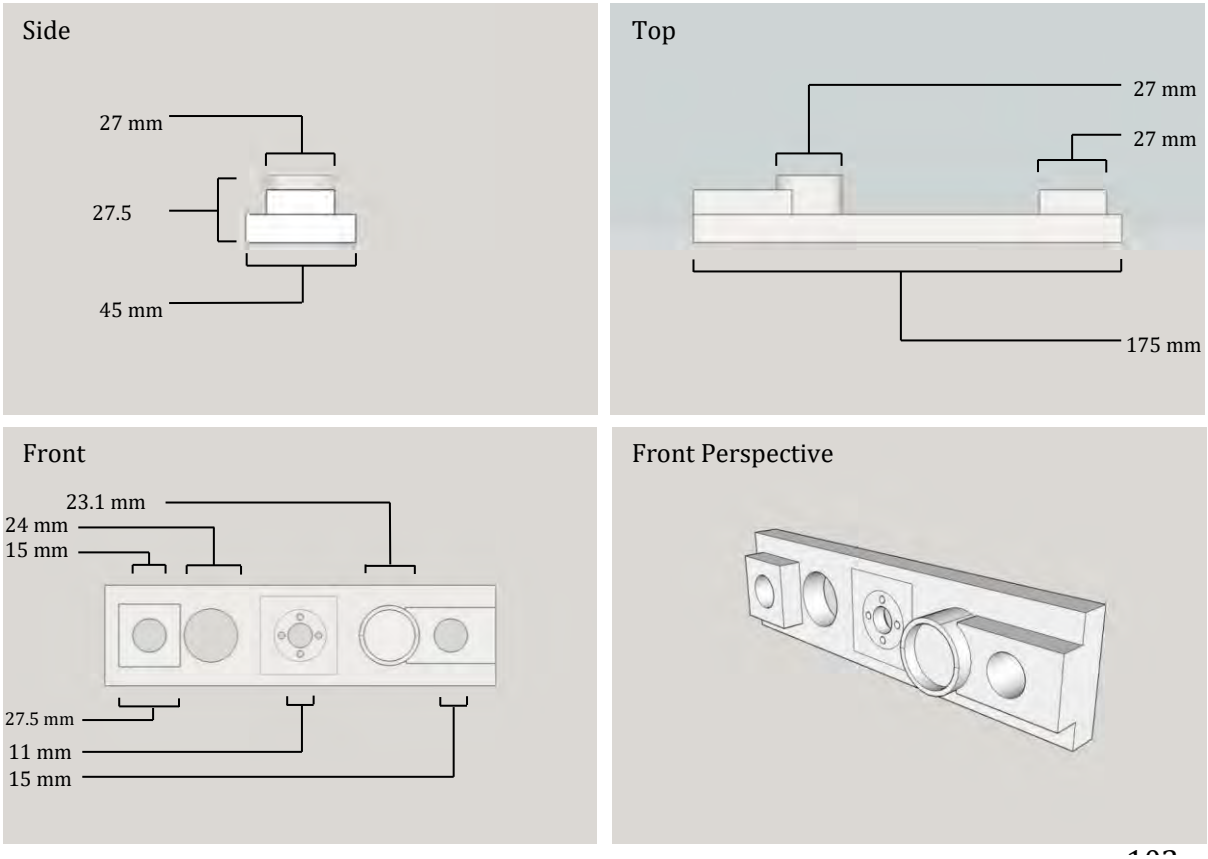

Figure 3.6: CAD model of the 3D printed connective bar component of the completed motorized media pumping system.

3.3.4 Development and production of the bioreactor chamber

The bioreactor chamber exists to contain the cell culture scaffold in an enclosed environment and allow media to be passed through over time. The chamber consists of three individual parts, each 3D printed and combined to produce the finished unit. The first part is a central, 35 mm long cylinder shape that will make up the volume area of the reactor, with internal diameter of 19 mm, making in internal volume of 9.92 cm^3. At either end is a 10 mm long bevelled section for the full diameter of the cylinder, with 4 mm wide attachment groove at the top and bottom as can be seen in Figure 3.8. This grooved and bevelled area allows for the firm and watertight attachment of the cylinder to the two connective parts at either end shown in Figure 3.9. The walls of the main cylinder area were made to be 3 mm thick, providing a sturdy frame in which to house the cell scaffold during operation.

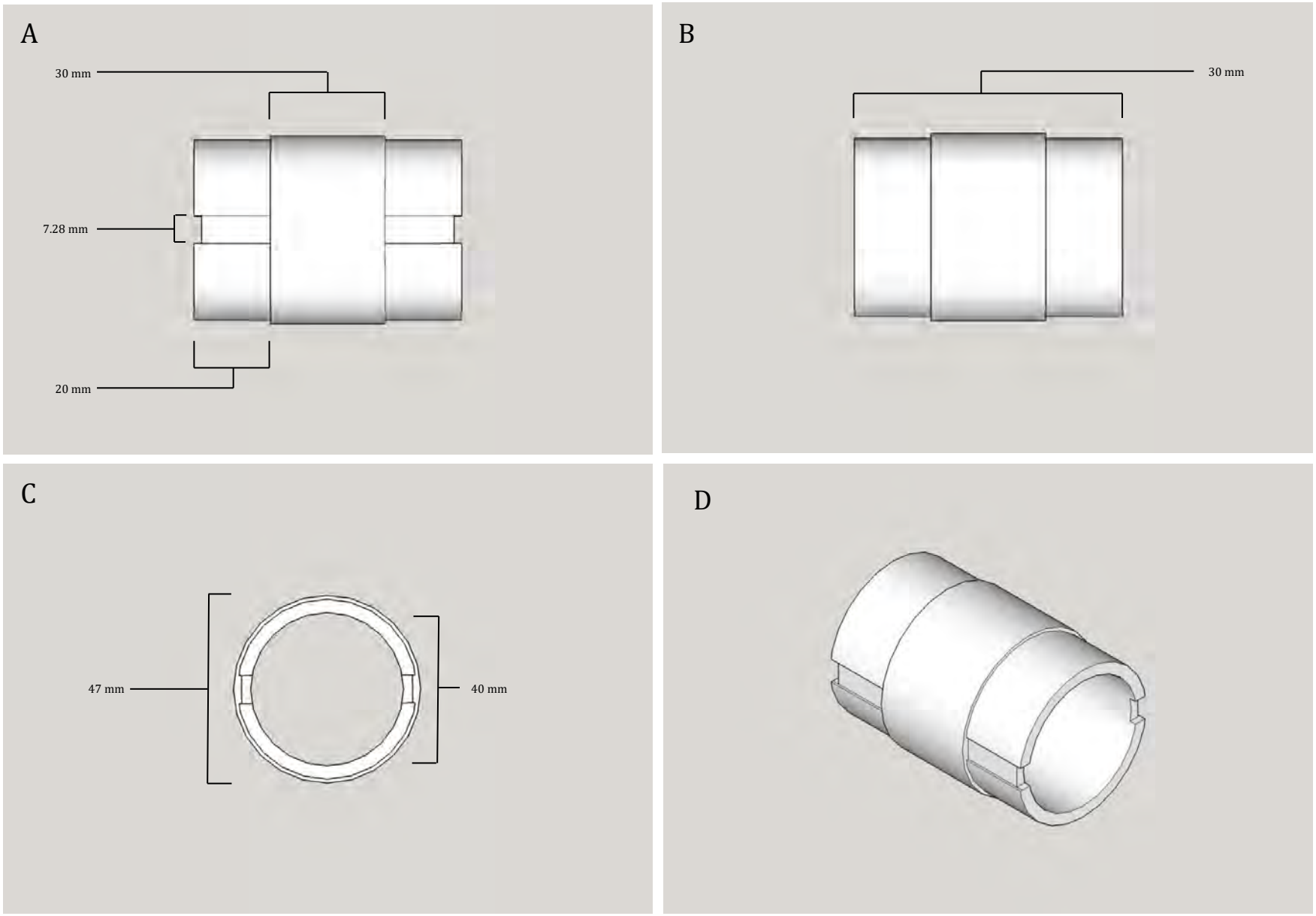

Figure 3.8: Schematic CAD layout of the central chamber of the bioreactor chamber. A: Side view; B: Top view; C: Front view; D: Front perspective.

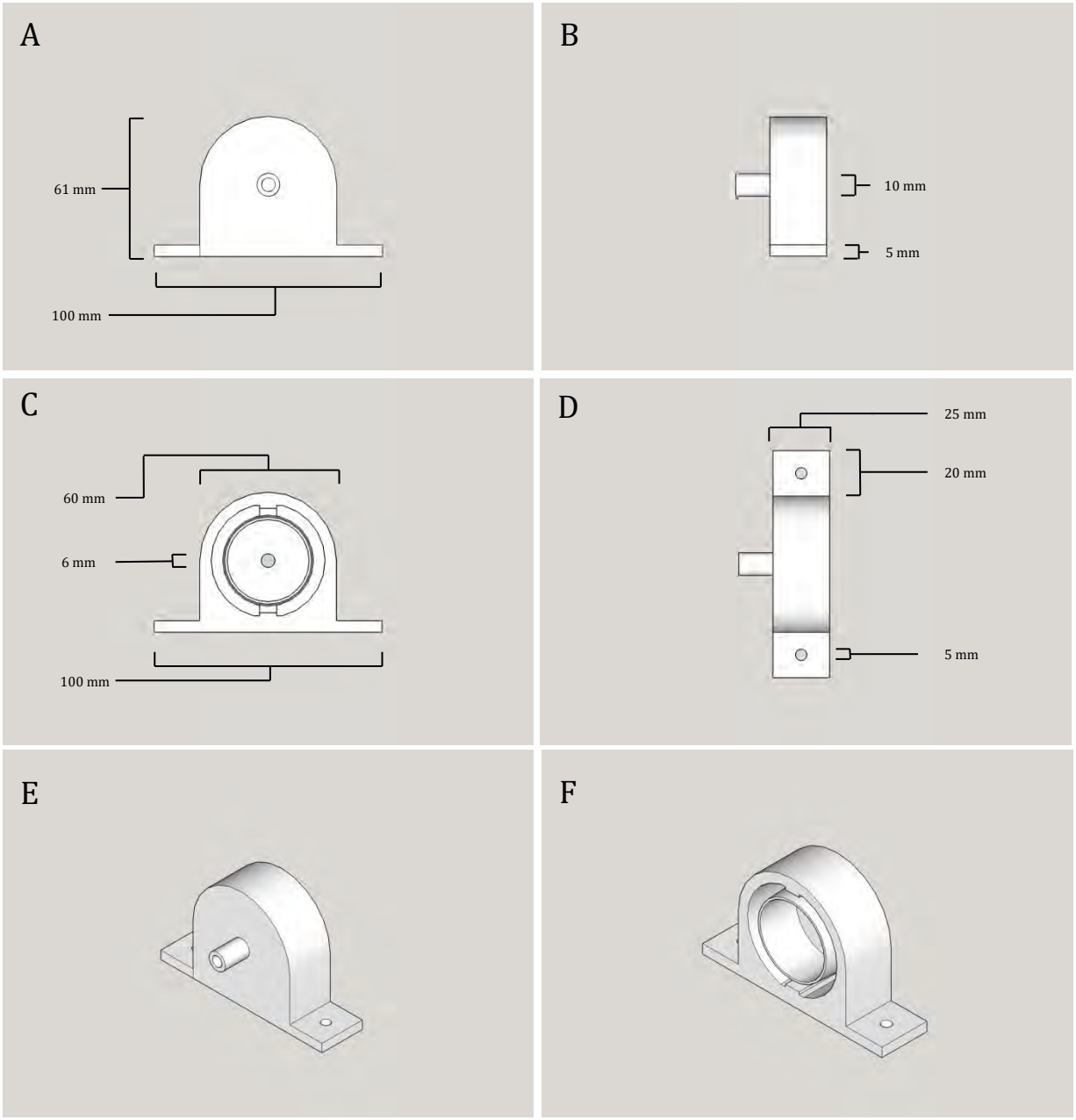

Figure 3.9: Schematic CAD layout of the cylinder ends of the bioreactor chamber. A: Front view; B: Side view; C: Rear view. D: Top view; E: Front perspective; F: Rear perspective.

The end pieces, shown in Figure 3.6, were produced identically in design, and provided end walls to the bioreactor chamber, mounting connections to the base plate, and attachment to the connective silicone tubing and from the pump system. The connective portion of this part consists of an inner and outer wall matching the shape and structure of the bevelled and grooved portion of the cylinder. When firmly pressed together these parts form a watertight seal on either end of the cylinder structure, producing a single enclosed chamber with an internal volume of 9.92 cm^3. The bottom section of this part was designed to be positioned horizontally along the base plate of the bioreactor unit, and has capacity for attachment via 4 mm nuts and bolts to the base plate. This should allow for stability of the system during movement in or out of an incubator, and maintains a constant orientation. Finally, opposite the cylinder attachment side of the part, an extruded connective piece was added to allow for connection of the reactor to the pumping system via silicone tubing. This extrusion had an inner diameter of 2.5 mm and an outer diameter of 5 mm. All of the components of the bioreactor chamber were produced using a Wanhao D7 3D printer. The final completed bioreactor chamber can be seen in Figure 3.10.

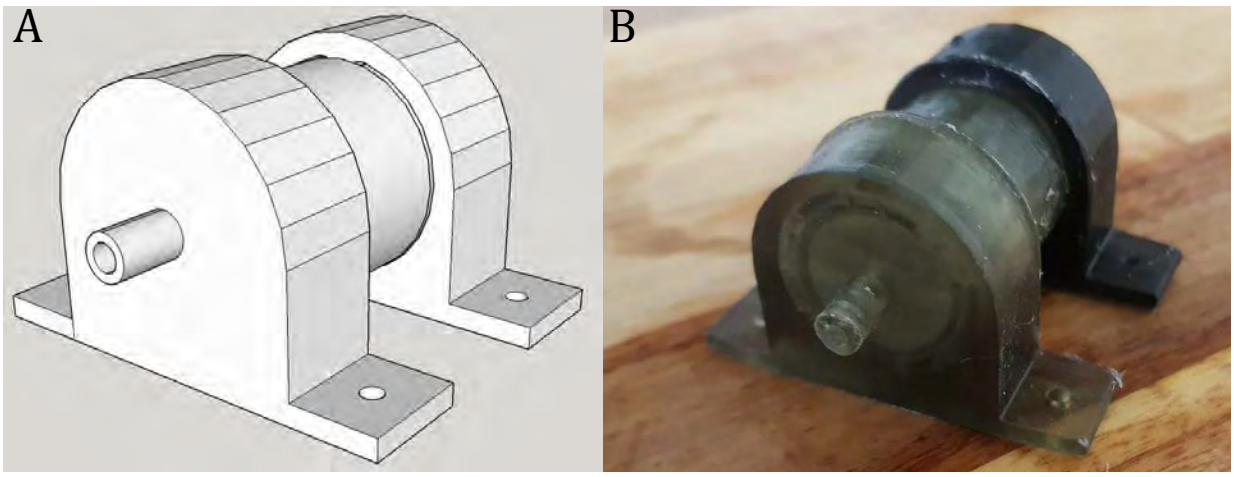

Figure 3.10: The completed bioreactor chamber assembly. A: CAD model illustrating the intended design. B: Final 3D printed design.

3.3.5 Control systems implementation

To allow for control of the unit once assembled the central motor was connected to an UNO R3 control board with pinned CNC shield via its Y-axis motor control pins. The UNO control board was then connected to a controlling windows PC via standard USB-B to USB-A cable. The CNC shield was additionally connected to a standard 12V power supply via its power input. Section 2.3.6, Figure 2.5 and Figure 2.6 illustrates the Arduino CNC-shield and underlying Arduino UNO R3 control board with reference to individual components mentioned.

Movement of the motor, and thus the flow of media through the system, was controlled on a Windows 10 PC, through the use of preinstalled Creation Workshop software. This software allowed for specific actions to be sent and executed by the system as determined an inputted .gcode, or through manual interaction with move-command linked hotkeys. In the case .gcode based command inputs, the following commands were utilized in repeating sequence to achieve specific motor action over time:

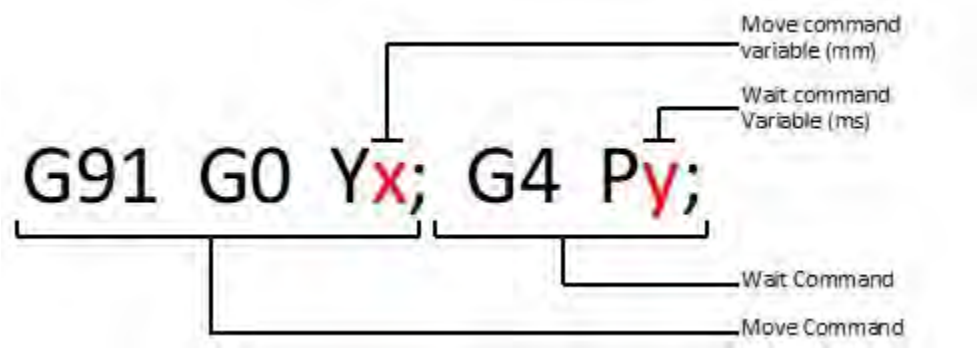

In the first move function, G91 denotes the .gcode command to set the proceeding movement type to incremental. This means that the motor will move from its current position, as opposed to moving to a position in relation to the homed state. G0 then denotes a move function itself, based on the variables that

follow. The “Y” character codes that the move is to be conducted on the Y-axis, to the value of the variable “x”, measured on millimetres. The speed and calibration of this movement is based on flashed grbl firmware settings. Firmware details of have already been described in section 2.3.7, but briefly, relevant settings used were a speed of 200 mm/min, and a steps_per_mm setting of 4000. The command is ended by the use of a “;”. The wait function is then coded by the G4 command. The “P” character is then used to denote that the following variable “y” should be used for the length of time of the wait command, measured in milliseconds. When repeated in sequence, these two commands could be sent to the pump hardware through the Creation Workshop software, to allow for a semi-continuous flow over time.

3.4 Troubleshooting and Discussion

The bioreactor portion of this research was set out to produce a continuous perfusion-based system in which a produced hydrogel scaffold could be supported in an enclosed environment. In these aims, the developed syringe pump and bioreactor unit can be said to have succeeded but demonstrates many areas in which future designs can improve. The completed unit can be seen in Figure 3.11. This section will discuss the troubleshooting in the development, construction and implementation of the system and suggest improvements to be made in future iterations.

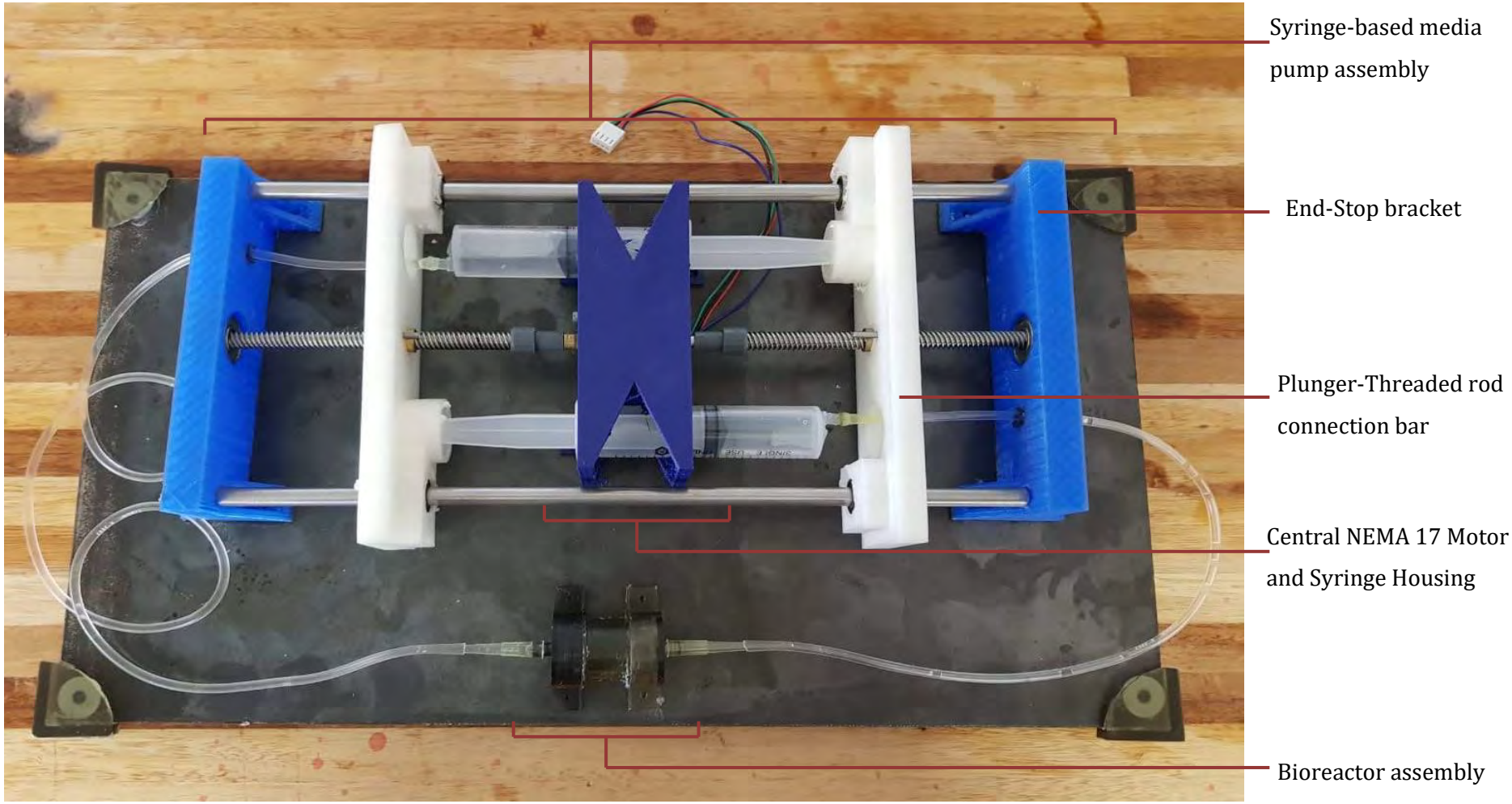

Figure 3.11: Proof of concept bioreactor and syringe pump system in the final working configuration, filled with water to demonstrate capacity for watertight operation.

3.4.1 Bioreactor chamber

The central component of the bioreactor unit, as the name suggests, is the bioreactor chamber itself which is designed to house a scaffold during operation. This enclosed environment allows for a scaffold to remain in a submerged and sterile environment and facilitates the perfusion of media over and through the scaffold from the inlet and outlet connections.

The final design of the three-piece bioreactor successfully achieves these goals. The design presented in this chapter is the product of the testing three distinct prototype iterations. The snap-fit, three-piece system was designed to be printable on a desktop Wanhao D7 3D printer using the Wanhao UV photopolymer resin (black). This production method was chosen over conventional fused filament fabrication based 3D printing for the manufacturing of high resolution, watertight parts. Once assembled, the unit was water tight due to the tight fitting joint sections, and had an internal volume of 9.92 cm^3. This can be seen demonstrated in Figure 3.9. The three-piece design was utilized to easily allow for the insertion and removal of printed scaffolds, and for this purpose the design was very effective. It was decided to use a 'squeeze together'/snap-fit method of connection over a printed nut and bolt design when it was found that hardened material became damaged during friction caused by the screwing action. A similar effect should be noted to have occurred in the current design iteration, but to a far lesser degree. Using the current design, individual pieces could be taken apart and put together around four or five times before the loss of water retentiveness, using no form of sealant. This manageable while developing the presented set-up, as new bioreactor parts could be reprinted in a few hours with little effort, but is a factor to be improved upon in future iterations. Some of the major developmental design iterations are shown in Figure 3.12.

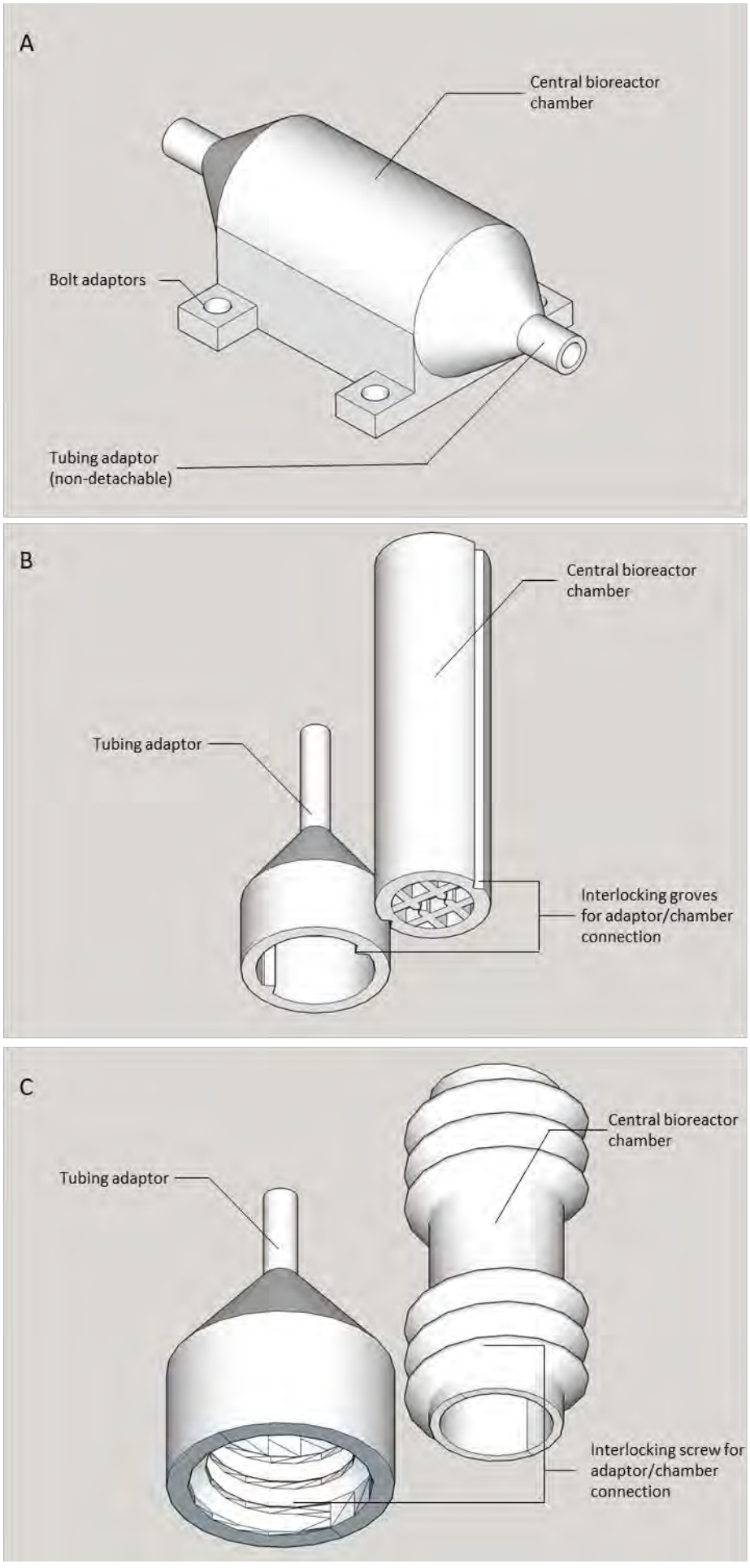

Figure 3.12: CAD designs of bioreactor chambers tested during development. A: Fully enclosed bioreactor without detachable ends; B: Simple column design with grove for end connection and column chamber disassembly; C: Bioreactor chamber with screw attached ends.

While successful in its primary goals, the design of the bioreactor still leaves plenty more to be desired regarding functionality. While the design does allow for investigation into the interior before and after operation, it does not allow for any form of monitoring during experiment proceedings. To address this, future iterations of this design should include functionality for sensor integration, to allow for data to be extracted from the internals of the reactor during testing. Sensors detecting factors such as temperature and O_2 levels will not only be needed for many experimental protocols, but will also be critical in the continued development of the bioreactor unit itself.

Another unexplored issue is the potential toxicity from components of the resin leeching into media during extended culture periods. After washing, the internal polymerised resin of the chamber should not dissolve or release any compounds into solution. Additionally, any molecules that are still released would be quickly cleared due to the continuous nature of the system. However, three major components of the resin, tripropylene glycol diacrylate, pentaerythritol triacrylate and 4-Methoxyphenol, are noted as having the potential for acute toxicity in *in vivo* animal studies at various concentrations. There therefore exists the potential of any uncured residual resin components that are not removed by isopropanol washing and curing, to negatively impact a culture within the reactor. This hypothesis is unconfirmed in this research but is further examined in Chapter 4.3.

One final criticism of the current design is the need for standard medium sized auto-pipette tips to act as adapters between the bioreactor chamber and the inlet/outlet tubing. This was ultimately needed has the Wanhao D7 printer used to construct the chamber was unable to produce a tube of sufficiently small external diameter to fit within the 4 mm connective tubing. Any further

reduction in the diameter of the inlet would result in the internal channel being unintentionally polymerised. This could be corrected with post print modification by manually drilling the channel, but this was not consistently reproducible due to the small diameter. Another potential approach to overcome this issue was to rotate the printing orientation of the part, such that the printer could better handle the small diameter inner tube. This was investigated, but unfortunately no alternate orientation was found to produce better results.

Once connected to the motorized pumping system, the developed bioreactor chamber was able to pass media through the central chamber without leaking for extended periods. This is further elaborated on in Chapter 4.3, as the system was used to support a printed PEGDA scaffold over a period of 48 hours.

3.4.2 Motorized syringe-based pump system

The general aim of the pumping system was to produce the continuous flow of media through the bioreactor chamber at a defined rate. This was achieved through the development of a motorized pump system featuring a centralized motor unit that controls extrusion and intake of two 20 ml syringes simultaneously. The syringes function as reservoirs for cell culture media that it then fed through the bioreactor chamber in response to the computer-controlled motor movement.

The central bracket in the system houses both the central motor and two syringe reservoirs, fixing them in place to the base plate (Figure 3.2 and Figure 3.3). This part was produced with standard PLA, and proved to be strong enough to provide resistance for the motor during operation, as well as hold the syringes in place through friction alone. While this part was suitable with regard to the

desired application within this research, it could still be improved with regard to user accessibility. One of the characteristics desirable in a system such as this would be the easy exchanging of syringes with those containing fresh media. In the current configuration, rapid replacement of syringes within the incubator would not be possible. The redesign of the friction-based approach to securing the syringes in future iterations would alleviate this issue.

On either end of the system, a bracket was added to support the smooth rods and the central leadscrews. The purpose of this part was thus to secure these parts during operation and prevent movement, and for this the designed brackets were highly effective. When bolted down into the base plate, the brackets were well fitted and adequate to secure the beams with little to no observed movement detected during operation. The central part of the bracket featured a circular bearing, in which the threaded rod from the motor was able to freely rotate but did not allow any translational movement.

The final component of the pumping system was the 3D printed connective bars that transferred lateral movement to the syringe plungers in response to rotational movement from the motor. Initial designs for these parts did not include connection to any stabilizing bars on either side. Initial testing revealed significant torsional strain being caused during operation, leading to the bending of the syringe plunger. The reinforced build structure and attachment to the stabilization rods seen in the current version (Figure 3.5) alleviated this issue. In its current version, the connective bars showed no sign of twisting or flexing during operation, and successfully provide linear movement to the syringes. During testing it was shown that after continuous use, the connection bracket for the syringe plungers on the connective bars would become worn out. This resulted in the syringe plungers becoming detached when being pulled by the bars, causing them to be moved solely by the pressure of the syringe pressing

from the opposite side. This issue would result in a high internal backpressure, a factor that was intended to be avoided by the twin syringe system. An uncontrolled high-pressure environment would have a negative impact on any cell culture being maintained within. This was ultimately not solved in this research, but should be addressed in future iterations of the design. To fix this in future prototypes, the connective bars should be redesigned to accommodate an improved attachment with the ends of the syringe plungers. A more major alternative solution could be to redesign the system to use a single reservoir delivery system with other measures to avoid excessive pressure, for instance having a gravity fed inlet.

Incorporation of a gravity-based input or output may also help to alleviate the issue of flow rate through the system, which in its current incarnation was limited to a minimum residence time of 19.84 h (theoretical time a free moving particle is expected to remain in the system) and a dilution rate of 0.0504 h^{-1} (The number of complete volume changes per hour). These were calculated as follows, where D = dilution rate as calculated as a function of F = Flow rate divided by V = volume of the system:

Equation 3.4: Calculation of the dilution rate (D) of the prototype bioreactor setup.

$$D = \frac{F}{V}$$

$$D = \frac{0.5\ ml/h}{9.92\ ml}$$

$$D = 0.0504\ h^{-1}$$

Residence time (μ) of a particle within the reactor is therefor then simply calculated by the equivalent relationship:

Equation 3.5: Calculation of particle residence time (μ) of the prototype bioreactor setup.

$$\mu = \frac{1}{D}$$

$$\mu = \frac{1}{0.0504}$$

$$\mu = 19.8413\ h$$

The specific residence time of a bioreactor system is an issue when it is lower than the doubling time of the organism it is intended to support. If this is the case, then the reactor runs the risk of washing out individual cells faster than the cells are able to replace themselves, depleting the culture. This was found to be the case for this bioreactor setup, and will be discussed after the calculation of cell doubling time in Chapter 4. This problem could be alleviated by either reducing the flow rate, which would require a different input system as suggested, or by increasing the volume of the reactor itself.

3.4.3 Control Software Implementation

Once assembled, the motor was connected to the controlling PC via a CNC-Shield and UNO R3 control board, to USB. The software used to control the system was Creation Workshop. The Creation Workshop software allowed for manual control of the motor during the initial phases of testing. This allows for basic rotation of the motor at a set rate in response to a bound forward and backward softkey. Additionally this software allowed for a .gcode script to inputted and be executed over time. This functionality was utilized later for longer-term testing and experimentation. Overall, this method of software control worked well for its intended purpose, being easy to use during initial testing and running longer automated tests running without issue.

If future iterations of this design deem it significant enough an issue, a dedicated application could be developed to make the inputting of commands much easier. As it stands, using Creation Workshop for this application requires the user to manually determine the .gcode string and enter it into the appropriate field in the program. Inputting the desired commands directly though the Arduino IDE is also an option to achieve this, but falls short for the same reasons. The production of a simple application that would allow a user to select the flow rate and total run time, converting this to .gcode automatically would be far more elegant of a solution. To add on to this idea, the application could be linked over the Internet to a mobile-paired app, allowing a user to view the status of an operation in real time, or receive notifications when an operation is complete. With the implementation of internal sensors with regard to improvement of the bioreactor system earlier discussed, a developed application for PC and mobile could provide researchers using the equipment with large amounts of relevant data without the need to stop a given operation or even be in the lab at all. Further, the data could be relayed to the rest of the equipment involved, adjusting parameters to maintain optimal culture conditions at all time. An example would be autonomous adjustment of the outer incubator's temperature to counter any fluctuations in internal temperature.

4 Chapter 4: Mammalian cell culture and PEGDA hydrogel scaffold printing

4.1 Introduction

Poly (ethylene glycol) diacrylate (PEGDA) is a synthetic monomer capable of rapid crosslinking at room temperature by means of a variety of initiation reactions (Fairbanks, *et al.*, 2009). It can be polymerized by light activated systems, in both the UV and visible light spectrums through the addition of photoinitiation agents. This characteristic has illustrated the effectiveness of PEG based systems in application for 3D bioprinting and scaffold production. The visible light-based polymerization of PEGDA used in this research was demonstrated by Wang *et al.* (2016), and includes the light sensitizer and initiator Eosin Y, catalyzing agent N-Vinylpyrrolidone (NVP), and co-initiator Triethylamine (TEA). The utilization of visible light over UV based systems allowed for the possibility of 'live prints'; something that would have resulted in DNA damaging effects of UV based systems (Ikehata & Ono 2011). Visible light however, has been documented to still have an impact on the cells *in vitro,* but the effects vary widely between cell types, exposure time, wavelength and intensity (Moore, *et al.*, 2005)(Smith, *et al.,* 2009). Additionally, visible light can have an impact on components of cell culture media, indirectly affecting the cells in culture (Nielsen & Bertheussen, 1991).

As a polymerized matrix, PEGDA is biologically inert in nature, and thus resists biological degradation over time (Browning, *et al.,* 2015). This feature makes it suitable for sustained use in a bioreactor system, as the scaffold would need to remain firmly in place during culture. The disadvantage to this resistance to

biological action means that mammalian cells do not readily adhere to PEGDA. However, PEGDA has been shown to allow for effective and rapid modification with functional small molecules and peptides, such as RGD peptides, to alter its biological affinity and characteristics (Zhu, 2011) (Bahney, *et al.,* 2016) (Yang, *et al.,* 2005). Through modification, PEGDA has been shown to be an effective scaffold for cell culture and tissue engineering (Son & Lee, 2016) (Burdick, & Anseth, 2002).

Table 4.1: List of characteristics for which PEGDA was chosen for application in 3D bioprinting and cell culture.

Characteristic	Functionality
Photopolymerisable	Critical the production of spatially defined bioscaffolds using light-based 3D printing.
Biologically Inert	Resists biological degradation, thus having the potential to provide a support scaffold for long term cell culture.
Chemically modifiable	Can be modified using a variety of biologic and synthetic molecules to tailor characteristics to a specific use.
Physically modifiable	Can be modified to produce a wide variety of elastic modulus and structural features at the micro scale

Finally, PEGDA has been shown to be widely variable in terms of elastic modulus, stiffness and structural rigidity (Durst *et al.,* 2015) (Grigoryan, *et al.,* 2019).

Altering the concentration or chain length of the PEGDA used will modify these characteristics (Mazzoccoli, *et al,.* 2011). Additionally, PEGDA can be used in conjunction with other polymers to produce a range of hydrogels with unique

characteristics (Son & Lee, 2016). Mammalian cells have been shown to be adapted to their specific niche environments *in vivo*, and thus are impacted by the physical characteristics of their culture environment *in vitro* (Kfoury & Scadden, 2015). PEGDA makes for an interesting case study for this research, as it allows for easily modifiable physical and chemical scaffold characteristics.

It is for these reasons (Summarized in Table 4.1) that PEGDA was chosen as the primary case study with which to test the 3D bioprinter and bioreactor set up. In addition, PEGDA was evaluated for its biocompatibility, to ensure that it acts as an effective scaffold post-print.

In order to assess the toxicity of PEGDA and visible light exposure on mammalian cells *in vitro,* the ACEA xCELLigence Real-time Cell Analyzer (RTCA) was utilized. The RTCA system allows label free monitoring of cultures based on the electrical impedance produced by cells grown on a 96-well plate with a gold electrode microarray. The electrical impedance of a culture is influenced by attached cell quantity, size, morphology and composition. The electrical impedance of a culture is subtracted from the background impedance to produce a Cell Index unit (CI). The equation for the cell index can be seen below, where the cell index (CI) calculated from changes in electrical impedance. Zi: electrical impedance at given time points. ZO: background reading.

Equation 4.1: Equation to determine Cell Index (CI), as a measure of electrical impedance (Zi) less the background impedance divided by a constant of 15.

$$Cell\ Index\ (CI)\ = \frac{Z_i - Z_o}{15}$$

4.2 Methods and materials

4.2.1 Culture of 3T3-L1 cell lineage and microscopic evaluation

Murine preadipocyte 3T3-L1 cells were maintained in basal culture media (DMEM containing 5%(v/v) Fetal Calf Serum (FCS), 1% (v/v) Penicillin/Streptomycin) in a humidified incubator (37°C; 5% CO_2). Sub-culture was carried out as needed by routine trypsinization. Cell viability was determined using trypan blue staining: Cell suspension diluted 1:1 with trypan blue, and the ratio of stained to unstained cells calculated from a standard hemocytometer cell count.

4.2.2 Visible light PEGDA hydrogel synthesis for swelling analysis, SEM and 3D bioprinting.

The visible light polymerizing, PEGDA hydrogel cocktail produced in this research combined various concentrations of PEGDA 10-100% (v/v), in sterile deionized water. Regardless of PEGDA concentration, the photoinitiator cocktail was then added consisting of 0.01 mM Eosin Y, 37 nM NVP and 0.1 % TEA (v/v) (Bahney et al. 2016). The mixture was stirred overnight using a magnetic stirring bed, and kept in a light protected container at room temperature. This formulation was repeated throughout the following experiments, unless otherwise stated. The capacity for photopolymerization for the PEGDA cocktail was initially tested by projecting static shapes onto the hydrogel using an Optoma (Model HD141X) Full HD projector (See supplementary materials; Figure 7.1).

4.2.3 Swelling analysis of PEGDA hydrogels

Poly (ethylene glycol) diacrylate (PEGDA) disks were produced by 60 seconds of exposure to high intensity white light (3000 lumens) from an Optoma projector (Model HD141X) within a clear own ended 20 ml syringe. The PEGDA disks were produced using concentrations of 10 and 20% (v/v) PEGDA to deionized water, and the standard cocktail as described earlier (see Section 4.2.2). The polymerized PEGDA gels were then extruded from the syringe and sliced at a thickness of 5 mm to produce uniform disks using a scalpel, producing uniform disks with a 20 mm initial diameter. Disks of the same densities were also produced in the same way using Irgacure 2959 instead of the standard cocktail, and polymerized under UV light for 60 seconds. The disks were then submerged in either standard culture media or PBS, in the wells of 6 well plates (n=3 for each PEGDA concentration vs media type vs polymerization method). These plates were then incubated in standard mammalian incubation conditions (37^{o}C; 5% CO_2), with periodic removal every 24 hours for 2 days. During each removal, the disks were measured along the X- and Y- axis and the average taken to assess swelling over time.

4.2.4 Toxicity analysis of PEGDA hydrogel components on 3T3-L1 preadipocytes

A 3T3-L1 mouse preadipocyte culture was grown to confluence on a standard T75 culture flask, trypsinised, and enumerated via hemocytometer counting after 1:1 trypan blue staining. The cells were then seeded uniformly on an xCELLigence plate at 5000 cells per well, which was then transferred into a standard mammalian culture incubator (37˚C; 5% CO_2). The culture was allowed to adhere to the plate for 1 hour before monitoring began. The xCELLigence unit

then monitored the electrical impedance of the cells for 24 hours in standard culture media. The xCELLigence unit was set up to take readings at 15-minute intervals for this phase of the experiment.

The media from all wells were removed after the 24-hour adherence period, and replaced with media containing each of the components of the PEGDA visible light cocktail at various concentrations in triplicate. Positive control wells simply contained fresh culture media during experimentation. Negative control wells did not have cells seeded but did include fresh culture media. The xCELLigence unit was set-up to take electrical impedance readings at 30-minute intervals over 48 hours. Three internal replicates were done for each concentration of each cocktail component during the single xCELLigence experiment.

Negative control wells across all experiments were used to calculate average culture doubling time between 48h and 72h. IC50 values were determined for each component tested. These calculations were carried out using the relevant automated functions in the xCELLigence software.

4.2.5 Analysis of 3T3-L1 growths with exposure to high intensity light

A 3T3-L1 mouse preadipocyte cell line was cultured to confluence in a standard T75 culture flask, trypsinised and were then seeded uniformly on an xCELLigence plate at 5000 cells per well. Two lanes of wells that bisected the plate were filled with Wanhao printing resin (Black), to provide a barrier to light exposure to control samples. The xCELLigence unit monitored the electrical impedance of the cells adhering to the plate for 24 hours in standard culture media. The xCELLigence unit was set up to take readings at 15-minute intervals for this phase of the experiment.

After 24 hours, the media of all wells containing cells were changed for fresh culture media. Control wells were then briefly covered with tinfoil. The remaining wells were then exposed to high intensity white light from the Optoma (Model HD141X) DLP projector and a distance of 100 mm. Cells were exposed for either 60 or 120 second. After exposure, the plate was returned to the xCELLigence unit which monitored electrical impedance every 30 minutes for 48 hours at 37^{o}C and 5% CO_2. 24 internal replicate wells were run for each exposure time, for the single xCELLigence experement.

4.2.6 Scanning Electron Microscopy analysis of PEGDA hydrogels

The PEGDA visible light polymerization cocktails containing 10, 20 and 100% (v/v) PEGDA were produced as described in section 4.2.1. A 1 ml sample of each was then aspirated into a 1 ml clear syringe with removed front end. The gels were then polymerized by exposure to 3000 lumen, white light from an Optoma HD (Model HD141X) DLP projector directed to the side of the syringe. To ensure even polymerization, the syringe was rotated 180 degrees at the 30 second mark during polymerization. Gels were then extruded, and disks of approximately 3 mm height cut using a scalpel (n=3). Disks for each density of PEGDA were placed on SEM pedestals, before being vacuum gold coated using a Quorum Q150R S Gold sputter in preparation for viewing (n=3). Samples were then viewed under Tescan Vega scanning electron microscope, at various magnifications.

4.2.7 Viability of PEGDA as a Bioprinting Material.

A 3 L volume of 20% (v/v) PEGDA cocktail was produced as described earlier and stirred overnight using a magnetic stirrer bed at room temperature, in the

dark. The 3 L volume PEGDA cocktail was then transferred into the print tank of the 3D bioprinter, described in Chapter 2 with the projector not initially positioned above the tank. The projector unit of the printer was then switched on, and allowed to fully warm up, while the print parameters were set up on the connecting computer. Once ready the PEGDA solution tank was then moved into position below the projector using the computer-controlled X-axis bed. The printer build platform was then lowered to just below the surface level of the PEGDA solution. Finally, the print was initiated using the settings input onto the Creation Workshop software, on the controlling computer. This process was repeated until the printability with the system was optimal. The parts printed during the testing phase were simple cylinders, but as printability improved, internal crosslinking structures were added.

4.2.8 Attachment analysis 3T3-L1 cell line on PEGDA hydrogel scaffolds

A 20% (v/v) PEGDA visible light cocktail was prepared as described earlier in section 4.2.1. A volume of 2ml of this cocktail was aliquoted into each of the wells of a 6 well plate (n=6). Each well of the plate was then exposed to direct high intensity white light from the developed 3D printer unit for 60 seconds. The light was passed through the closed lid of the 6 well plate to maintain sterility. The polymerized gels were then covered with 2ml of PBS, with half containing 1% poly-l-lysine. These were then incubated for 2 hours at 37^{o}C and 5% CO_2. After incubation, the PBS solutions were aspirated in preparation to be seeded. 3T3-L1 preadipocytes were cultured in a T25 culture flask to confluence in DMEM at 37^{o}C and 5% CO_2. These cells were then trypsinised and seeded into the wells of the 6 well plate at 20 000 cells per well. The plates were then incubated at 37^{o}C and 5% CO_2 for 48 hours. A second 6 well plate without PEGDA had cells seeded and was incubated in the same manner for comparison. The culture media was then aspirated and replaced with live/dead staining solution consisting of DMEM, 1 % (v/v) PSA, 19.2 μM fluorescein diacetate (FDA, Sigma Cat. No. F7378)

and 30 μM propidium iodide (PI, Sigma Cat. No. P4170) and incubated for 5 minutes. The staining solution was then aspirated and rinsed with PBS. Each well was then visualized under a Zeiss AxioVert A1 Fluorescence Microscope using the dsRed filter (563 nm/581 nm) for visualization of PI, the FITC filter (495 nm/519 nm) for the visualization of fluorescein diacetate. Brightfield microscopy was also included for morphological analysis. All 6 experimental replicate wells were imaged 3 times, maintaining the image position each time for the images to later be overlayed.

A 20% PEGDA hydrogel scaffold was then produced using the developed 3D bioprinter unit as described in section using a crosslinked cylinder design described in section (4.2.7). Once printed, the scaffold was inserted into the bioreactor chamber, which was then sealed. The chamber was then filled with PBS containing 1% poly-L-lysine and incubated for 2 hours at 37^{o}C and 5% CO_2. The poly-L-lysine solution was drained, and the chamber gently rinsed with PBS. The bioreactor chamber was then filled with DMEM culture media, containing trypsinised 3T3-L1 preadipocytes. The sealed chamber was then incubated for 24 hours at 37^{o}C and 5% CO_2. The sealed reactor was then connected to the motorized pump system that supplied fresh media at a flow rate of approximately 0.5 ml per hour at 37^{o}C and 5% CO_2. After 24 hours, media was replenished in the inlet reservoir, and emptied in the outlet reservoir. After 48 hours, the bioreactor was disconnected, unsealed and the scaffold carefully removed by hand into a sterile PBS bath. Portions of the scaffold were dissected by scalpel, and examined by Brightfield microscopy using a Zeiss Axiovert A1 fluorescent microscope (n = 1).

4.3 Results and Discussion

4.3.1 Culture of 3T3-L1 cell lineage and microscopic evaluation

The 3T3-L1 murine preadipocyte cell line was grown in standard 2D cell culture conditions with periodic media replacement until confluent. The culture was then observed under microscopy to assess cell morphology and culture characteristics. The 3T3-L1 cultures at 90 – 100% confluence can be seen in Figure 4.1 below.

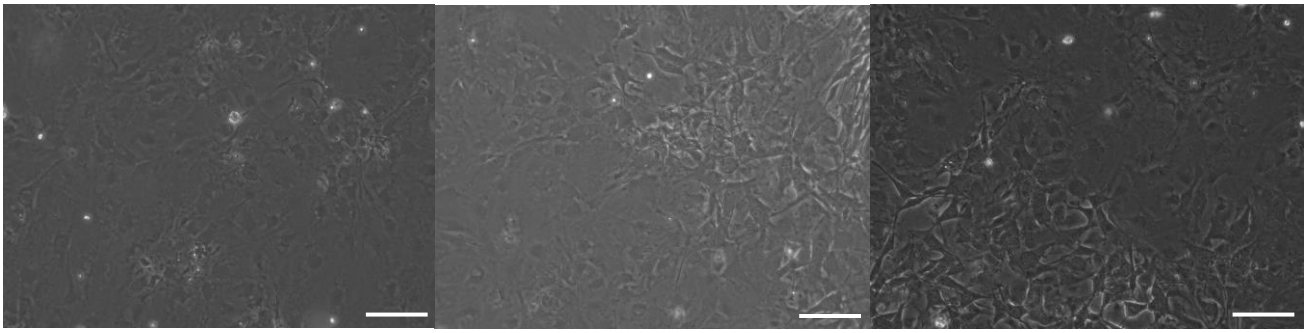

Figure 4.1: Culture of 3T3-L1 cells under standard culture conditions. The culture was grown in DMEM with 5% v/v FCS and 1% v/v Pen/Strep. Images denote microscopic evaluation of the culture at 90 – 100% confluence. Scale bars represent 200 µm. n = 3.

Figure 4.1 illustrates the culture characteristics of the 3T3-L1 cell line under standard culture conditions. It can be seen that the cells have maintained their fibroblastic morphology, and had minimal to no observable lipid droplet formation. This suggests that the culture maintained the pre-adipogenic phenotype as expected for this cell line.

4.3.2 Swelling analysis of PEGDA hydrogels

To analyze the swelling characteristics of PEGDA hydrogel scaffolds in standard culture conditions, the diameter change over time in uniformly produced PEGDA hydrogel disks was assessed. In addition, the impact of PEGDA concentration within the hydrogel with regard to swelling was investigated. This can be seen in Figure 4.2 below.

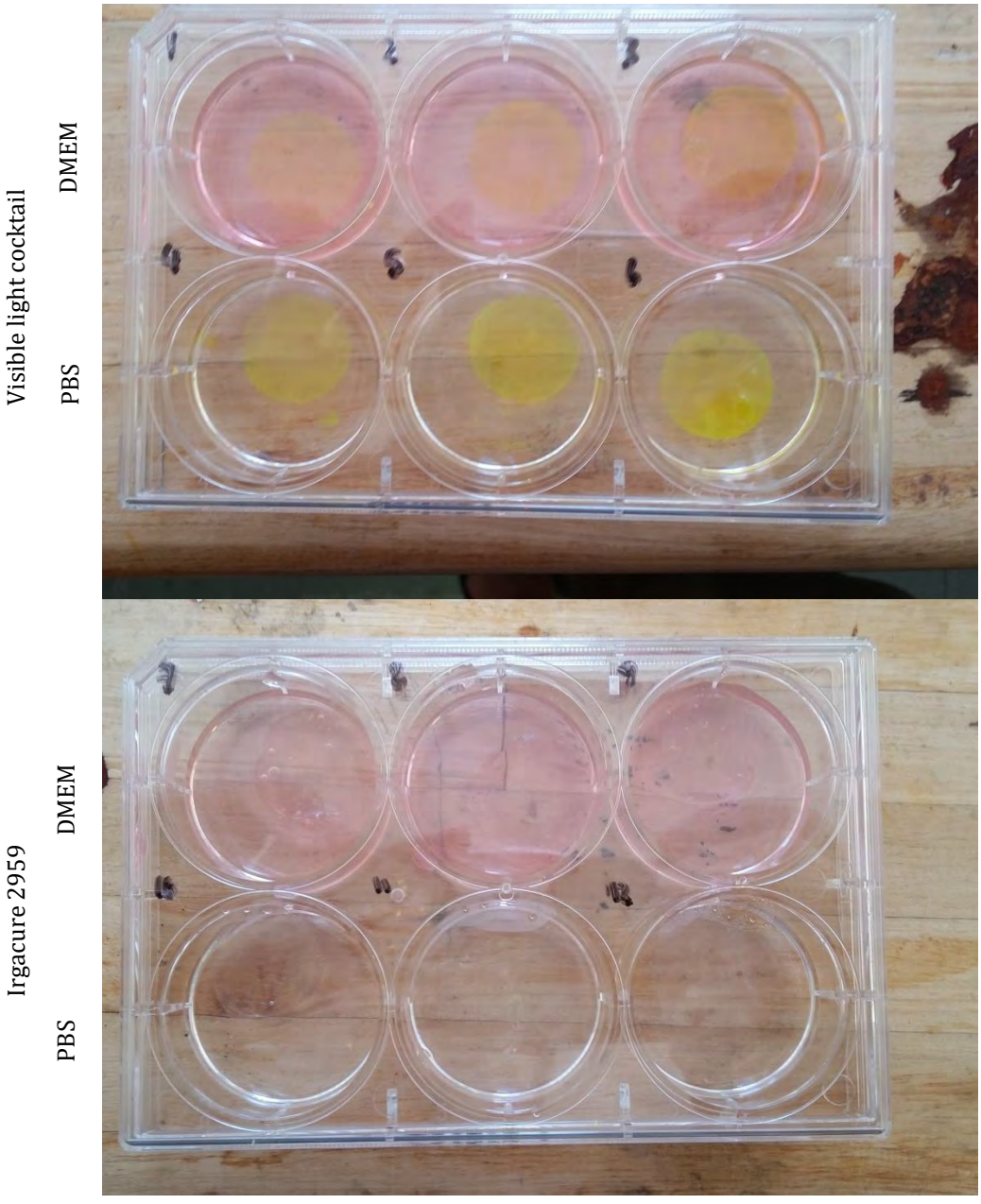

Figure 4.2: Experimental set up for the swelling analysis of PEGDA hydrogel disks of various PEGDA concentrations produced either by visible (using standard visible light cocktail) or UV light (Igracure 2959) polymerization. Each disk submerged in either 1X DPBS or DMEM. The diameter change over time recorded. (n = 3).

The understanding of the fundamental swelling characteristics of any hydrogel is critical, as any change in scaffold size over time could lead to a number of unexpected variables when implemented into a given experimental set-up. With regard to the 3D printing utility described in Chapter 2 of this dissertation, the swelling of the PEGDA hydrogel will affect the potential final resolution of any print, as it remains submerged over time, altering the intended design. Once a printed scaffold is implemented into the enclosed bioreactor system described in section 3, any change in volume may lead internal outward pressure, changes to available surface area or alterations in media flow characteristics.

The swelling of the PEGDA hydrogel must thus be well understood and then accounted for, during the design phase of hydrogel production, prior to printing. After testing, it was found that regardless of PEGDA concentration or polymerization technique, all hydrogels observed reached peak swelling sizes within 24 hours after exposure to culture conditions, after which no further increase in size was observed. Additionally, regardless of PEGDA concentration, diameter increase in the PEGDA hydrogel disks was limited to around 5%, summarized in Table 4.2 below. The predictable swelling characteristics presented by the PEGDA hydrogel made it a suitable candidate for application in the bioreactor system described.

Table 4.2: Average final diameter (mm) of 20 mm diameter PEGDA hydrogel disks at a concentration of 10% and 20% after polymerization by visible and UV light (n=3).

PEGDA Concentration:		10%	20%
Visible Light:	DMEM	20.83 +- 0.18	20.67 +- 0.12
	PBS	20.47 +- 0.24	20.58 +- 0.31
UV:	DMEM	20.75 +- 0.20	20.50 +- 0.20
	PBS	20.25 +- 0.20	20.33 +- 0.24

4.3.3 Toxicity analysis of PEGDA hydrogel components on 3T3-L1 murine preadipocytes

An analysis into the toxicity of the various components making up the PEGDA visible light polymerizing cocktail was investigated using ACEA xCELLigence Real-Time Cell Analyzer (RTCA) Single Plate (SP) system. This was performed in order to investigate the effect of each individual component making up the hydrogel, to confirm its suitability for application within the bioreactor system. The electrical impedance data for 3T3-L1 preadipocyte cells during exposure to the PEGDA hydrogel components at varying concentrations was averaged and represented in Figure 4.3. The IC50 values for each hydrogel component after 72 hours were calculated and included in Figure 4.3. Individual non-averaged replicate data can be found represented in Chapter 7, Figure 7.2 – 7.5.

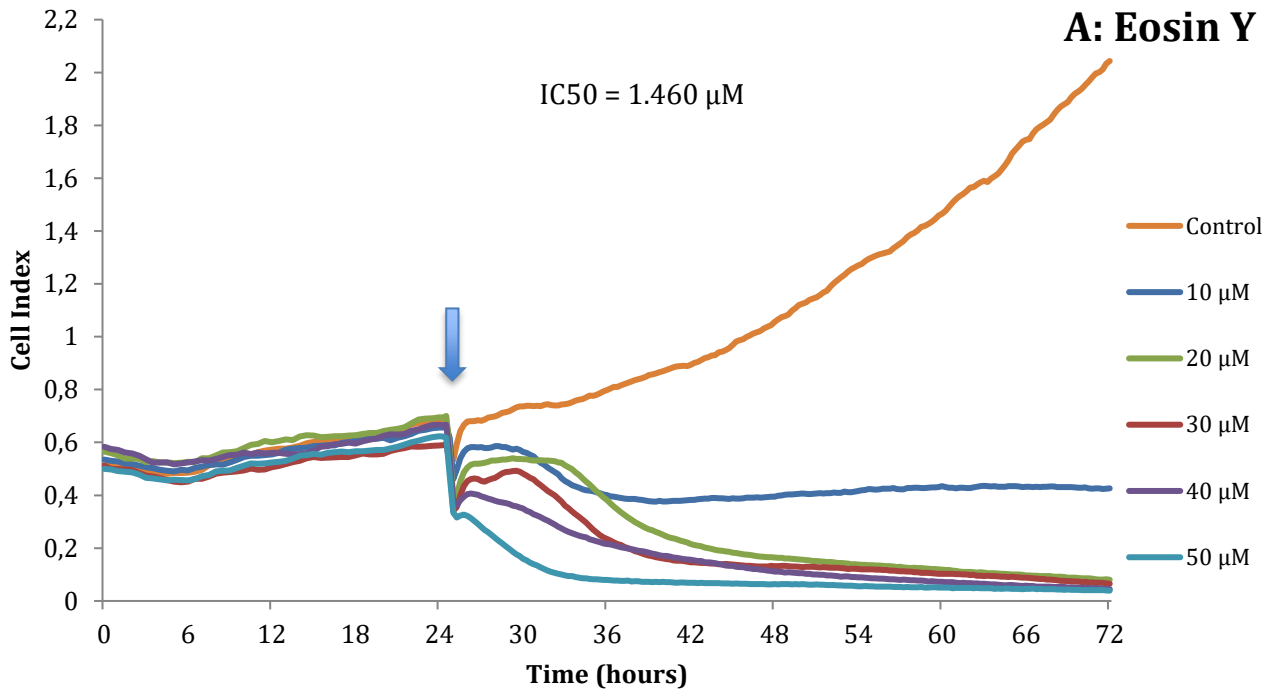
A: Eosin Y
IC50 = 1.460 µM
Cell Index
Time (hours)
Control
10 µM
20 µM
30 µM
40 µM
50 µM

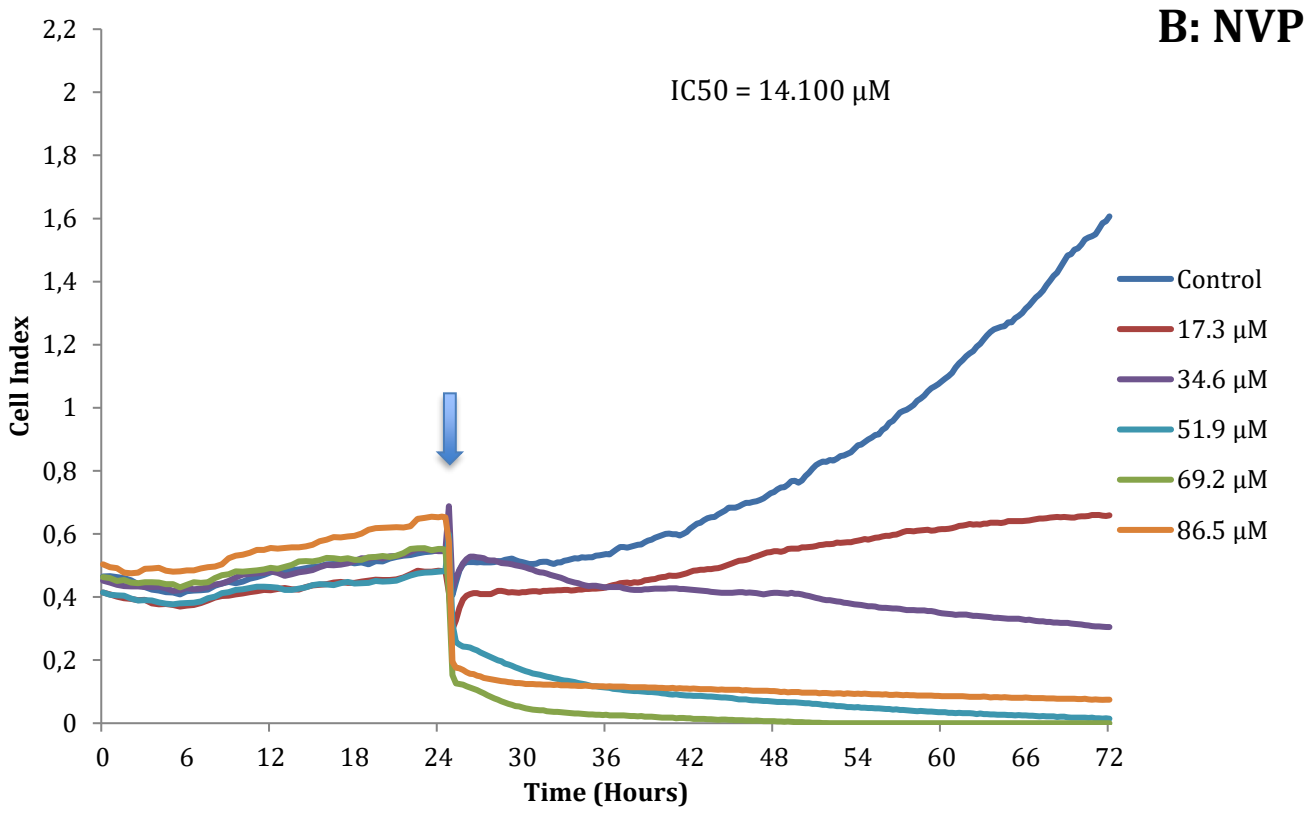
B: NVP
IC50 = 14.100 µM
Cell Index
Time (Hours)
Control
17.3 µM
34.6 µM
51.9 µM
69.2 µM
86.5 µM

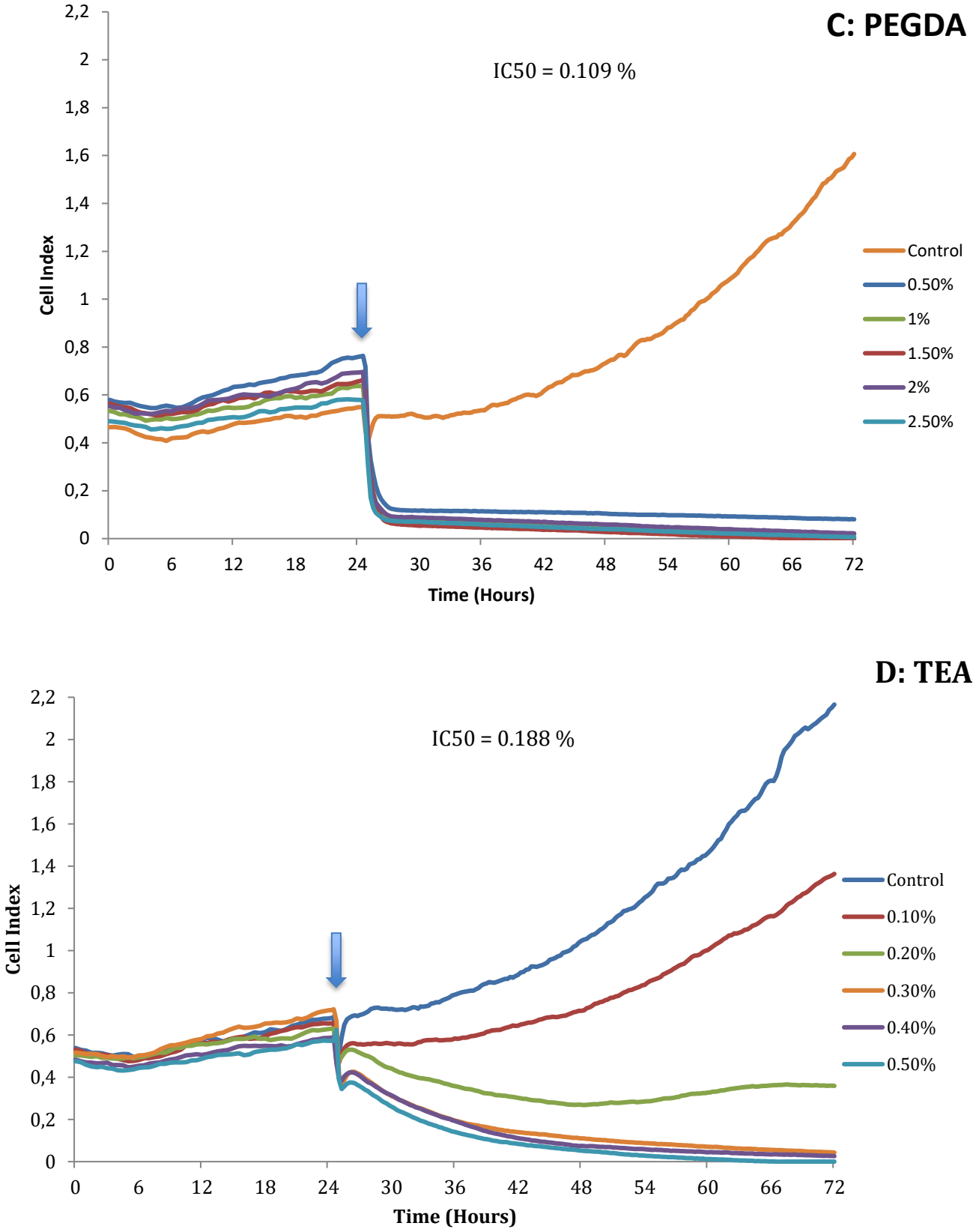

Figure 4.3: Electrical impedance of 3T3-L1 preadipocyte cell cultures during exposure to individual PEGDA hydrogel compounds (A:Eosin Y;B: NVP; C: PEGDA; D: TEA) at varying concentrations. In each case, exposure was carried out at 24 hours (indicated by arrows) and the cultures kept at 37°C throughout. Graphs are each representative of 3 averaged replicates. Each of these replicates can be found in supplementary material, Figure 7.2 -7.5.

Eosin Y is a visible light sensitizing agent within the PEGDA cocktail, and is present at a concentration of 10 μM in with working solution used in this research. This concentration also represented the lowest concentration tested in this experiment, as an increased concentration of eosin Y was anticipated to improve the printing characteristics of the PEGDA cocktail. What can be seen in the xCELLigence analysis (Figure 4.3A) is that eosin Y at the 10 μM concentration halted cell proliferation relative to the control, but did not cause cells to die and lift from the culture surface altogether. An increase in eosin Y concentration past this point was shown to then increase the rate of cell death that scaled relative to the increase in eosin Y concentration. The survival of cells in media containing 10 μM of eosin Y would point towards it's suitability for successful live-printing using this formulation, but this certainly warrants further investigation to determine if it's concentration should be lowered in the standard polymerization cocktail. The IC50 value calculated from these data of 1.460 μM would indicate that any polymerized hydrogel would need to achieve a soluble concentration lower than this to prevent significant toxicity. This value is not representative of the impact of Eosin-Y post polymerization though, so short term exposure in a live printing system may not be significantly detrimental.

The second compound to be tested was NVP (N-vinylpyrrolidone), which serves to enhance and adjust the polymerization rate and final stiffness of the hydrogel. Similar to the observations made for eosin Y, NVP at lower concentrations had a halting effect of cellular proliferation (Figure 4.3B). The lowest concentration of NVP tested (17.3 μM) greatly reduced proliferation rate in relation to the control but still produced a positive overall growth trend after exposure. The next concentration of 34.6 μM was also non-fatal to the cultures, but caused a slightly negative trend. Increasing the concentration of NVP further however, caused culture death within a number of hours. These data produce an IC50 value of 14.1 μM, well above what is present in the unpolymerized hydrogel cocktail (37

nM). Thus, at such a low concentration in the cocktail, the data would indicate that NVP as a component would have low toxicity in live print application.

PEGDA is the main component of the hydrogel cocktail used in this research. It can be seen in Figure 4.2C that all concentrations of PEGDA tested caused absolute cell death, despite the concentrations being well below those found in the working solution. This would suggest that a live-print using the cocktail defined in this research would not be possible due to the PEGDA concentrations used (20%). However, this concentration is not indicative of what would be present in the PEGDA hydrogel post-polymerization, but does highlight the need for adequate wash steps prior to culture inoculation. This is supported in literature as others have reported significantly improved cell viability after multiple wash steps, removing excess monomer from the culture environment (Rekowska, *et al.,* 2019). In a live print setting, Desi, *et al*., found that, while unpolymerized PEGDA was fatal to sustained culture at 15% (in standard culture conditions), short term exposure of 10 minutes before polymerization and encapsulation was not significantly detrimental to cell viability. The low IC50 value of 0.109% calculated in this experiment corroborates the toxicity to the PEGDA solution in culture media, but is not indicative of post-polymerized culture sustainability.

Finally, TEA (triethanolamine) acted as a co-initiator of polymerization in the PEGDA hydrogel cocktail used. At the working concentration of 0.1%, TEA was shown to slow the rate of culture proliferation in relation to the control. Despite this, the culture trend at 0.1% remained strongly positive, and remained below the calculated IC50 value of 0.188%. At the increased concentration of 0.2% TEA, cell proliferation was halted, but was insufficient to cause cell death altogether, which would have produced a downward trend in cell index over time as cells

lifted from the plate surface. At concentrations higher than these, TEA was shown to be fatal to the cultures tested, causing cell death within the 48 hours tested.

The doubling time was calculated for the control curves of each test between 48h and 72h. The average doubling time was found to be 22.74h.

In addition to these data, cells were also visually monitored to examine the effect individual cocktail components might have on morphology or differentiation of the 3T3-L1 cells. In the case of all components tested, no sign of any morphologic abnormalities were detected in cells that remained attached. Additionally, no visible signs of differentiation had occurred, but this was not confirmed through adipogenic staining.

4.3.4 Analysis of 3T3-L1 growths with exposure to high intensity light

Similarly to component toxicity, exposure to the high intensity visible light produced by the bioprinter was investigated for its potential impact on cell culture over time. This aspect was investigated to simulate the feasibility of the printer for use in a "live print", one in which cells are added before the scaffold print has taken place, and would thus be exposed to the high intensity light used for the printing process. The high intensity light likely contains both a UV and IR component, which may be harmful to cells after prolonged exposure. This was tested by exposing 3T3-L1 murine preadipocyte cell cultures within the 96-well ACEA xCELLigence (RTCA) Single Plate (SP) to direct white light from the projector at 3000 lumens from a distance of 15 cm. Exposure was performed for 60 and 120 seconds after which, the change in electrical impedance of the cultures was monitored by the ACEA xCELLigence (RTCA) system for 7 days. The observed data is shown in Figure 4.4.

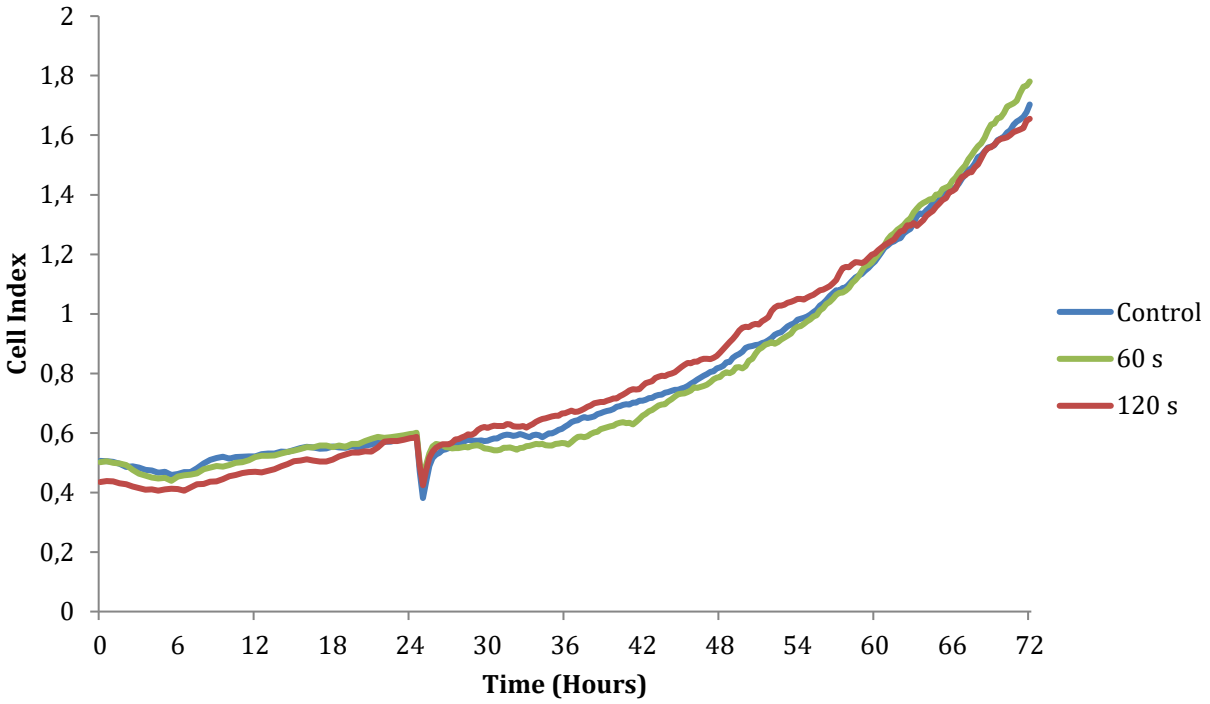

Figure 4.4: Electrical impedance of 3T3-L1 preadipocyte cell culture after exposure to visible light at 3000 lumens for 0, 60 and 120 seconds at an exposure distance of 15 cm. Curves were produced from an average of 16 replicate wells each.

An investigation into the impact of high intensity visible light on cell culture was critical, as the developed printer system used this as a way to overcome the mutagenic effect of conventional UV-based DLP printers. The data revealed in Figure 4.4 shows that regardless of exposure time, cell culture over time was not meaningfully affected by comparison to the unexposed control sample. The average cell doubling time in this experiment between 48h and 72h of measurement for the Control, 30s exposure and 60s exposure were: 22.39, 20.60 and 25.86h respectively, as calculated by the xCELLigence software version 1.2.1.

This would suggest that light at the 3000 lumen intensity would be viable for live-printing, should the printer be used to do so in the future. The exposure time of up to 120 seconds was well above 45 seconds ultimately needed by the PEGDA system to achieve polymerization at 100 µm, highlighting the flexibility of the

printing system to implement longer curing hydrogels, without causing adverse effects to any live-printed samples.

4.3.5 SEM analysis of PEGDA hydrogels

The surface characteristics of a hydrogel can be critical to the facilitation of an effective cell culture, through the impact of factors including surface area, cell-cell accessibility and mechanical forces placed on the cells (Ventre & Netti 2016). It is thus important to investigate the surface characteristics of any applied hydrogel in order to understand the potential impact on cellular attachment and proliferation. In this investigation the applied PEGDA visible light hydrogel at various concentration of PEGDA was viewed by SEM, to assess the affect that this change would have of surface morphology at the cellular scale.

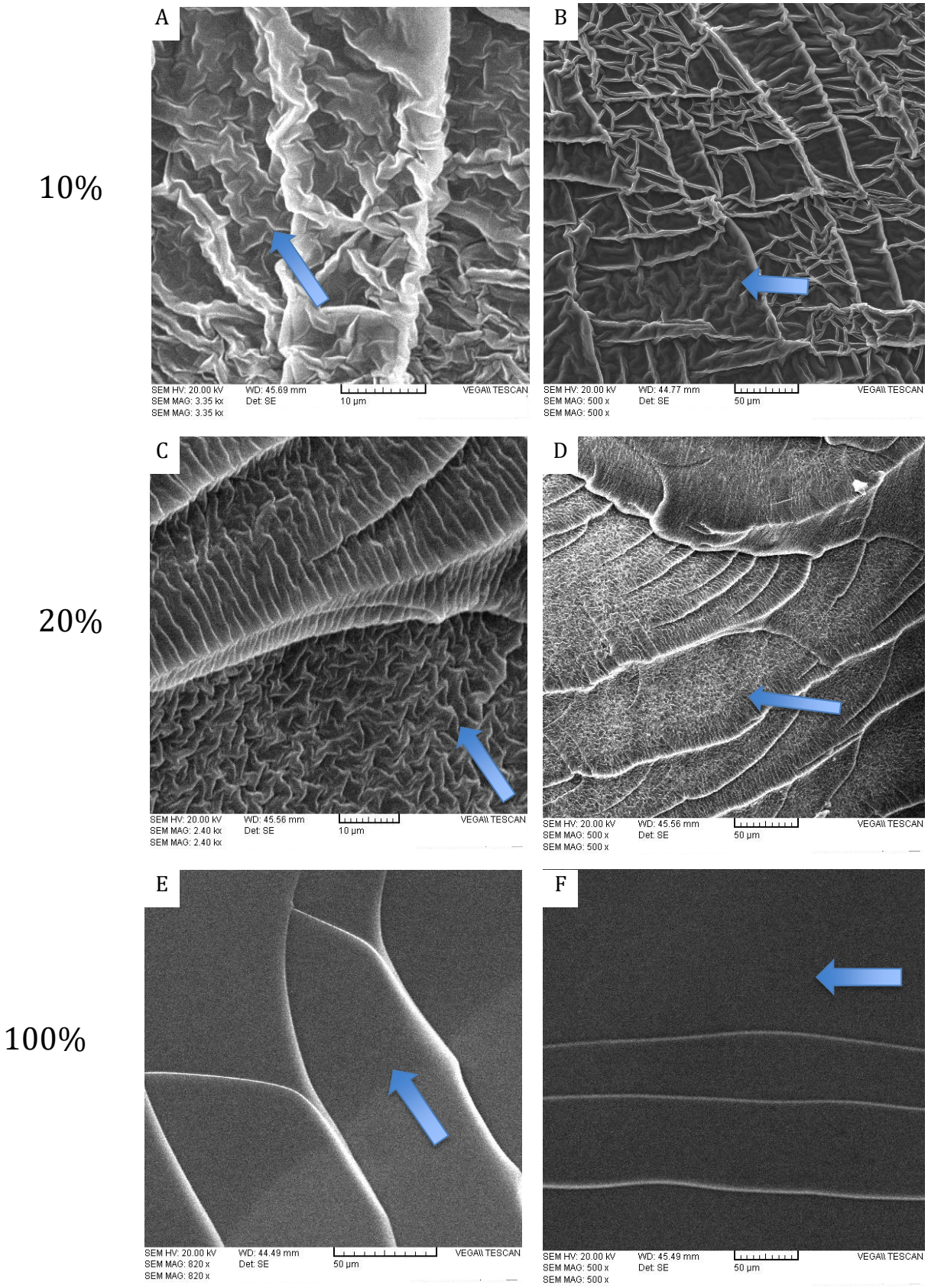

Figure 4.5: SEM analysis of PEGDA hydrogel of various concentrations at multiple scales A: and B: 10% PEGDA hydrogel; C and D: 20% PEGDA hydrogel; E and F: 100% PEGDA hydrogel; Images representative of multiple images. Arrows indicate areas of the overarching surface texture.

Figure 4.5 shows a clear distinction between the surface morphologies of the 10%, and 20% PEGDA hydrogels, and then a stark contrast between these and the 100% PEGDA sample. Panels A and B, in Figure 4.5, represent the lowest concentration of PEGDA tested and demonstrate the highest degree of surface folding and texturing. Panels C and D were produced from a 20% PEGDA hydrogel, producing a texture similar to the 10% gel, but in a more compacted manner. This difference can be seen between the texture density between panels B and D. Finally, panels E and F were produced from a polymerized 100% PEGDA hydrogel, and no texturing can be seen to have occurred. Further magnification than that shown in Figure 4.5 revealed no evidence of surface texture of any kind.

The SEM analysis reveals a clear increase in surface smoothness, as the concentration of PEGDA increases. This result is in concurrence with images taken by a Tescan Vega scanning electron microscope that saw identical surface morphologies. The surface area and surface roughness of a hydrogel would likely facilitate cell attachment and increase cell density within a culture and was thus one of the contributing factors in choosing to utilize a PEGDA hydrogel of as low density as possible in the development of the hydrogel printing system. It should be mentioned that this analysis was done prior to swelling of the gels, as SEM could not effectively take place on wet samples. Thus, additional analysis in the future using alternate techniques to view the PEGDA hydrogels post swelling would be beneficial for a more accurate representation of surface structure in a functioning sample. Atomic Force Microscopy (AFM) would be ideal for this, as the sample could remain hydrated, as this technique does not require a vacuum.

4.3.6 Testing of PEGDA with developed 3D bioprinter unit.

Once testing of the PEGDA hydrogel had taken place, a 20% PEGDA hydrogel had been decided upon for use in the bioreactor system, for its balance between

structural rigidity and surface morphology. Initial testing began by implementing this 20% PEGDA cocktail into the developed 3D bioprinting system and performed prints of increasing complexity on an iterative rapid prototyping basis in order to fine-tune the settings needed for effective printing. The final settings seen to be optimal for the 20% PEGDA hydrogel are shown in Figure 4.6.

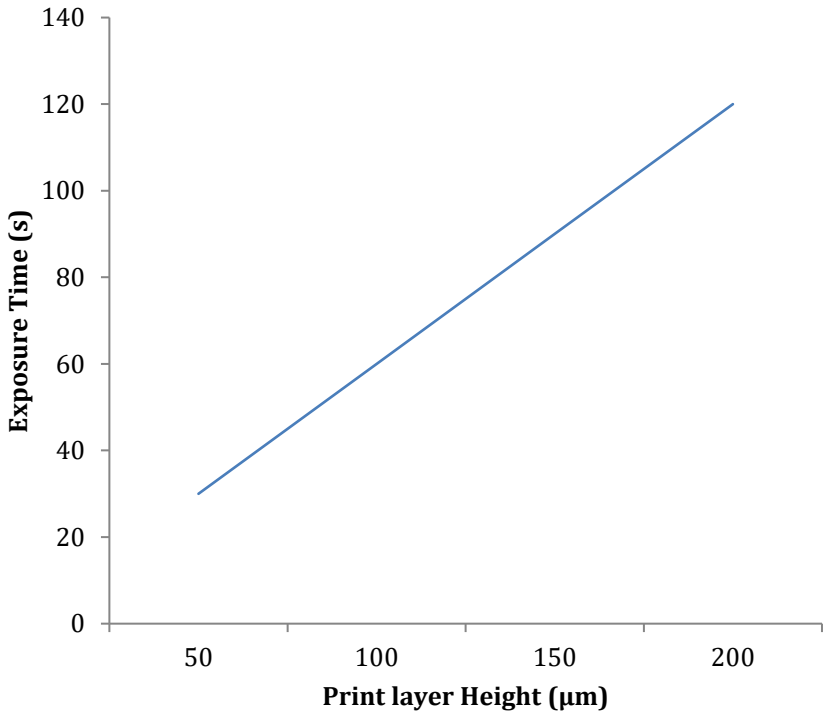

Figure 4.6: Optimal exposure settings for different layer heights found for the developed 3D DLP viable light bioprinter utilizing a 20% PEGDA hydrogel applied through the 'Creation Workshop' printing software.

The settings illustrated in Figure 4.6 were determined through simple trial and error based testing of trial columns containing internal architecture as shown in Figure 4.6, to determine the effective ranges of layer height and exposure time that allowed for an effective print to be produced. These values also represent the limits of layer height, which were achieved using the developed 3D printer and PEGDA hydrogel.

At the lower end, the liquid PEGDA hydrogel itself becomes a limiting factor due to its viscosity and surface tension. When lowering the build layer to below 50 μm on the software, the solid printed layers start to 'pull' the surrounding surface material up over the print surface and hold it in place through surface tension alone, producing a print height of approximately 50 μm regardless of fine-tuning. When forcing the build platform above the surface for each layer to avoid this, the liquid PEGDA simply pools up on top of the print surface in a continuous droplet held together by sheer viscosity and surface tension. If allowed to print in this manner, the print will be produced at a layer height of approximately 75 μm. This is one of the major limiting factors of using a top-down printer configuration, as a bottom-up printer would not be interacting with the liquid surface as its point of solidification. To solve this problem, future iterations of this design could include a skimmer, to run over the surface of the print between each layer.

At the high end, the printer showed capacity to accurately print up to a layer height of around 200 μm. This limit is due to the increased scattering of light through the somewhat opaque liquid as layer height increases, leading to unintentional polymerization of material outside of the intended build shape. This effect is amplified by apparent micro-currents formed within the tank, moving material through the larger layer height space, but can be mitigated by increasing the "wait time" before the projector activates. This allows the movement within the tank to settle, but has a large impact on overall print time. The printer could technically achieve a greater layer height given increased exposure time and longer 'wait-time', but the trade-off with increased print times and decreased print resolution made this unfeasible. To improve upon this, utilizing a more viscous material to prevent fluid movement or one with decreased opacity to decrease scattering may yield better results. It should be also be noted that decreasing the speed of the z-axis motor during layer transitions would also serve to decrease fluid movement within the tank, but

again would significantly add to print time. While an increase in print time would not affect the production of scaffolds for downstream use, it would negatively impact the usability of the printing system for live print applications.

With regard to exposure times, the time required to produce complete layer polymerization depended directly on the size of the layer height but fell within the 30 to 120 second range as described in Figure 4.6. With 30 seconds of exposure time, the printer was able to accurately solidify a layer of the PEGDA hydrogel at an expected layer height of 50 μm. When decreasing the exposure time further, new layers would form inconsistently, leading to subsequent layers to print inaccurately, or detach completely. Increasing the exposure time without changing layer height shows little or no adverse effects aside from increased overall print times. However, after exceedingly long exposure times, printed layers of the PEGDA scaffold become increasingly brittle, no doubt due to the drying out caused by the heat generated during direct light exposure, causing excessive evaporation within the scaffold. At 50 μm, this occurred at around 120 seconds of exposure and greater.

In order to confirm the layer heights were as expected, microscopic imaging was carried out to measure the produced scaffolds post-print. Representative images are shown in Figure 4.7.

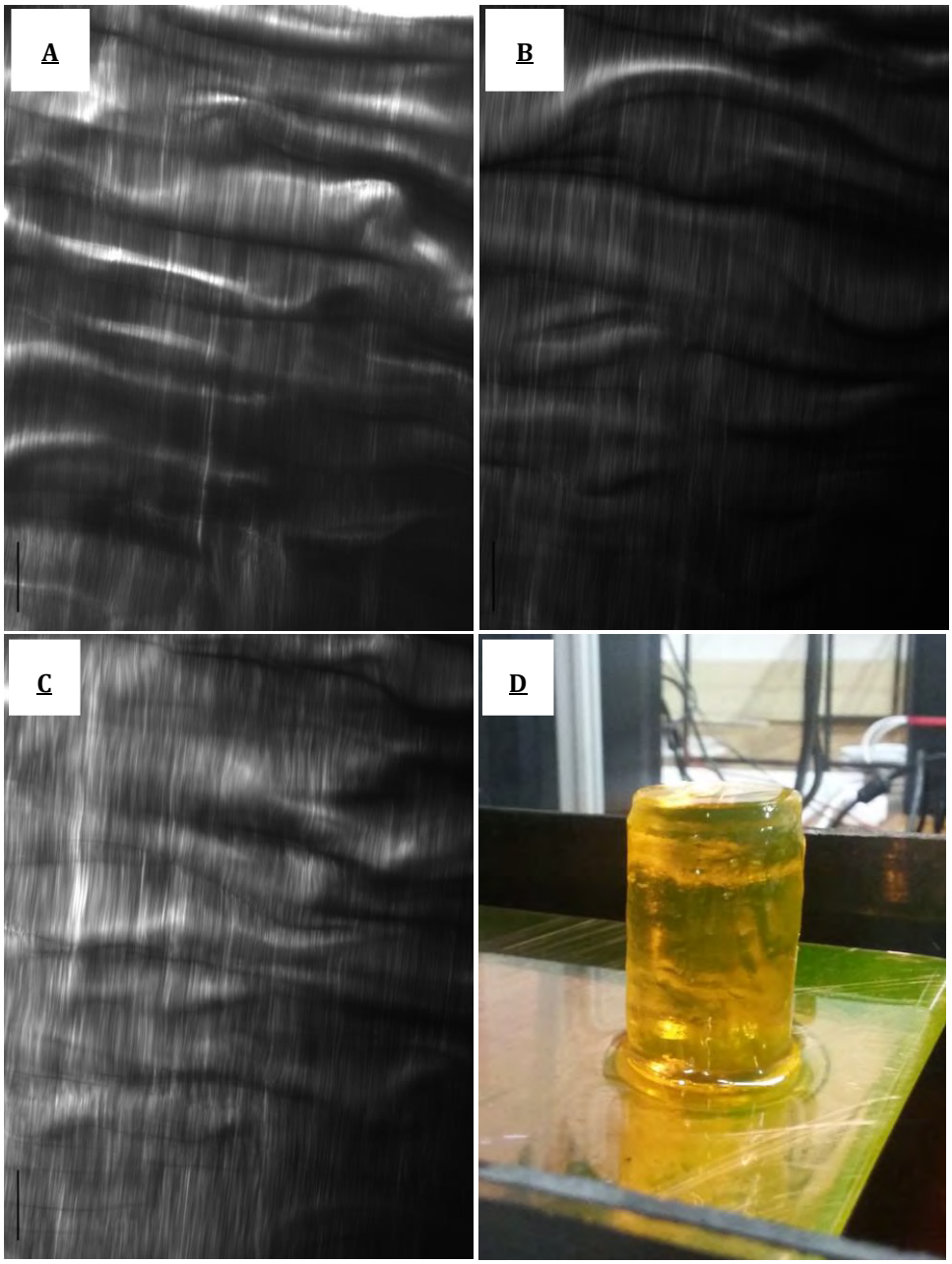

Figure 4.7: Microscopic cross-sections of PEGDA scaffold 3D prints along the Z-axis illustrating individual layer heights (A:C) from a 100 µm print (D) (Vertical scale-bars on images A-C represent 100 µm). Individual layers can be seen running horizontally in images A:C.

Revealed through light microscopy shown in Figure 4.7 is that the layers produced in a single print can vary layer-to-layer. The layer height for a given print is thus better expressed as an "average layer height". It is unclear what is causing the production of these differing layer heights, but differing micro flows of the liquid PEGDA hydrogel in the tank caused by heating and cooling during light exposure may be the cause. These differences seem to occur at a consistent rate, allowing for predictably sized and proportioned prints to be produced regardless. Using the settings described, it was found that the given set up could

print down to an observed average layer height of around 50 µm, and up to a maximum of around 200 µm without loss of print precision or accuracy.

Overall, the PEGDA hydrogel worked well in conjunction with the developed 3D bioprinter, successfully producing spatially defined scaffolds in a consistent manner. An example of a printed scaffold structure is illustrated in Figure 4.8.

Figure 4.8: Images of a 20% PEGDA hydrogel scaffold, 3D printed using the developed visible light 3D bioprinting system at a 100 µm layer height with an intended outer diameter of 17.5 mm (Actual diameter 19 mm) and intended height of 12 mm (Actual height 12 mm).

As noted in the figure legend of Figure 4.8, the actual height of the scaffold produced accurately matched the CAD model of the structure. Once taking into account the troubleshooting steps discussed in Section 2.4.5 to rescale the CAD model, the program accurately slices the model into 120 individual 100 μm slices, printed, and produced a structure of 12 mm height. However, the diameter on the structure, governed by the X/Y resolution of the printer, did inaccurately produce an outer diameter of 19 mm instead of the intended 17.5 mm. This was no doubt due to unintended polymerization of material through light diffraction in the material, thickening the walls and of the structure during printing. This inaccuracy was consistent over the course of the prints but could not be reduced any further with the current setup.

4.3.7 Attachment and culture analysis 3T3-L1 cell line on PEGDA hydrogel scaffolds

The effectiveness of *in vitro* culture on the defined 20% visible light polymerized PEGDA hydrogel was investigated using 3T3-L1 preadipocytes. PEGDA hydrogels were produced to cover the bottom of standard 6-well culture plates, and culture was assessed using trypsinised 3T3-L1 cells at 20 000 cells per well. Attachment to 20% PEGDA was investigated. To improve upon cellular attachment, samples of 20% PEGDA hydrogel incubated with 1% poly-l-lysine were also tested. Staining was then performed using fluorescein diacetate and propidium iodide to assess cell viability on the scaffold. The images taken by florescence and Brightfield microscopy are illustrated in Figure 4.9.

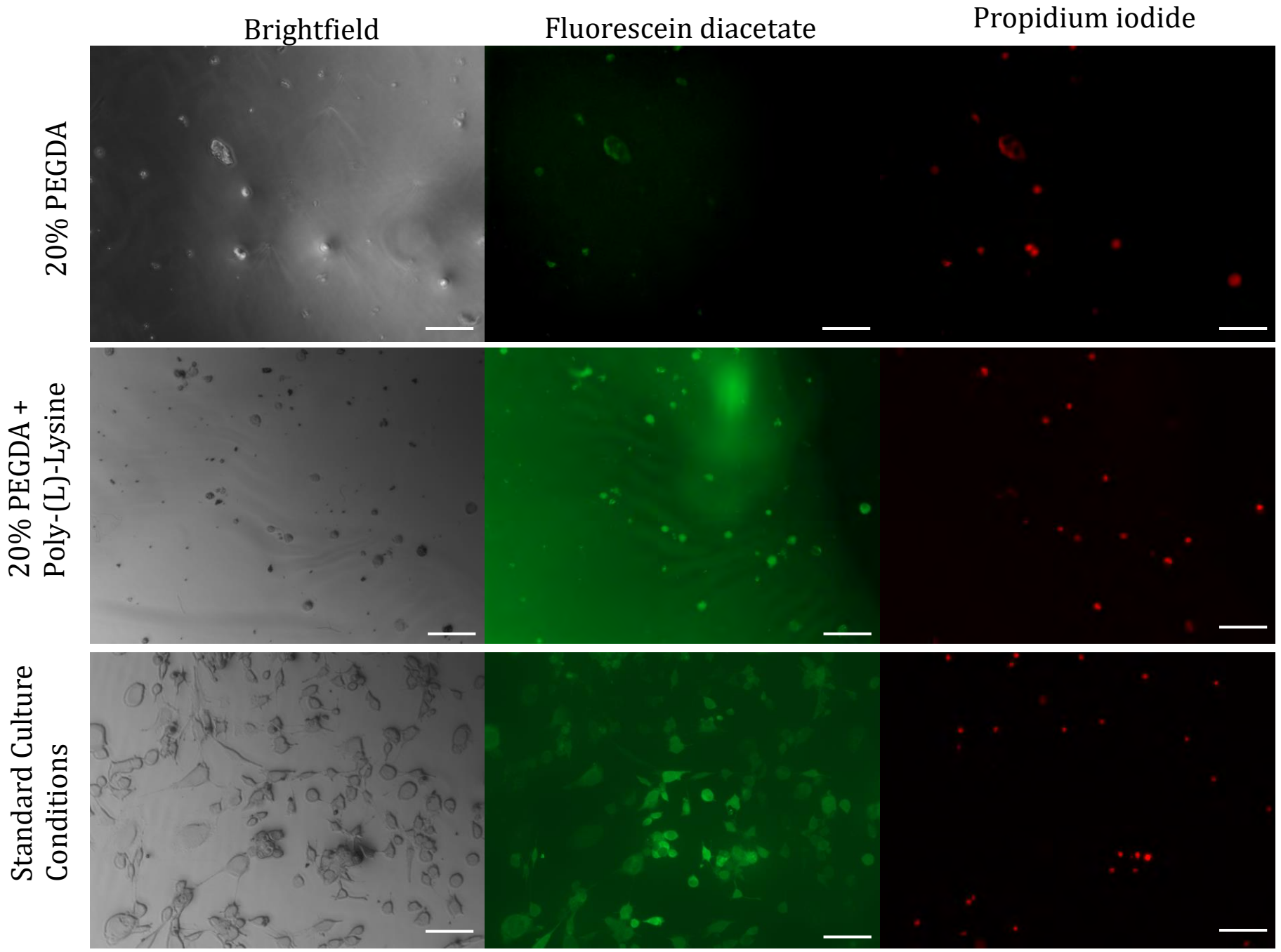

Figure 4.9: Fluorescein diacetate and propidium iodide staining of 3T3-L1 preadipocytes on 20% PEGDA hydrogel; 20% PEGDA hydrogel after incubation with Poly-(L)-Lysine; and under standard culture conditions. Scale bars represent 200 µm. Images representative of multiple images.

The results illustrated in Figure 4.9 illustrate a lack of cellular attachment and proliferation on the 20% PEGDA scaffold in relation to what was achieved on the control surface. This was however not completely unexpected, as many sources have reported PEGDA to be an ineffective culture surface prior to functionalization. The addition of poly-l-lysine did increase the number of cells attached, but had no effect of the survival or proliferation of these cells. In all samples (n=3), the cells that attached to the PEGDA surface were shown to be non-viable through fluorescein diacetate and propidium iodide staining. This is exhibited by the taking up of both dyes, as the taking up of only fluorescein diacetate would indicate a healthy, non-apoptotic phenotype.

Additionally, all cells that successfully attached to the PEGDA hydrogel surface exhibited a rounded morphology, with a greatly reduced diameter in comparison to cells in standard culture conditions. A similar morphology has been observed by (Zhu et al. 2010), showing that this shape was taken by endothelial cells in the hours after seeding on standard PEGDA scaffolds. However, after 24 hours the cells were observed expanding outwards, adopting morphology similar to that of standard 2D culture, which did not occur in the case of the research presented here. It is likely that if the 3T3-L1 cells in this research had remained viable post attachment, a 2D morphology may have been observed. Research by numerous others has demonstrated that through the modification of the PEGDA hydrogel cocktail (Wang, *et al,* 2015), addition of attachment enhancing compounds (Zhu, *et al.,* 2010), and hydrogel charge modification (Tan, *et al,* 2012), can all significantly enhance these attachment characteristics.

It is clear from the attachment profile exhibited that more work is needed to improve the PEGDA cocktail or alter the culture conditions in order to create a viable cell culture environment. The presence of attaching cells and indeed the

literature on the topic does show this being possible, and should be explored further.

The capacity of the bioreactor unit to contain a 3D printed bioscaffold containing cells was then investigated. This was intended to determine whether PEGDA incubated with poly-l-lysine would be able to support cells within the continuous bioreactor environment. Further, the stability of the PEGDA scaffold given the current formulation would be assessed within the bioreactor environment.

The PEGDA scaffold seen in Figure 4.7 was reproduced and incubated in PBS within the bioreactor chamber with 1% poly-l-lysine for 2 hours, after which time it was rinsed with PBS and filled with culture media containing 3T3-L1 cells in suspension. After 24 hours for the cells to adhere, the pumping system was attached and set to supply media at 0.5 ml per hour for 48 hours, including a media change after 24 hours.

Once removed from the chamber and examined under microscopy, no cells were found to have remained attached to the PEGDA scaffold. This is most likely due to the flow of media washing off the cells during culture, resulting from a combination of factors, including the poor attachment and proliferation characteristics observed in section 4.3.7. Further, the dilution factor of 0.05 h^{-1} and associated residence time of 20 h calculated in Section 3.4.2 was lower than the observed cell doubling time of 22.74h calculated in Section 4.3.3. This difference over time would have washed out any unattached cells, as their growth rate would not sufficiently replace those lost.. These characteristics of the system should be improved in future iterations of this project to overcome these limitations, as earlier discussed.

It was observed that the PEGDA hydrogel scaffold had swollen as expected, but maintained its shape and structure within the bioreactor during the experiment.

This result was positive, as any hydrogel used in this application would have to maintain its structure in order to support the culture attached cells long term. While this experiment was relatively brief, it pointed towards the ability of PEGDA based hydrogels to achieve this.

Finally, during experimentation it was noted that the system remained leak-free within the cell culture incubator for the 48 hours of media perfusion, including the single media reservoir exchange. The maintenance of an enclosed and sterile environment is critical for a system designed to maintain mammalian cell culture to prevent contamination. While this alone did not confirm that no contamination occurred, it did illustrate that one of the major objectives of the designed bioreactor and pump system had been achieved. Further testing should be done on even longer term cultures that include a syringe media change to further test this capacity.

5 Chapter 5: Conclusions and future work

5.1. Conclusions

Three dimensional (3D) *in vitro* cell culture is becoming increasingly recognized as the future for tissue engineering and regenerative medicine technologies, as it has the potential to produce cultures far more representative of the native tissue (Antoni et al. 2015). Thus, the development of technologies able to rapidly produce and support 3D mammalian cell cultures will be essential for these fields to develop. The current cost associated with commercial bioprinters is relatively high, decreasing the accessibility of these technologies and slowing progress. In addition, the printing materials themselves are not easily accessible at a low cost. This research was intended to illustrate the feasibility for the development and production of a 3D bioprinter and bioreactor unit at relatively lower cost, and illustrate its implementation for manufacturing of printable hydrogel scaffolds using PEGDA, as a case study.

5.1.1 3D Bioprinter

The developed 3D bioprinter succeeded in the broad aim of allowing for the rapid production of 3D bioscaffolds, in a spatially defined manner. Using the visible light sensitive PEGDA hydrogel system, the developed printer was able to consistently produce designs at a minimum average layer height of approximately 50 μm. Additionally, the printer had the functionality to include two separate print materials, through the implementation of an X-axis sliding tank exchange system. This allows for the potential to include two separate materials within a single print if needed. The entire system successfully utilized

and demonstrated the use of visible light as a polymerization mechanism, avoiding the potential mutagenic effects of UV based DLP systems, expanding its potential for application in live-print applications. This conclusion is backed up by the non-toxic effects of visible light observed by xCELLigence analysis after exposure. However, other similar projects have indicated unfiltered visible light from DLP projectors can have a negative impact when printed with higher exposure times (Wang, 2016).

While the final 3D bioprinter was an effective proof of concept, it suffered a number of shortfalls. In relation to commercially available conventional DLP 3D printers, the prototype was chosen to be top-down, with the intention to help improve adherence of softer hydrogels to the build plate during printing. This, however, forced the printer to be exceptionally large, and require a relatively high substrate volume. With the ultimate goal of live-printing in mind, this larger necessary volume decreased usability in that it would require a high quantity of cells to achieve the same working concentration. The issue of substrate surface tension also became an issue with this top-down approach, with a bottom-up approach being likely able to achieve finer layer height increments. In terms of final cost, the bioprinting unit was R11 000 to produce, far cheaper than commercially available bioprinters. Commercially available bioprinters range from R300 000 ($20 000 USD) up to R4.5m ($300 000 USD) (https://www.aniwaa.com/buyers-guide/3d-printers/3d-bioprinting-3d-bioprinters/, Accessed 05 Sept 2021). Commercial units are also almost exclusively extrusion bioprinters, without the benefits of the DLP system discussed in this thesis.

In relation to the bioprinter developed by Wang *et al* (2015), the prototype developed for this thesis was comparative in many ways. Both systems utilized visible light to avoid the damaging effects of UV based systems on living cells. Further, both systems utilizing the same PEGDA + Eosin Y visible light based substrate approach, although this formulation was modified by Wang *et al* through the addition of gelatin methacrylate.

The two systems differed in that the system developed by Wang *et al* had a primary focus on XY resolution, while the prototype printer developed here sacrificed in this area to provide significantly greater Z axis utility. A future prototype and final product should ideally have the best of both, being able to achieve excellent XY profiles at a functional overall height made from equally fine layering. This difference was at the heart of the differences demonstrated by either system. For instance, Wang *et al* utilized a polymerization time of 2 minutes per layer, while the prototype developed here required only 30 seconds. This difference is accounted for by the Z-axis motor keeping the polymerization depth to a minimum (50 μm) on each layer, while the prints achieved by Wang *et al* were initially deeper requiring the light to diffuse through more material (100 μm). Perhaps more importantly to polymerization speed though, the substrate used in this work used a higher PEGDA concentration of 20%. The work done by Wang *et al* did show impressive live cell encapsulation and micro-patterning thereof, something that was not achieved in this work.

5.1.2 Bioreactor

The developed bioreactor system addressed the issue of continuous 3D cell culture over time within a printed hydrogel. The produced system utilized a forced-perfusion based approach to allow for constant supply of media to 3D hydrogel scaffolds and cultures post-print. Extremely small scaffold designs have a small enough surface area to volume ratio for nutrient transfer by simple diffusion (Asthana & Kisaalita 2012). Larger scaffolds by comparison have been shown to produce nutrient and oxygen deficient areas within their design, leading to unhealthy and ultimately apoptotic cell phenotypes in these instances (Rouwkema et al. 2009). The bioreactor system successfully contained a 3D printed hydrogel scaffold in a watertight environment, and provided fresh media to the bioreactor chamber for a number of days at a consistent rate.

Despite these achievements, a continuous cell culture was not achieved in this thesis, due in combination to attachment, proliferation and flow rate issues. The bioreactor system itself was responsible for the flow rate component of this, and should be one of the main considerations for future designs. The current design likely supplied a flow rate too high for cellular surface attachment to be sustainable, but may have worked for cell encapsulated hydrogel scaffolds.

5.1.3 PEGDA as a substrate for bioprinting

The visible light polymerized PEGDA cocktail was investigated for application within the developed 3D bioprinter and bioreactor system. Its efficacy with regard to subsequent cell adhesion and culture was also explored. PEGDA was shown to be exceedingly effective as a substrate with which to produce 3D scaffolds with the developed 3D printing system. The PEGDA hydrogel cocktail could be printed at a layer height of between 50 μm to 200 μm and produced scaffolds of sufficient strength to be handled and resisted any noticeable degradation within the bioreactor system for 7 days. Exposure time needed to achieve these layer heights ranged from 30 seconds to 120 seconds. This was in line with polymerization times used by Wang. *et al.,* 2016, who found a polymerization time of 120 seconds per layer suitable for their setup. Unfortunately, the 20% PEGDA hydrogel tested resulted in unexceptional cell adhesion and culture characteristics, even after incubation with poly-l-lysine. This is most likely due to the ineffective incorporation of poly-l-lysine onto the PEGDA surface, resulting in a lack of molecular attachment sites available. Thus, this issue should be addressed in future work to produce scaffolds with improved attachment and culture characteristics. This issue has routinely been overcome in other work through the modification of the PEGDA hydrogel, either through the additional of attachment enhancing compounds such as RGD pepides, or though charge modification of the scaffold itself (Tan, *et al.,* 2012).

In summary, the developed bioprinting system, bioreactor and PEGDA hydrogel performed well, and achieved some of the aims set out initially in this research. The 3D bioprinter was able to effectively produce simple, spatially defined 3D scaffolds using a visible light-based controlled deposition system, as set out. The developed printer was affordable in relation to alternate market options, and was acceptably robust in its ability to produce prints that were well defined and consistent. The bioreactor system was successfully able to supply a printed hydrogel scaffold with fresh culture media consistently over a period of 2 days, within an enclosed environment. Finally, PEGDA proved to be exceptionally effective in terms of its printability use structural robustness, but showed to be ineffective for cellular attachment in the current formulation defined by this research. Future research and improvements could and should be implemented onto the work presented, improving upon the aspects presented here.

5.2 Future Work

While the research presented in this thesis did address the research questions set out initially, it has undoubtedly revealed the potential of the technologies presented and could thus be greatly improved. A detailed discussion of improvement that can be implemented to improve upon this research is laid out in the troubleshooting and discussion sections of each chapter. Broadly though, both the bioprinter and bioreactor systems developed have the potential to be improved upon, through either modification or augmentation of existing designs. The PEGDA hydrogel should also be further refined for better cell culture characteristics, as it showed potential within the current configuration. Alternatively, other hydrogel options could be investigated. Once improved, the technologies showcased here should be capable of exceedingly precise

production of hydrogel scaffolds and allow for their long-term maintenance for enhanced mammalian cell culture.

5.2.1 3D Bioprinter

The developed 3D bioprinter unit fulfilled the aims and expectations set out prior to design and construction. However, a number of alterations and additions to the current setup should be implemented to improve its effectiveness. Some of these improvements specific to particular components have already been discussed in Chapter 2.4, but there are still a number of general changes that should be considered for future versions.

One such major improvement is the inclusion of an enclosed casing for the printer. This casing would fully enclose and make up the walls of the printer, and would be slotted into the frame itself. A completed casing would be essential for version 2.0 of the printer, as it would provide an enclosed print space capable of being sterilized for cell culture work, taking inspiration from traditional biosafety cabinet designs with a HEPA filtration unit. Additionally, the casing should be dark tinted, to allow for work with hydrogels with increased light sensitivity. The implementation of an enclosure would bring about additional challenges such as the need for ventilation, to offset heat produced by the projector, which would potentially need to be monitored. A proposed design update to address this can be seen in Figure 5.1.

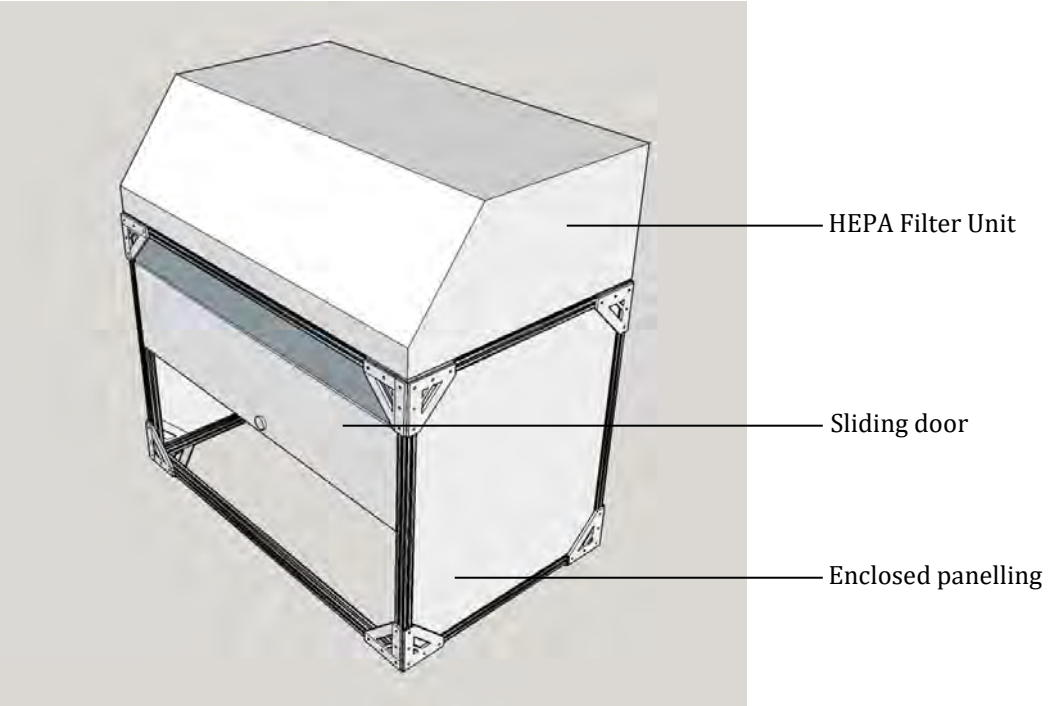

Figure 5.1: Updated 3D bioprinter frame design for improved sterility and protection from light through modification with an enclosed HEPA filter system.

Other augmentations of the design presented could be carried out through the inclusion of upgraded components. The increasing of fill density of all 3D printed PLA parts would lead to all round better structural integrity, now that designs for these parts have been confirmed to be effective. The use of different plastics such as ABS in part manufacture could further improve upon this. All parts fixed to the frame of the unit were done so via 4 mm x 12 mm bolts and standard conjoining nuts. In some of the later added components however, 4 mm T-slot specific nuts with bearing sliders replaced these standard nuts. While the standard nuts worked sufficiently, it is recommended that future iterations should include T-slot specific nuts in all part for their ease of access and effectiveness within the T-slot profile framework.

Finally, the dual tank system implemented in the printer design was not utilized in this research. Future versions of the printer would make use of this feature to

provide a streamlined exchange between tanks during a single print. The printing software used for the current set up does not include this functionality, and thus custom software would need to be developed to fully take advantage of this feature. In addition, the design software used to design the scaffold shapes does not have functionality to designate multiple materials on a single construct. These issues could be temporarily overcome by running separate prints of complimentary scaffold models in sequence. However, for an elegant and seamless system, a significant amount of software development will be required to allow for the system to be used at its full potential. When put into place, a two-tank system would be able to produce scaffolds with combined structural or biological properties. This would significantly expand upon experimental capability of the system as a whole, as it would be able to accommodate the production of more complex experimental setups.

5.2.2 Bioreactor and media pump system

Overall, the bioreactor and pumping system worked as intended, but still leaves lots of room for improvement. The unit was successfully able to maintain the flow of media through the developed bioreactor unit at a constant rate over time. The system remained sealed and entirely free of leaks during media perfusion, with no sign of internal contamination during testing. That being said, the system could benefit from a number of improvements for future iterations, particularly in the area of user friendliness and overall functionality.

The major issue facing the current generation design of the bioreactor and pump system is the difficulty encountered when resetting or refilling the media in the unit. This is caused by the lack of an effective way to detach components while maintaining a seal for both the component, and the rest of the system. This was crudely countered by using crocodile clips on the silicone tubing during exchanges, but still introduced small amounts of air into the system on occasion.

In addition, filling the system with media prior to running an experiment was difficult to manage. Briefly, this was achieved by holding a disconnected outflow tube above the level of the mounted components and allowing media be extruded into the system until reaching the end of the outflow pipe. Once the media level reaches the end, it is carefully connected to a filled syringe reservoir that would then act at input for the subsequent run, with the syringe having just extruded to fill the system becoming the output. If this technology intends to replace standard 2D culture techniques, it needs to be just as easy to use if not more so. Ideally, future iterations will address this concern and make the system as easy to use as simply removing an emptied reservoir and clipping a new one into place when required.

Future iterations of this prototype should also seek to improve upon and accommodate a far better flow rate of media over time. The current system was limited to a reservoir of 20 ml, making long-term and truly continuous culture impossible without frequent refilling. Further, the use of a stepper motor to drive the pump meant that the movement of media through the system occurred in infrequent steps. While this did achieve a consistent flow of media over time, it was discontinuous in nature. The flow rate of the current system was also likely fast relative the growth rate and adherence capability of the cells being tested. A more optimal flow rate should be investigated going forward, to provide improved long term culture conditions in future experiments. Accommodating this change will almost certainly require a fundamental redesign of the pumping mechanism.

Finally, future iterations of the bioreactor system should include a suite of sensors to monitor the temperature, oxygen/CO^2 content and flow rate parameters throughout the system during operation. This would allow for a better understanding of the conditions present within the reactor, and allow them to be adjusted accordingly. Ideally, the system would be set up to modify itself based on predetermined operational parameters, for example adjusting external incubator temperature to keep the bioreactor's internal temperature at

a set point. This concept could be applied to any of the key operating conditions of the bioreactor system. A diagrammatic representation of this concept can be seen below in Figure 5.2.

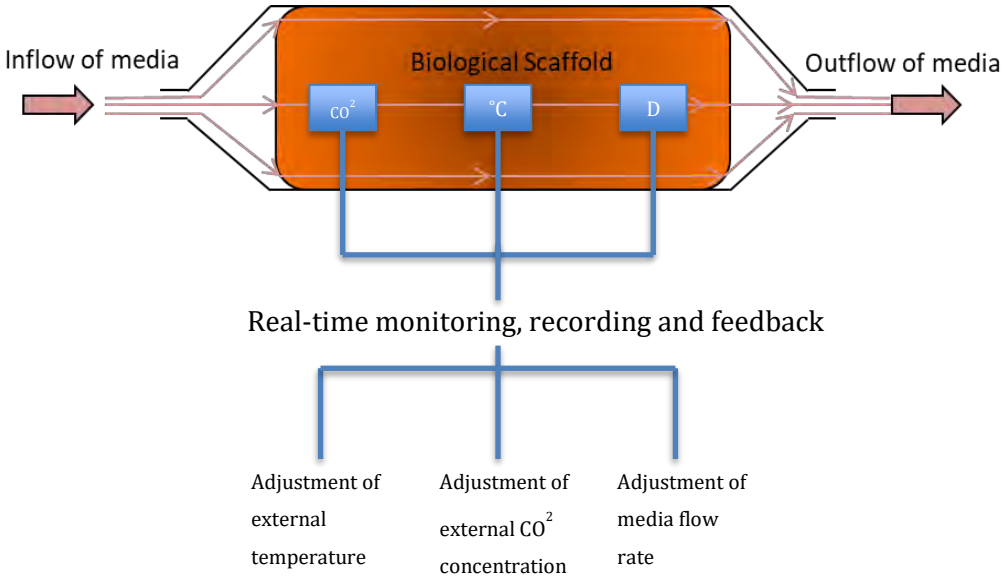

Figure 5.2: Diagrammatic representation of potential internal bioreactor sensor system, demonstrating feedback mechanisms for CO2, temperature, or flow rate (D).

5.2.3 PEGDA hydrogel

The PEGDA hydrogel formulation tested was partially successful in terms of achieving the overall aims. In terms of printability, the 20% PEGDA solution was shown to be highly effective in producing spatially defined 3D scaffolds with minimal post print swelling. In addition, initial toxicity analysis demonstrated that the reagents used in the formulation were sufficiently non-toxic at well above their working concentrations. Despite this, culture testing showed that cells had difficulty remaining attached and surviving on printed scaffolds.

To overcome these difficulties, a number of steps can be taken in future work to pinpoint and overcome these issues. It was decided to move ahead with using a 20% PEGDA solution for its improved printability, in terms of both print speed and structural integrity. Therefore, future experiments should consider a comparative study of cellular attachment on gels of varying density, followed by an optimization of printability for the formulation that exhibits optimal attachment. This could be further investigated by using PEGDA of different molecular mass, as this study only focused on PEGDA of 700 Da. PEGDA of increased molecular weight may reduce printability, but may allow for increased cellular attachment due to increased pore sizes.

Future experimentation should focus on the functionalization and attachment protocols used. In this research, gels were only briefly rinsed with PBS before functionalization with PLL. Further experimentation may reveal the need to allow the gels to more fully swell before rinsing, or indeed need to be rinsed more thoroughly before experimentation. While the reagents used to produce the PEGDA gel was shown to be non-toxic, they may be inhibiting the attachment of cells to the hydrogel surface.

Finally, it would be important to investigate other avenues of functionalization of the PEGDA scaffold post-print. Other groups have shown improved attachment and viability after functionalization various compounds. Most notable of these are RGD peptides, which have been shown to directly influence and enhance cell adhesion on PEGDA hydrogels (Wang, *et al.,* 2005)(Xueshan, 2006). Future testing into PEGDA as a scaffold material should include an in-depth analysis of the various functionalization options available with regard to their ability to improve cell viability during culture over time. In conjunction, the entrapment of

cells within the PEGDA hydrogel should be investigated to assess the capacity of the scaffold to produce cultures of this nature.

By refining both the printability and improved cellular attachment and viability issues that have presented in v1.0, future work will be able to focus on the application of the printer in producing scaffolds that incorporate more complex biomimetic structures. Ultimately, improved versions of this prototype should be able to effectively replicate highly complex structures for a variety of applications.

6 Chapter 6: References

Abu-Absi, N.R. et al., 2011. Real time monitoring of multiple parameters in mammalian cell culture bioreactors using an in-line Raman spectroscopy probe. *Biotechnology and Bioengineering*, 108(5).

Ahmad, S. et al., 2007. Differentiation of Human Embryonic Stem Cells into Corneal Epithelial-Like Cells by In Vitro Replication of the Corneal Epithelial Stem Cell Niche. *Stem Cells*, 25(5), pp.1145–1155.

Ahmed, T.A.E., Dare, E. V. & Hincke, M., 2008. Fibrin: a versatile scaffold for tissue engineering applications. *Tissue Engineering Part B: Reviews*, 14(2), pp.199–215.

Almany, L. & Seliktar, D., 2005. Biosynthetic hydrogel scaffolds made from fibrinogen and polyethylene glycol for 3D cell cultures. *Biomaterials*, 26(15), pp.2467–2477.

Ameri, K., Samurkashian, R. & Yeghiazarians, Y., 2017. Three-Dimensional Bioprinting Emerging Technology in Cardiovascular Medicine. *Circulation*, 135(14), pp.1281–1283.

Anjum, F. et al., 2017. Tough , Semisynthetic Hydrogels for Adipose Derived Stem Cell Delivery for Chondral Defect Repair. *Macromolecular Bioscience*, pp.1–13.

Antoine, E.E., Vlachos, P.P. & Rylander, M.N., 2014. Review of Collagen I Hydrogels for Bioengineered Tissue Microenvironments: Characterization of Mechanics, Structure, and Transport. *Tissue Engineering Part B: Reviews*, 20(6), pp.683–696.

Antoni, D. et al., 2015. Three-Dimensional Cell Culture : A Breakthrough in Vivo. *International Journal of Molecular Sciences*, 16, pp.5517–5527.

Arcaute, K., Mann, B. & Wicker, R., 2014. Stereolithography of Three-Dimensional Bioactive Poly (Ethylene Glycol) Constructs with Encapsulated Cells Stereolithography of Three-Dimensional Bioactive Poly (Ethylene Glycol) Constructs with Encapsulated Cells. *Annals of Biomedical Engineering*, 34(9), pp.1429–1441.

Asthana, A. & Kisaalita, W., 2012. Microtissue size and hypoxia in HTS with 3D cultures. *Drug Discovery Today*, 17(15–16), pp.810–817. Available at: http://dx.doi.org/10.1016/j.drudis.2012.03.004.

Attar, E., 2011. *Simulation of Selective Electron Beam Melting Processes*

Augst, A. Kong, H. Mooney, D. 2006. Alginate Hydrogels as Biomaterials. Macromolecular Bioscience. 6(8), pp. 623-633.

Baden, T. Chagas, AM. Gage, GJ. Marzullo, TC. Prieto-Godino, LL. Euler, T. 2015. Open Labware: 3-D Printing Your Own Lab Equipment. PLoS Biol 13(3): e1002086. pmid:25794301

Bahney, C. et al., 2016. VISIBLE LIGHT PHOTOINITIATION OF MESENCHYMAL STEM CELL-LADEN BIORESPONSIVE HYDROGELS. *European Cells & Materials*, 22, pp.43–55.

Bail, R. et al., 2013. The effect of a type I photoinitiator on cure kinetics and cell toxicity in projection-microstereolithography. *Procedia - Social and Behavioral Sciences*, 5, pp.222–225. Available at: http://dx.doi.org/10.1016/j.procir.2013.01.044.

Birgersdotter, A., Sandberg, R. & Ernberg, I., 2005. Gene expression perturbation in vitro—A growing case for three-dimensional (3D) culture systems. *Seminars in Cancer Biology*, 15(5), pp.405–412.

Brajlih, T. et al., 2011. Speed and accuracy evaluation of additive manufacturing machines. *Rapid Prototyping Journal*, 17(1), pp.64–75.

Brash, D.E. et al., 1991. A role for sunlight in skin cancer : UV-induced p53

mutations in squamous cell carcinoma. *Proceedings of the National Academy of Sciences of the United States of America*, 88(November), pp.10124–10128.

Brennand, K.J. et al., 2011. Modelling schizophrenia using human induced pluripotent stem cells. *Nature*, 473(7346), pp.221–225.

Briggs, J. et al., 2007. OPERATIONAL REVIEW OF THE NORTH HEAD MEMBRANE BIOREACTOR IN SYDNEY, AUSTRALIA. *Proceedings of the Water Environment Federation*, pp.8567–8581.

Browne, S.M. & Al-Rubeai, M., 2007. Selection methods for high-producing mammalian cell lines. *Trends in Biotechnology*, 25(9), pp.425–432.

Browning, M. et al., 2015. Determination of the in vivo degradation mechanism of PEGDA hydrogels. *Journal of Biomedical Materials Research - Part A*, 102(12), pp.4244–4251.

Caliari, S.R. & Burdick, J.A., 2016. A practical guide to hydrogels for cell culture. *Nature Methods*, 13(5), pp.405–414.

Carlson, A.L. et al., 2016. Generation and transplantation of reprogrammed human neurons in the brain using 3D microtopographic scaffolds. *Nature Communications*, 7.

Chen, C. et al., 2015. 3D Porous Calcium-Alginate Scaffolds Cell Culture System Improved Human Osteoblast Cell Clusters for Cell Therapy. *Theranostics*, 5(6), pp.643–655.

Cheung, H.Y. et al., 2007. A critical review on polymer-based bio-engineered materials for scaffold development. *Composites Part B: Engineering*, 38(3), pp.291–300.

Chiu, Y.C. et al., 2011. The role of pore size on vascularization and tissue remodeling in PEG hydrogels. *Biomaterials*, 32(26), pp.6045–6051.

Cui, X. et al., 2012. Thermal inkjet printing in tissue engineering and regenerative medicine. *Recent patents on drug delivery & formulation*, 6(2), pp.149–155.

Cukierman, E. et al., 2001. Taking cell-matrix adhesions to the third dimension. *Science*, 294(5547), pp.1708–1712.

Deforest, C.A., Sims, E.A. & Anseth, K.S., 2010. Peptide-functionalized click hydrogels with independently tunable mechanics and chemical functionality for 3D cell culture. *Chemistry of Materials*, 22(16), pp.4783–4790.

Derby, B., 2008. Bioprinting: Inkjet printing proteins and hybrid cell-containing materials and structures. *Journal of Materials Chemistry*, 18(47), pp.5717–5721.

Desi, E. et al., 2012. Critical factors affecting cell encapsulation in superporous hydrogels. *Biomedical Materials*, 7(2):024108.

Di, L. & Obach, R.S., 2015. Addressing the Challenges of Low Clearance in Drug Research. *The AAPS Journal*, 17(2), pp.352–357.

Drury, J.L. & Mooney, D.J., 2003. Hydrogels for tissue engineering: Scaffold design variables and applications. *Biomaterials*, 24(24), pp.4337–4351.

Du Plessis, A., et al., 2019. Beautiful and functional: a review of biomimetic design in additive manufacturing. Additive Manufacturing, 27, pp.408-427.

Dudek, P., 2013. FDM 3D printing technology in manufacturing composite elements. *Archives of Metallurgy and Materials*, 58(4), pp.1415–1418.

Durst, C.A. et al., 2015. Flexural characterization of cell encapsulated PEGDA hydrogels with applications for tissue engineered heart valves. *Acta Biomaterialia*, 7(6), pp.2467–2476.

Duval, K. et al., 2017. Modeling Physiological Events in 2D vs. 3D Cell Culture. *Physiology*, 32(4), pp.266–277.

Edalat, F. et al., 2012. Material strategies for creating artificial cell-instructive niches. *Current Opinion in Biotechnology*, 23(5), pp.820–825.

Edmondson, R. et al., 2014. Three-Dimensional Cell Culture Systems and Their

Applications in Drug Discovery and Cell-Based Biosensors. *ASSAY and Drug Development Technologies*, 12(4), pp.207–218.

Engler, A.J. et al., 2006. Matrix Elasticity Directs Stem Cell Lineage Specification. *Cell*, pp.677–689.

El-Sherbiny, I. & Yacoub, M., 2013. Hydrogel scaffolds for tissue engineering: Progress and challenges. *Global cardiology science & practice*,(3), pp.316–342.

Fairbanks, B. et al., 2009. Photoinitiated polymerization of PEG-diacrylate with lithium phenyl-2,4,6-trimethylbenzoylphosphinate: polymerization rate and cytocompatibility. *Biomaterials*, 30(35), pp.6702–6707.

Fantini, M. & Curto, M., 2018. Interactive design and manufacturing of a Voronoi-based biomimetic bone scaffold for morphological characterization. *International Journal on Interactive Design and Manufacturing*, 12(2), pp.585–596.

Finnes, T., 2015. High Definition 3D Printing – Comparing SLA and FDM Printing Technologies. *The Journal of Undergraduate Research*, 13(13).

Freshney, R.I., 2011. *Culture of Animal Cells: A Manual of Basic Technique and Specialized Applications: Sixth Edition*,

Gospodarowicz, D., Greenburg, G. & Birdwell, C.R., 1978. Determination of Cellular Shape by the Extracellular Matrix and Its Correlation with the Control of Cellular Growth. *Cancer Research*, 38(11), pp.4155–4171.

Gross, B.C. et al., 2014. Evaluation of 3D printing and its potential impact on biotechnology and the chemical sciences. *Analytical Chemistry*, 86(7), pp.3240–3253.

Gudapati, H., Dey, M. & Ozbolat, I., 2016. A comprehensive review on droplet-based bioprinting: Past, present and future. *Biomaterials*, 102, pp.20–42.

Gupta, N. et al., 2016. Micro fluidics-based 3D cell culture models : Utility in novel drug discovery and delivery research. *Bioengineering and Translational Medicine*, pp.63–81.

Gungor-Ozkerim, S. et al., 2018. Bioinks for 3D bioprinting: an overview. *Biomaterial Science* 6(5) pp 915 - 946.

Grigoryan, B. et al., 2019. Multivascular networks and functional intravascular topologies within biocompatible hydrogels. *Biomedicine*, 364(6439), pp.458–464.

He, Y. et al., 2014. Cell-culture models of the blood-brain barrier. *Stroke*, 45(8), pp.2514–2526.

Hess, M.W. et al., 2010. 3D versus 2D cell culture. Implications for electron microscopy. *Methods in Cell Biology*, 96, pp.649–670.

Hidalgo-Bastida, L.A. et al., 2012. Modeling and design of optimal flow perfusion bioreactors for tissue engineering applications. *Biotechnology and Bioengineering*, 109(4), pp.1095–1099.

Hongisto, V. et al., 2013. High-Throughput 3D Screening Reveals Differences in Drug Sensitivities between Culture Models of JIMT1 Breast Cancer Cells. *PLoS ONE*, 8(10).

Horch, R.E. et al., 2005. Tissue engineering of cultured skin substitutes. *Journal of Cellular and Molecular Medicine*, 9(3).

Hospodiuk, M. et al., 2017. The bioink: A comprehensive review on bioprintable materials. *Biotechnology Advances*, 35(2), pp.217–239.

Huh, D. et al., 2012. Microengineered physiological biomimicry: Organs-on-Chips. *Lab on a Chip*, 12(12), pp.2156–2164.

Hwang, S. et al., 2015. Thermo-mechanical Characterization of Metal/Polymer Composite Filaments and Printing Parameter Study for Fused Deposition Modeling in the 3D Printing Process. *Journal of Electronic Materials*, 44(3),

pp.771–777.

Ikehata, H. & Ono, T., 2011. The Mechanisms of UV Mutagenesis. *Journal of Radiation Research*, 125, pp.115–125.

Imamura, Y. et al., 2015. Comparison of 2D- and 3D-culture models as drug-testing platforms in breast cancer. *Oncology Reports*, 33(4), pp.1837–1844.

Jain, P. & Kuthe, A.M., 2013. Feasibility study of manufacturing using rapid prototyping: FDM approach. *Procedia Engineering*, 63, pp.4–11.

Kandow, C.E. et al., 2007. Polyacrylamide Hydrogels for Cell Mechanics: Steps Toward Optimization and Alternative Uses. *Methods in Cell Biology*, 83, pp.29–46.

Kenny, P.A. et al., 2007. The morphologies of breast cancer cell lines in three-dimensional assays correlate with their profiles of gene expression. *Molecular Oncology*, 1(1), pp.84–96.

Kerbrat, O., Mognol, P. & Hascoet, J.Y., 2010. Manufacturability analysis to combine additive and subtractive processes. *Rapid Prototyping Journal*, 16(1), pp.63–72.

Kfoury, Y. & Scadden, D.T., 2015. Mesenchymal cell contributions to the stem cell niche. *Cell Stem Cell*, 16(3), pp.239–253.

Khoruzhenko, A.I., 2011. 2D- and 3D-cell culture. *Biopolymers and Cell*, 27(1), pp.17–24.

Kim, M. et al., 2017. Passage-dependent accumulation of somatic mutations in mesenchymal stromal cells during in vitro culture revealed by whole genome sequencing. *Scientific Reports*, 7, pp.1–10. Available at: http://dx.doi.org/10.1038/s41598-017-15155-5.

Krish, S., 2011. A practical generative design method. *Computer-Aided Design*, 43(1), pp.88–100.

Kurniawan, N., 2019. The ins and outs of engineering functional tissues and organs: evaluating the in-vitro and in-situ processes, *Current Opinion in Organ Transplantation*. 24(5), pp.590-597

Lamhamedi-Cherradi, S.E. et al., 2014. 3D tissue-engineered model of Ewing's sarcoma. *Advanced Drug Delivery Reviews*, 79–80, pp.155–171.

Lee, J. et al., 2009. In vitro toxicity testing of nanoparticles in 3D cell culture. *Small*, 5(10), pp.1213–1221.

Lee, J.M. & Yeong, W.Y., 2016. Design and Printing Strategies in 3D Bioprinting of Cell-Hydrogels: A Review. *Advanced Healthcare Materials*, 5(22), pp.2956–2865.

Leipzig, N.D. & Shoichet, M.S., 2009. The effect of substrate stiffness on adult neural stem cell behavior. *Biomaterials*, 30(36), pp.6867–6878.

Lim, K.S. et al., 2016. New Visible-Light Photoinitiating System for Improved Print Fidelity in Gelatin-Based Bioinks. *ACS Biomaterials Science and Engineering*, 2(10), pp.1752–1762.

Lutolf, M.P., Gilbert, P.M. & Blau, H.M., 2009. Designing materials to direct stem-cell fate. *Nature*, 462, pp.433–441.

Lutolf, M.P. & Hubbell, J.A., 2005. Synthetic biomaterials as instructive extracellular microenvironments for morphogenesis in tissue engineering. *Nature Biotechnology*, 23(1), pp.47–55.

Malda, J., Klein, T.J. & Upton, Z., 2007. The Roles of Hypoxia in the In Vitro Engineering of Tissues. *Tissue Engineering*, 13(9), pp.2153–2162.

Mannoor, M.S. et al., 2013. 3D printed bionic ears. *Nano Letters*, 13(6), pp.2634–2639.

Matsuda, Y. et al., 2010. Morphological and cytoskeletal changes of pancreatic cancer cells in three-dimensional spheroidal culture. *Medical Molecular Morphology*, 43, pp.211–217.

Mazzoccoli, J. et al., 2011. Mechanical and Cell Viability Properties of Crosslinked Low and High Molecular Weight Poly(ethylene glycol) Diacrylate Blends. *Journal of Biomedical Materials Research - Part A*, 93(2), pp.558–566.

Meli, L. et al., 2012. Influence of a three-dimensional, microarray environment on human Cell culture in drug screening systems. *Biomaterials*, 33(35), pp.9087–9096.

Min, S., Ko, I. K., & Yoo, J. J. 2019. State-of-the-Art Strategies for the Vascularization of Three-Dimensional Engineered Organs. Vascular specialist international, 35(2), 77–89.

Moore, P. et al., 2005. Brief Report Effect of Wavelength on Low-Intensity Laser Irradiation-Stimulated Cell Proliferation In Vitro. *Lasers in Surgery and Medicine*, 12(October 2004), pp.8–12.

Mulukutla, B.C., Gramer, M. & Hu, W.S., 2012. On metabolic shift to lactate consumption in fed-batch culture of mammalian cells. *Metabolic Engineering*, 14(2), pp.138–149.

Murr, L.E. et al., 2012. Fabrication of metal and alloy components by additive manufacturing: Examples of 3D materials science. *Journal of Materials Research and Technology*, 1(1), pp.42–54.

Nagel, B., Dellweg, H. & Gierasch, L., 1992. GLOSSARY FOR CHEMISTS OF TERMS USED. *Pure and Applied Chemistry*, 64(1), pp.143–168.

Nair, L.S. & Laurencin, C.T., 2007. Biodegradable polymers as biomaterials. *Progress in Polymer Science (Oxford)*, 32(8–9), pp.762–798.

Newman, S.T. et al., 2015. Process planning for additive and subtractive manufacturing technologies. *CIRP Annals - Manufacturing Technology*, 64(1), pp.467–470.

Nguyen, K. & West, J., 2002. Photopolymerizable hydrogels for tissue engineering applications. *Biomaterials*, 23, pp.4307–4314.

Nielsen, H.I. & Bertheussen, K., 1991. *DEGRADING EFFECT OF LIGHT ON CELL CULTURE MEDIA*, Butterworth-Heinemann Ltd. Available at: http://dx.doi.org/10.1016/B978-0-7506-1103-9.50026-3.

Nikitina, V. et al., 2018. Clonal chromosomal and genomic instability during human multipotent mesenchymal stromal cells long-term culture. *PLoS ONE*, pp.1–14.O'Brien, F.J., 2011. Biomaterials & scaffolds for tissue engineering. *Materials Today*, 14(3), pp.88–95.

Obradovic, B. et al., 1999. Gas exchange is essential for bioreactor cultivation of tissue engineered cartilage. *Biotechnology and Bioengineering*, 63(2), pp.197–205.

Ozbolat, I.T. & Hospodiuk, M., 2016. Current advances and future perspectives in extrusion-based bioprinting. *Biomaterials*, 76, pp.321–343.

Page, H., Flood, P. & Reynaud, E.G., 2013. Three-dimensional tissue cultures: Current trends and beyond. *Cell and Tissue Research*, 352(1), pp.123–131.

Pampaloni, F., Reynaud, E.G. & Stelzer, E.H.K., 2007. The third dimension bridges the gap between cell culture and live tissue. *Nature Reviews Molecular Cell Biology*, 8(10), pp.829–845.

Pandian, A. & Belavek, C., 2016. A review of recent trends and challenges in 3D printing. In *Proceedings of the 2016 ASEE North Central Section Conference*. pp. 1–17.

Paris, H. et al., 2016. Comparative environmental impacts of additive and subtractive manufacturing technologies. *CIRP Annals - Manufacturing Technology*, 65(1), pp.29–32.

Park, J. et al., 2018. A 3D human triculture system modeling neurodegeneration and neuroinflammation in Alzheimer's disease. *Nature Neuroscience*, 21, pp.941–951. Available at: http://dx.doi.org/10.1038/s41593-018-0175-4.

Passino, K.M., 2005. *Biomimicry for Optimization, Control, and Automation*,

Pati, F. et al., 2015. Extrusion bioprinting. In *Essentials of 3D Biofabrication and Translation*. pp. 123–152.

Pearce, J.M. et al., 2010. 3-D Printing of Open Source Appropriate Technologies for Self-Directed Sustainable Development. *Journal of Sustainable Development*, 3(4), pp.17–29.

Pennesi, G. et al., 2011. Regulatory influence of scaffolds on cell behavior: how cells decode biomaterials. *Current pharmaceutical biotechnology*, 12(2), pp.151–159.

Persano, L. et al., 2018. 3D printing of optical materials: an investigation of the microscopic properties. *Organic Photonic Materials and Devices*, 10529.

Phelan, M.C., 2007. Basic techniques in mammalian cell tissue culture. *Current Protocols in Cell Biology*, 36(1).

Powers, M.J. et al., 2002. A Microfabricated Array Bioreactor for Perfused 3D Liver Culture. *Biotechnology and Bioengineering*, 78(3), pp.257–269.

Raman, R. & Bashir, R., 2015. Stereolithographic 3D bioprinting for biomedical applications. *Essentials of 3D Biofabrication and Translation*, pp.89–121.

Rekowska, N. et al., 2019. Biocompatibility and thermodynamic properties of PEGDA and two of its copolymers. In *1st Annual International Conference of the IEEE Engineering in Medicine and Biology Society (EMBC)*. IEEE, pp. 1093–1096.

Rouwkema, J. et al., 2009. Supply of Nutrients to Cells in Engineered Tissues. *Biotechnology and Genetic Engineering Reviews*, 26, pp.163–178.

Saha, K. et al., 2007. Designing synthetic materials to control stem cell phenotype. *Current Opinion in Chemical Biology*, 11(4), pp.381–387.

Sass, L. & Oxman, R., 2006. Materializing design: The implications of rapid prototyping in digital design. *Design Studies*, 27(3), pp.325–355.

Scadden, D.T., 2006. The stem-cell niche as an entity of action. *Nature*, 441,

pp.1075–1079.

Schmidt, S. et al., 2013. Impact of the 3D Microenvironment on Phenotype , Gene Expression , and EGFR Inhibition of Colorectal Cancer Cell Lines. *PLoS ONE*, 8(3).

Sekine, H. et al., 2013. In vitro fabrication of functional three-dimensional tissues with perfusable blood vessels. *Nature Communications*, 4.

Selden, C. and Fuller, B. 2018. Role of Bioreactor Technology in Tissue Engineering for Clinical Use and Therapeutic Target Design. *Bioengineering*. 5(2).

Seliktar, D. (2012). Designing Cell-Compatible Hydrogels for Biomedical Applications. Science, 336(6085), 1124–1128.

Sen, A., Kallos, M.S. & Behie, L.A., 2001. Effects of hydrodynamics on cultures of mammalian neural stem cell aggregates in suspension bioreactors. *Industrial and Engineering Chemistry Research*, 40(23), pp.5350–5357.

Sing, S.L. et al., 2016. Laser and electron-beam powder-bed additive manufacturing of metallic implants: A review on processes, materials and designs. *Journal of Orthopaedic Research*, 34(3), pp.369–385.

Smith, S. et al., 2009. Exposure of 3T3 mouse Fibroblasts and Collagen to High Intensity Blue Light. *13th International Conference on Biomedical Engineering*, 23, pp.1352–1353.

Son, K.H. & Lee, J.W., 2016. Synthesis and Characterization of Hydrogels for Cell Sheet Engineering. *Materials*, 9(10), p.854.

Spier, *et al.,* 2011. Application of different types of bioreactors in bioprocesses. *Bioreactors: Design, Properties and Applications.* Nova Science Publishers Inc: New York, pp.55-90.

Sucosky, P. et al., 2004. Fluid Mechanics of a Spinner-Flask Bioreactor. *Biotechnology and Bioengineering*, 85(1), pp.34–46.

Sun, J. et al., 2015. An Overview of 3D Printing Technologies for Food Fabrication. *Food and Bioprocess Technology*, 8(8), pp.1605–1615.

Sun, T. et al., 2006. Culture of skin cells in 3D rather than 2D improves their ability to survive exposure to cytotoxic agents. *Journal of Biotechnology*, 122(3), pp.372–381.

Takayama, K. et al., 2013. 3D spheroid culture of hESC/hiPSC-derived hepatocyte-like cells for drug toxicity testing. *Biomaterials*, 34(7), pp.1781–1789.

Tan, F et al., (2012). Fabrication of positively charged poly(ethylene glycol)-diacrylate hydrogel as a bone tissue engineering scaffold. *Biomedical materials,* 7 (5).

Tambi, G. et al., 2014. Bioprinting Technology: A Current State-of-the-Art Review. *Journal of Manufacturing Science and Engineering*, 136(6).

Tan, H. & Marra, K.G., 2010. Injectable, biodegradable hydrogels for tissue engineering applications. *Materials*, 3(3), pp.1746–1767.

Taormina, G. et al., 2018. Special resins for stereolithography: In situ generation of silver nanoparticles. *Polymers*, 10(2), p.212.

Tarun, G. 2011. Scaffold: Tissue engineering and regenerative medicine. International *Research Journal of Pharmacy*. 2.

Thankam, F.G. & Muthu, J., 2014. Biosynthetic hydrogels - Studies on chemical and physical characteristics on long-term cellular response for tissue engineering. *Journal of Biomedical Materials Research - Part A*, 102(7), pp.2238–2247.

Tibbitt, M.W. & Anseth, K.S., 2009. Hydrogels as extracellular matrix mimics for 3D cell culture. *Biotechnology and Bioengineering*, 103(4), pp.655–663.

Vargo-Gogola, T. & Rosen, J.M., 2007. Modelling breast cancer: One size does not fit all. *Nature Reviews Cancer*, 7, pp.659–672.

Ventre, M. & Netti, P., 2016. Controlling Cell Functions and Fate with Surfaces and Hydrogels : The Role of Material Features in Cell Adhesion and Signal Transduction. *Gels*, 2(1), p.12.

Vitale, A. & Cabral, J.T., 2016. Frontal conversion and uniformity in 3D printing by photopolymerisation. *Materials*, 9(9), p.760.

Vriezema, D. et al., 2005. Self-Assembled Nanoreactors. *Chemical Reviews*, 105, p.1445–1489.

Wang, L.D. & Wagers, A.J., 2011. Dynamic niches in the origination and differentiation of haematopoietic stem cells. *Nature Reviews Molecular Cell Biology*, 12(10), pp.643–655.

Wang, Z. et al., 2015. A simple and high-resolution stereolithography-based 3D bioprinting system using visible light crosslinkable bioinks. *Biofabrication*, 7(4).

Wang, Z., 2016. *Development of A Visible Light Stereo Lithography-Based Bio Printing System for Tissue Engineering Zongjie Wang Master of Applied Science*.

Weber, L.M. et al., 2007. The effects of cell-matrix interactions on encapsulated β-cell function within hydrogels functionalized with matrix-derived adhesive peptides. *Biomaterials*, 28(19), pp.3004–3011.

Williams, C.G. et al., 2005. Variable cytocompatibility of six cell lines with photoinitiators used for polymerizing hydrogels and cell encapsulation. *Biomaterials*, 26, pp.1211–1218.

Yahia, Lh., 2015. History and Applications of Hydrogels. *Journal of Biomedical Sciencies*, 4(2).

Yamada, K.M. & Cukierman, E., 2007. Modeling Tissue Morphogenesis and Cancer in 3D. *Cell*, 130(4), pp.601–610.

Yap, C.Y. et al., 2015. Review of selective laser melting: Materials and

applications. *Applied Physics Reviews*, 2(4).

Zaitseva, M., Vollenhoven, B. & Rogers, P., 2006. In vitro culture significantly alters gene expression profiles and reduces differences between myometrial and fibroid smooth muscle cells. *Molecular Human Reproduction*, 12(3), pp.187–207.

Zhang, G., 2012. Biomimicry in biomedical research. *Organogenesis*, 8(4), pp.101–102.

Zhang, J. et al., 2003. Identification of the haematopoietic stem cell niche and control of the niche size. *Nature*, 425(6960), pp.836–841.

Zhu, J., 2011. Bioactive Modification of Poly(ethylene glycol) Hydrogels for Tissue Engineering. *Biomaterials*, 31(17), pp.4639–4656.

Zhu, J. et al., 2010. Design and Synthesis of Biomimetic Hydrogel Scaffolds with Controlled Organization of Cyclic RGD Peptides. *Bioconjugate Chemistry*, 20(2), pp.333–339.

Zhu, W. et al., 2016. 3D printing of functional biomaterials for tissue engineering. *Current Opinion in Biotechnology*, 40, pp.103–112.

7 Chapter 7: Supplementary Materials

Video S1: Printing of a PEGDA hydrogel bioscaffold using the developed 3D bioprinting unit: https://figshare.com/s/47ad9fcad7908441693c

Video S2: Operation of the X and Z-axis of the developed 3D bioprinting unit: https://figshare.com/s/438659ba43df35384035

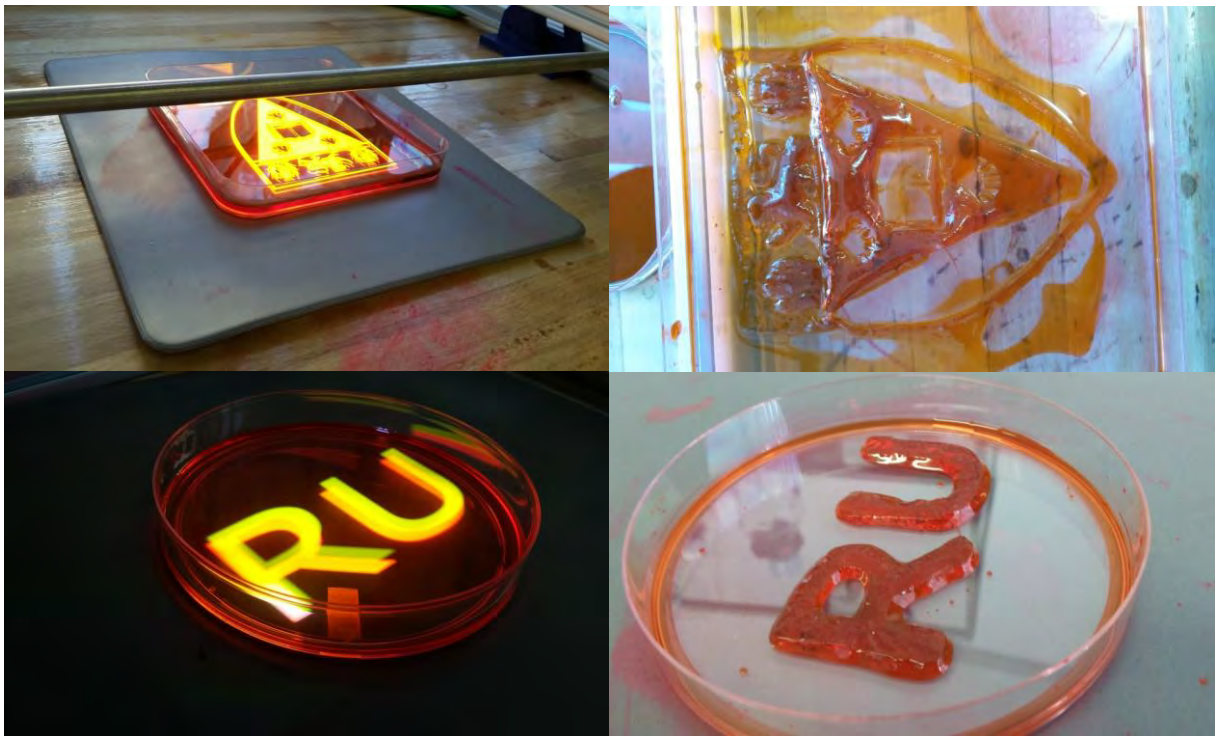

Figure 7.1: Initial testing of the PEGDA hydrogel cocktail polymerization using visible white light from an Optoma (Model HD141X) Full HD projector. Shapes used for testing include the letters "RU", and the Rhodes University Crest.

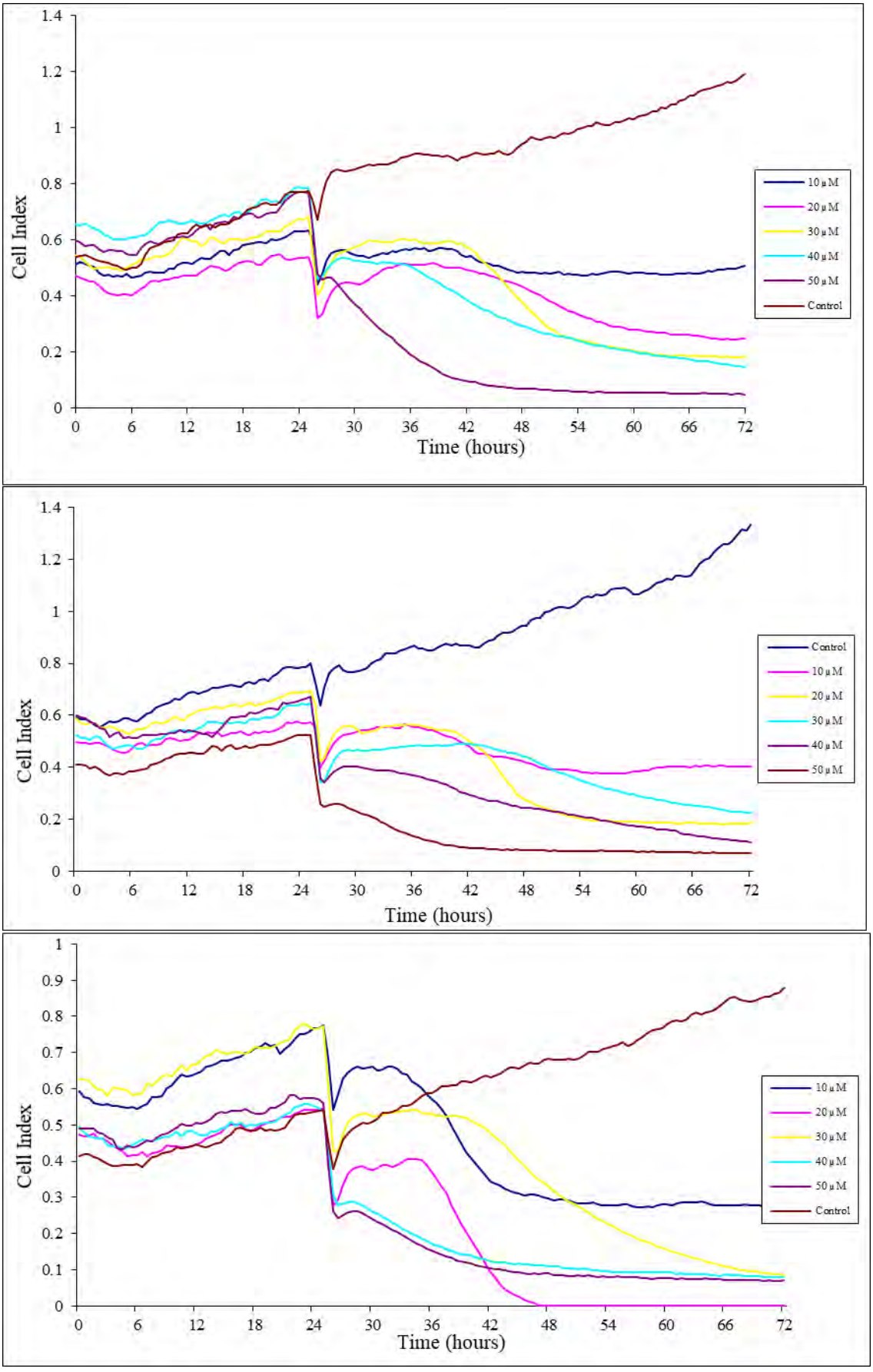

Figure 7.2: Electrical impedance of 3T3-L1 preadipocyte cell cultures during exposure to Eosin Y at various concentrations. Each graph represents one experimental replicate, which were averaged to produce the graph seen in Figure 4.3. Exposure to Eosin Y was carried out at 24h. Cultures were maintained at 37◦C.

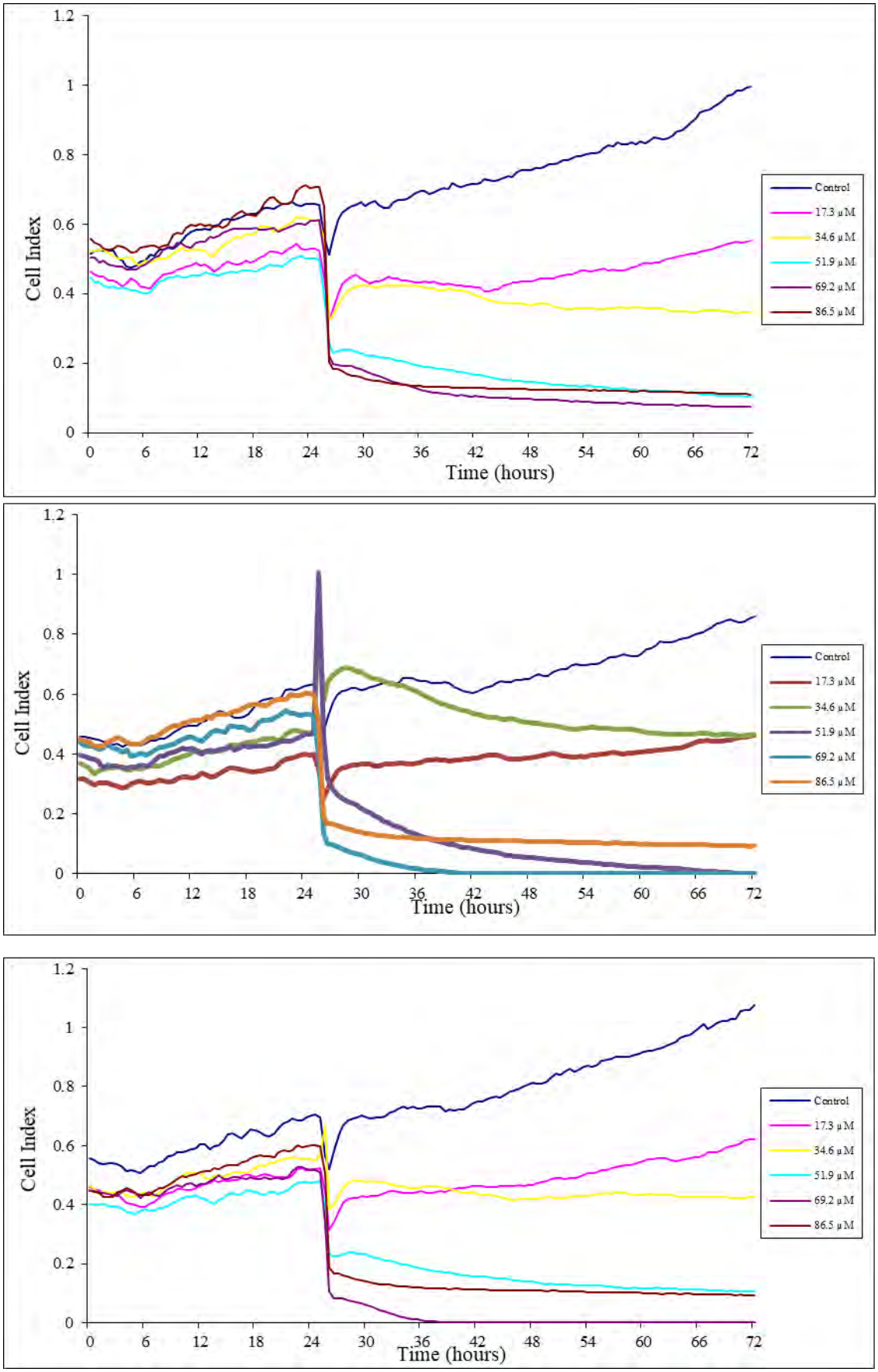

Figure 7.3: Electrical impedance of 3T3-L1 preadipocyte cell cultures during exposure to NVP at various concentrations. Each graph represents one experimental replicate, which were averaged to produce the graph seen in Figure 4.3. Exposure to NVP was carried out at 24h. Cultures were maintained at 37◦C.

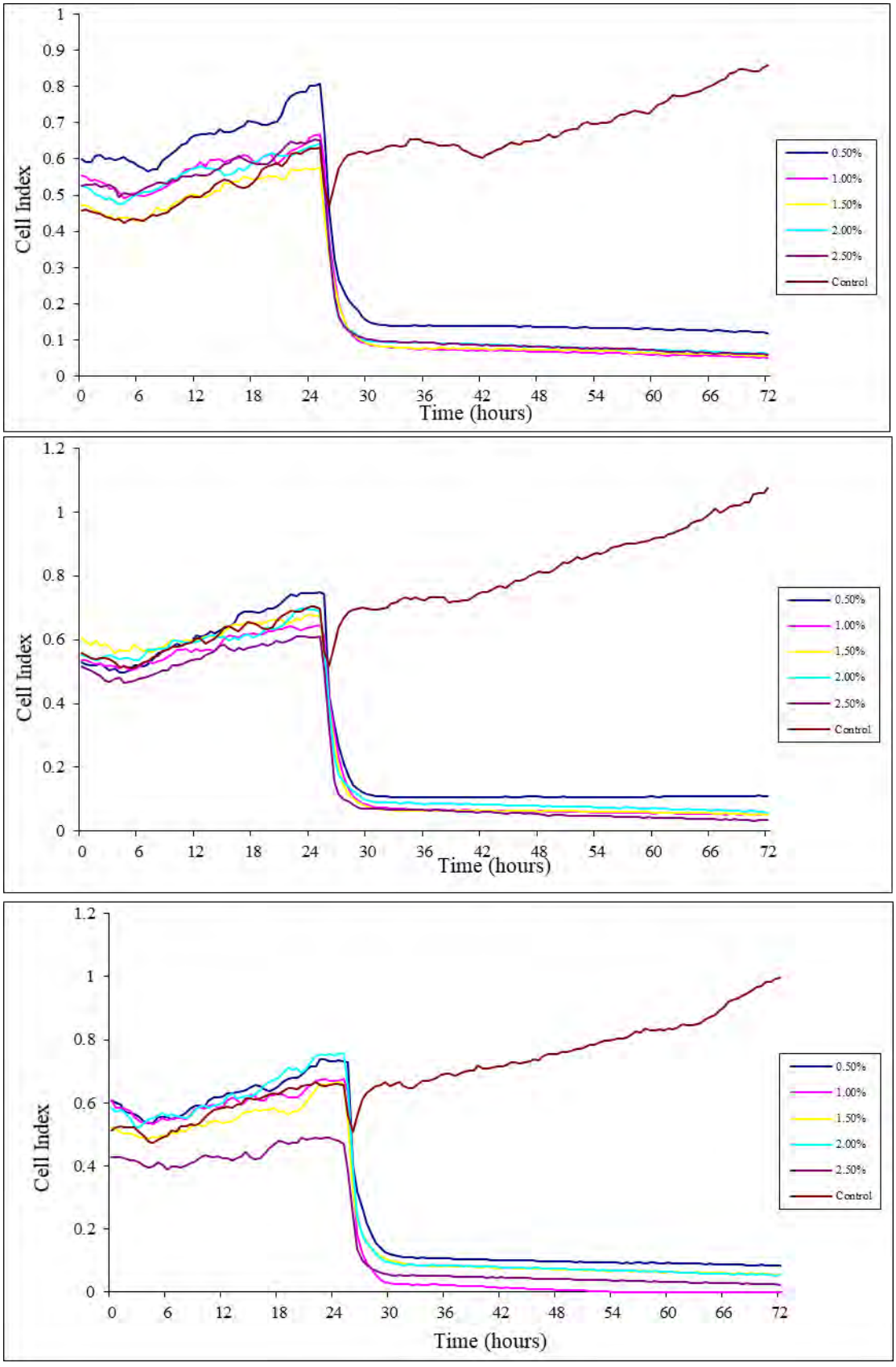

Figure 7.4: Electrical impedance of 3T3-L1 preadipocyte cell cultures during exposure to PEGDA at various concentrations. Each graph represents one experimental replicate, which were averaged to produce the graph seen in Figure 4.3. Exposure to PEGDA was carried out at 24h. Cultures were maintained at 37◦C.

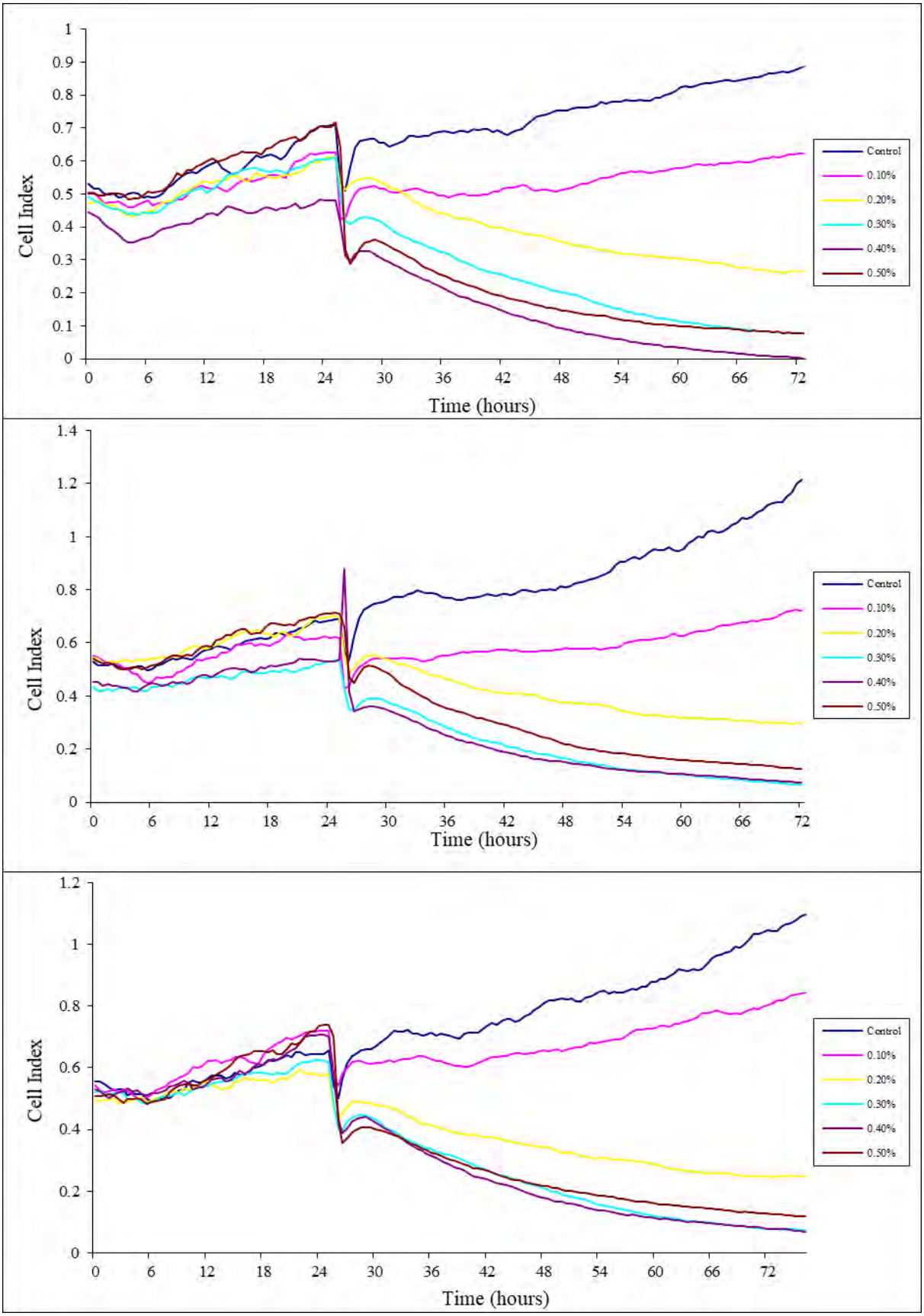

Figure 7.5: Electrical impedance of 3T3-L1 preadipocyte cell cultures during exposure to TEA at various concentrations. Each graph represents one experimental replicate, which were averaged to produce the graph seen in Figure 4.3. Exposure to TEA was carried out at 24h. Cultures were maintained at 37◦C.